UNIVERSITY OF CAPE COAST

DESIGN AND IMPLEMENTATION OF INTERFACED DIGITAL KYMOGRAPH AND ORGAN BATH

BENJAMIN OTENG

2023

UNIVERSITY OF CAPE COAST

DESIGN AND IMPLEMENTATION OF INTERFACED DIGITAL KYMOGRAPH AND ORGAN BATH

BY
BENJAMIN OTENG

Thesis submitted to the Department of Physics of the School of Physical Sciences, College of Agriculture and Natural Sciences, University of Cape Coast, in partial fulfilment of the requirements for the award of Doctor of Philosophy Degree in Physics

SEPTEMBER 2023

DECLARATION

Candidate's Declaration

I hereby declare that this thesis is the result of my own original research and that no part of it has been presented for another degree in this university or elsewhere.

Candidate's Signature……. Date: ……

Name: Benjamin Oteng

Supervisors' Declaration

We hereby declare that the preparation and presentation of the thesis were supervised in accordance with the guidelines on supervision of thesis laid down by the University of Cape Coast.

Principal Supervisor's Signature…….. Date: ……..

Name: Professor Anthony Kwabena Twum

1st Co-Supervisor's Signature……Date: ……..

Name: Professor Baah Sefa-Ntiri

2nd Co-Supervisor's Signature…….. Date: ……..

Name: Professor Benjamin Anderson

ABSTRACT

Kymographs are essential devices for investigating physiological parameters such as blood pressure, breathing rate and heart rate, and other pharmacological studies. However, high cost of acquiring a new kymograph has made the equipment nonexistent in most laboratories, especially in developing countries such as Ghana. In this research, an Arduino-based cost effective and easily available replacement parts prototype digital kymograph has been designed and built, together with an organ bath. A muscle contraction was used to evaluate the hardware and software systems that were developed to support the kymograph. Being more visually appealing than a traditional kymograph, the outcome demonstrates how well the instrument functions. All the materials used in this prototype are highly corrosion resistance. It also has a cooling fan, stepper-motor and driver, Arduino UNO R3 board, standby mode circuit, display unit, stop and start buttons, and speed regulator (0.25, 0.50, 0.75, 1.00, 1.25, 2.50, 3.00 mm/sec.). Proteus 8.7 SP3 Professional and NI Multisim 13.0 were used in the design and simulation of all the circuit diagrams. C++ was used for the programming of the microcontrollers used in this research. Unlike the traditional digital kymographs which employ steel, brass, iron and wood, this research uses Carbon fiber for the shaft, the drum was made of aluminum and the main chassis which houses the electrical system is made of galvanized steel. The organ bath is made up of Perspex glass, microcontroller and operates at a temperature of 37^{o}C. Researchers and students will have easy access to the sustainable and affordable kymograph for use in their teaching and research, particularly in developing laboratories. This makes it a novel device with overwhelming advantages for research and development in medicine and academia.

KEY WORDS

Arduino UNO R3

Carbon fiber

Kymograph

Muscular contractions

Organ bath

Physiology

ACKNOWLEDGEMENTS

My deepest gratitude goes out to Professor Anthony Kwabena Twum, Professor Baah Sefa-Ntiri and Professor Benjamin Anderson, Head of Department (Physics) who served as supervisors for their enormous contributions, direction, counsel, encouragement, and goodwill. Prof. Fredrick Sam, Professor Alex Boye, Prof. Raymond Edziah, and Doctor Anokye Dompreh, as well as Professor Robert Agbemafle, former Head of Department (Department of Laboratory Technology), Professor George Amoako, former Head of Department (Department of Physics) and Professor Ruphino Zugle, Vice-Dean School of Graduate Studies, are appreciated for their suggestions and support. For his assistance in improving this research, Professor John Kwesi Bentum of the Chemistry Department is also thanked. I appreciate the help from my family and friends, especially my mother, Comfort Annan.

DEDICATION

To Mr. Michael Amponsah, Miss Irene A.K. Tagoe and Children.

TABLE OF CONTENTS

LIST OF TABLES

LIST OF FIGURES

LIST OF ABBREVIATIONS

AC	Alternating Current
BDNF	Brain-Derived Neurotrophic Factor
CRC	Concentration Response Curve
CRO	Cathode Ray Oscilloscope
DC	Direct Current
DNA	Deoxyribonucleic Acid
EMCCD	Electron Multiplying Charge-Coupled Devices
ENA	Enable Pin A
ENB	Enable Pin B
IDE	Integrated Development Environment
IEEE	Institute of Electrical and Electronic Engineers
LCD	Liquid Crystal Display
LED	Light-Emitting Diode
NEMA	National Electrical Manufacturers Association
NTC	Negative Temperature Coefficient
SPDT	Single Pole Double Throw
SPST	Single Pole Single Throw
VFL	Voltage Full load
VNL	Voltage No Load

CHAPTER ONE

INTRODUCTION

The kymograph, also known as a myography, is an essential instrument for extended study in physiology, such as recording heart, skeletal and smooth muscle contractions, respiratory movements, and tissue examination in vivo or in vitro. It is also usually used in physics and engineering to analyse waveforms, vibrations, or other dynamic phenomena. However, various obstacles arise in practice, such as the cost of purchasing and servicing, which are critical challenges of using a kymograph. Traditional kymographs require sophisticated gear systems to operate, which might impair the accuracy of the spinning drum's speed. Furthermore, the kymograph is unavailable for study in several research and academic laboratories. In this chapter, the background to the study, history and the functions of the kymograph, statement of the problem, research objectives and significance of the study have been deliberated.

Background to the study

Kymograph is a Greek word, “kyma” meaning wave and “graphin” meaning write. Carl F.W. Ludwig invented the kymograph in 1847, which was employed to record variations in arterial blood pressure. A sample of a kymograph invented by Carl F.W. Ludwig is shown in Figure 1. His kymograph is comprised of an ivory float with a stylus attached to allow drawing or waving on a rotating drum, a brass pipe cannula, and a U-shaped mercury manometer tube. The curve generated had a twitch/cramp, which shows the period of contraction and relaxation of a muscle after a single stimulation. The three distinct phases of the twitch include (1) the latent period, (2) the contraction phase and (3) the relaxation phase, as shown in figure 3.

Ludwig made history by being the first to maintain animal organs alive in vitro. He found that the medulla oblongata, which is located at the base of the brain, has a blood vessel regulation system. He used frog hearts as models to measure blood pressure in capillaries by injecting a fluid that closely resembled blood plasma in composition. In collaboration with American scientist Henry Bowditch, he discovered the depressor and accelerator nerves of the heart. He developed the "all-or-none law" of cardiac muscle action, which states that “the heart muscle will either contract fully or not at all in response to any stimulus” (Britannica, 2020).

The idea of recording muscular contractions as graphs, displaying tension changes is demonstrated in Figure 1(B). During contraction, an isolated muscle pulls the pen (stylus) upward, and when the muscle relaxes, the weight pulls the muscle and stylus down. Muscle fibers are stimulated by electrical voltage, which mimics a nerve impulse. Computer-based devices that record similar muscle tension graphs are frequently used in modern myography. Figure 1 (A) is Ludwig’s kymograph which was copied from ‘Ludwig’s Lehrbuch der Physiologie’, It is made out of a bent glass tube that is attached to an animal's artery via d and contains mercury (a b c). The gear systems are represented by the letters h h and i i. e f is a thin, upright rod that swims on the surface of the mercury and has a brush at its free end, g, that records the movements of the mercury on the rotating cylinder.

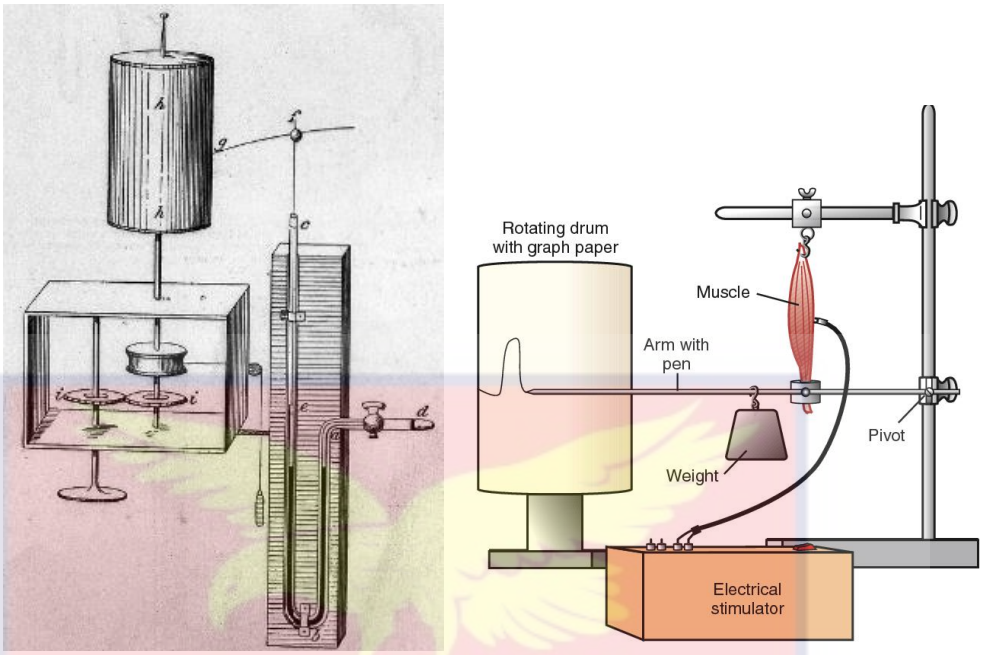

(A) (B)

Figure 1: (A) Carl F.W. Ludwig's invented kymograph (https://wellcomeimages.org, 2022) *(B)* A classical type of kymograph setup (https://www.semanticscholar.org, 2024)

The stylus attached to a kymograph moves up and down in response to the contraction and relaxation of muscle tissues. It has a rotating drum wrapped with a record sheet. The height of a wave can be used to examine the degree of movement, and horizontal distances can be used to measure how the movement relates to time as shown in Figure 2. (ww.vjinstruments.com, 2021).

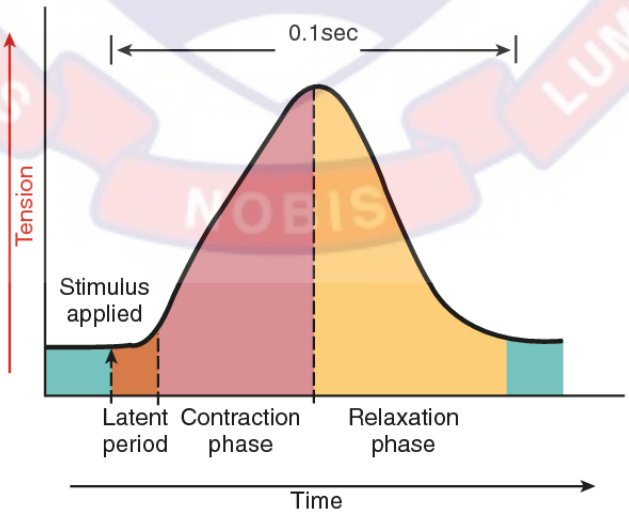

Figure 2: Twitch phases of a muscle (www.semanticscholar.org, 2024)

In a kymograph, the spatial axis doubles as the time axis to visually represent the geographical position over time. This clever gadget records variations in motion and pressure by having a stylus oscillate on a rotating drum that is covered with a sheet of recording paper. The main component of a kymograph is a revolving drum that is marked by a pen or stylus that moves perpendicular to the drum's revolution on a record sheet, which is usually made of smoked paper. The drum might be indicated by a time indicator on the sheet or rotated at a constant speed by a machine.

In its early stages, the kymograph was an analogue and hydraulic apparatus. It was the central apparatus used in physiology research during the 19th and 20th centuries. Researchers used it to determine physiological phenomena such as breathing, muscle movement, and speech. Over time, other researchers and technicians developed enhancements to the device and new sensory components like registration systems and electrical and electronic approaches. All of the data were recorded using ink (Alistair, 2016).

Kymographs were used in various fields such as medicine, atmospheric pressure, tuning fork vibrations, steam engines, animal behaviour, and movement of molecules in cells (dbpedia.org, 2021).

Kymographs can be either vertical or horizontal depending on the orientation of the drum. There are several varieties available as well, depending on the functioning mechanism. These include:

i. Clock work (spring movement)
ii. Mechanical (pulley driven)
iii. Electrical
iv. Digital

v. Long paper (research)

Statement of the Problem

The relatively high cost of acquiring a new kymograph has made the equipment nonexistent in most laboratories, especially in developing countries such as Ghana. An analogue kymograph produced in India came with a $1524 price tag; producing such an instrument in large quantities for research in institutions makes it expensive. Maintenance and service of the kymograph is another challenge since replacement components are not readily available. Most of these conventional kymographs use gear systems, which make the kymograph bulky and less accurate and require more precision. Hence, there is a need for readily available, efficient, and cost-effective customized kymographs that can be used for research in less-endowed laboratories. In addition, traditional and contemporary kymographs utilize materials such as aluminium alloy, steel and iron for the manufacturing of the shaft; however, using these materials in a digital kymograph shortens the lifespan of the stepper motor because of the weight these materials exert on the stepper motor. Therefore, there is a need to replace these materials with equally strong and lightweight materials like carbon fiber, used in this research to prolong the life span of the stepper motor.

Purpose of the Study

Design and construct a sustainable and inexpensive digital kymograph and organ bath for use in research and teaching on muscle movements, blood pressure fluctuations and other physiological phenomena.

Research Objective

To design and implement a sustainable, cost-effective digital prototype kymograph using available materials that will be interfaced with an organ bath for use in research laboratories.

Specific Objectives

The specific objectives of this study were to;

i. Design and simulate electronic circuits with CAD software for kymograph and organ bath.
ii. Physically design and construct the digital kymograph and organ bath.
iii. Develop a C++ program that interfaces and regulates the kymograph and organ bath.
iv. Calibrate and test for the efficiency.

Significance of the Study

Researchers and students will have easy access to the sustainable and affordable kymograph for use in their teaching and research, particularly in developing laboratories.

Delimitation

The developed kymograph is intended for usage in academic and research laboratories with speed range of 0.25 to 3.0 mm/sec.

Limitation

Lack of molds, specifically designed machines and tools for creating faster components (parts) of the kymograph served as a constraint in the prototype construction.

Organisation of the Study

Chapter One introduces the thesis and states the research work's problem and purpose. The rest of the thesis is organised as follows. Chapter Two focuses on the literature review, kymograph generation and data detection, acquisition techniques, and the materials used in the construction. Challenges in the use of kymograph are also covered. Chapter three deals with research methods, circuit design, simulation and procedure for constructing the kymograph and organ bath are emphasised. After that, Chapter Four discusses the findings and discussion related to data gathering and analysis. This chapter also focuses on the purpose of the study, techniques, interpretation and summary of the key findings. The overview of the entire thesis, summary of results, conclusions and recommendations of the critical findings of this study are presented in chapter five.

.

CHAPTER TWO

LITERATURE REVIEW

Introduction

A kymograph is an instrument that monitors the magnitude of physiological parameters such as muscular contraction. Traditional kymographs, however, have flaws such as lack of accuracy and high cost. As a result, a low-cost microcontrolled-kymograph with strong corrosion resistance and accurate speeds was created together with an organ bath. The results show that the equipment performs better at varied speeds than a typical kymograph with complicated gears. This chapter examines scholarly information on kymograph. It gives an overview of traditional and contemporary kymograph knowledge, enabling for the identification of important ideas, methodologies, and gaps in existing research that was applied to the design and implementation of this study.

Types of Kymograph

Kymographs can be categorized into two types based on their operational method and drum orientation - horizontal and vertical. Based on operational method, kymograph design include; Long paper/Research, Mechanical (pulley powered), Electrical, Digital, and Clockwork (spring movement) kymograph, as shown in Figures 3 a-c.

Horizontal and Vertical Kymographs

Various forms of kymographs exist, contingent upon the drum's orientation. When the drum rotates vertically, a vertical kymograph is produced; conversely, a horizontal kymograph is produced when the drum rotates horizontally. Vertical kymographs are commonly used in biological and

medical research to track the movement of cells or organisms over time. They are often used to study the motion of cilia, flagella, or muscle fibers.

Horizontal kymographs, on the other hand, are usually used in physics and engineering to analyze waveforms, vibrations, or other dynamic phenomena. Understanding the different types of kymographs and their applications is crucial in selecting the appropriate type of kymograph for a specific research or analysis task.

Horizontal Kymograph

The instrument is made up of a horizontally mounted brass drum (Figure 3A and 3B) between an anterior axle post and a posterior mechanical drive box. A rotating mechanical regulator protrudes from the drive box's top. The drum is secured to a metal base by three leveling screws.

(A) (B)

Figure 3: Horizontal kymograph. (A) Side view. (B) Back view (www.utsic.utoronto.ca, 2023)

In 1892, Charles Verdin built a horizontal kymograph, which is now housed in the Department of Psychology at the University of Toronto. The height = 33 cm, width = 21 cm and length = 59 cm. This Kymograph captured changes in physiological or muscle events throughout time. The revolving drum

was wrapped with smoked paper and tagged with a signal marker that recorded electrical or mechanical stimulus levels (www.utsic.utoronto.ca, 2023).

Vertical Kymographs

A vertically mounted drum is turned at a constant rate by a mechanism regulated by a governor (Figure 4a and 4b). The motor mechanism is mounted vertically on the heavy metal base behind the drum. The base has adjustable feet to level the instrument. Multiple gearing can adjust the overall speed of rotation. A paper is fixed to the drum. Primary Materials include: Brass, metal, Manufacturer's label "E. Zimmermann, Leipzig" Dimensions (cm): Height = 64, Width = 18, Length = 36. Function: Used in combination with other instruments to record the temporal variations of various physical events (usually related to the human body). Events are recorded in ink or smoked paper along the rotating drum.

Kymographs were originally developed by physiologists to record blood pressure. Later, experimental psychologists used them to record a variety of time-related phenomena, including muscle strain, response times, stimulus presentations, and tuning fork vibrations.

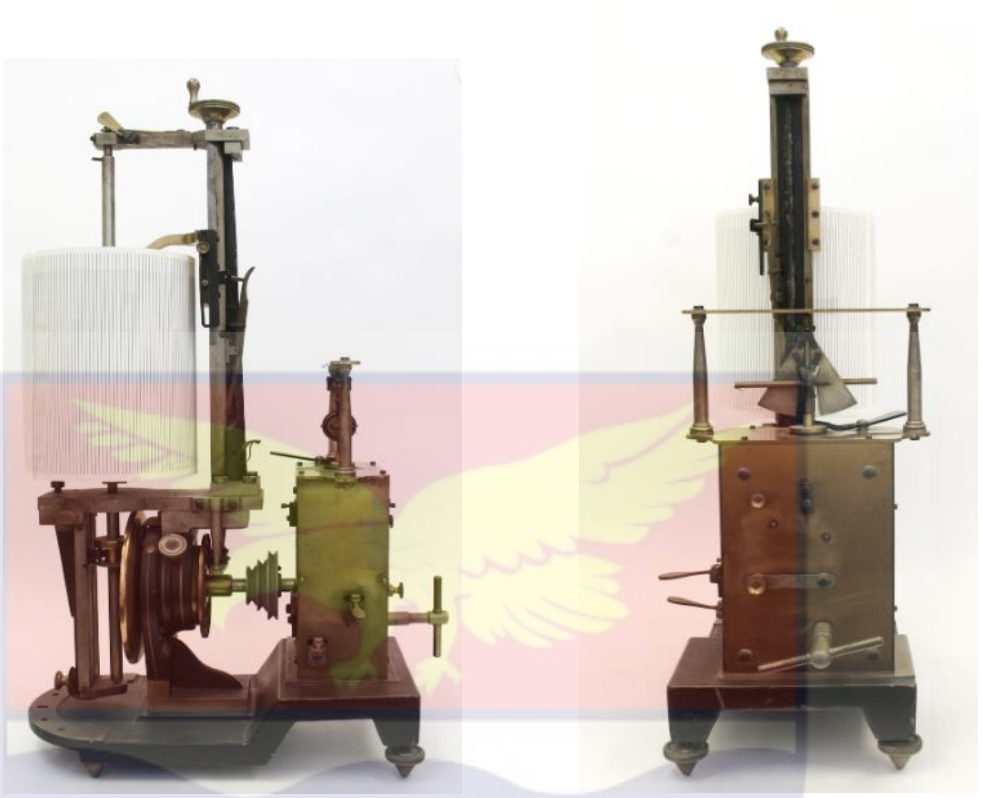

(A) (B)

Figure 4: Vertical Kymograph. (A) Front view. (B) Back view (University of Toronto, 2023)

Clock Work Kymograph

A kymograph is a clock-driven drum (Figure 5) that rotates at a very precise rate in order to provide a continuous surface for recording experimental data. The revolving drum would have been wrapped with smoked paper which was marked by a signal marker. A signal from a timekeeping device would also have been recorded alongside the experimental data in order to provide a time reference.

Figure 5: Clock work kymograph (vlp.mpiwg-berlin.mpg.de, 2022)

Pulley Driven Kymograph

The most common way to use a pulley-driven kymograph (Figure 6) is to clamp it to the back of a table over a quick-running cord. Two small pulleys guide a loop of this cord around a large pulley. The pulley that is driven in this way is fastened to a spindle that is horizontal and holds another pulley that uses a cotton cord loop to drive the instrument. This cord is led over a guide pulley and down to a pulley that is hooked to a weight that hangs at the back of the table in order to maintain uniform tension. This permits the instrument to have the same length as the cable loop. The instrument may be driven while standing in any position on the table since the driving pulley can be clamped at any location along the table's edge. These movements can be done while the cords are moving. A handle on the driving pulley can be turned to start and stop the instrument.

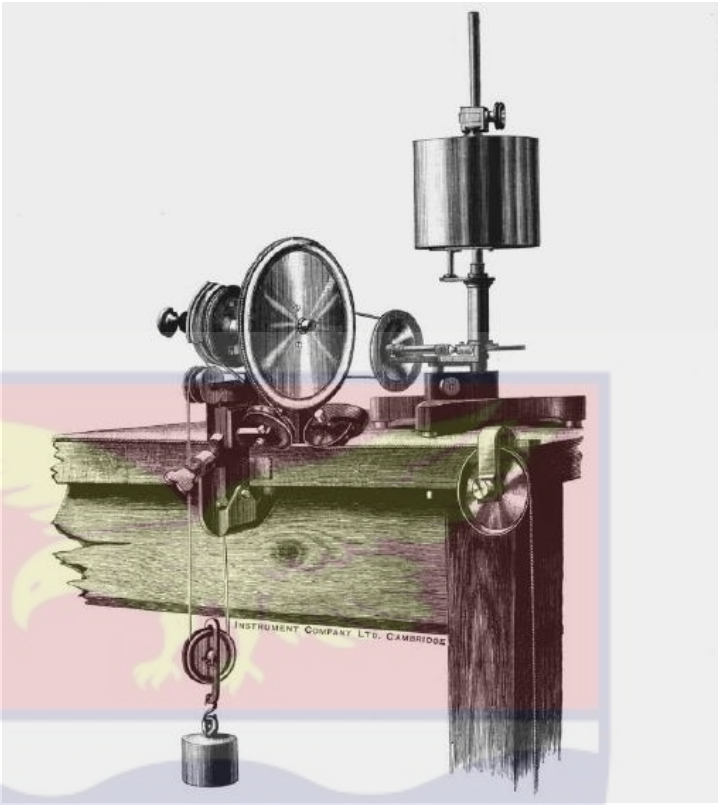

Figure 6: Pulley driven kymograph (www.sil.si.edu, 2024)

Electrical Kymograph

The components of an electrical kymograph (Figure 7) consist of stimulator knob, drum speed knob, stimulation pulse per second key and voltage key, make up the kymograph base. The most significant feature is a motor that spins the drum and is locked in place using a locking mechanism in the middle of the drum.

Figure 7: Electrical kymograph (www.indiamart.com, 2023)

The electric motor runs on a single phase 220 volts, 50 Hz Alternating Current (AC). The motor is enclosed in the base of the kymograph (Figure 8).

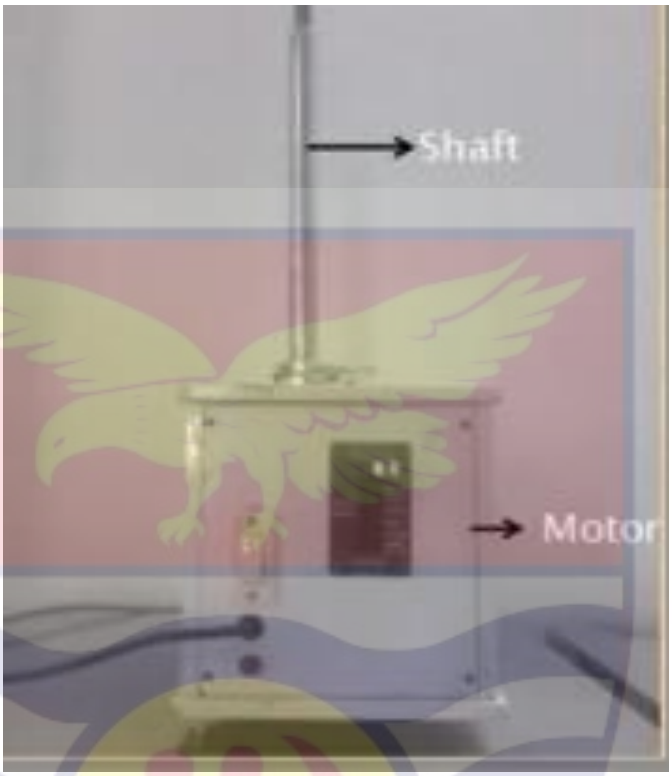

Figure 8: Kymograph shaft (Alwaz, 2021)

Kymograph Shaft

The shaft (Figures 9) is connected to the motor vertically and can be rotated at different speeds. Slowest: 0.12mm per second and fastest: 640 mm per second. Shaft has groove on one side and a screw lift at the top. A small rectangular plug mounted on the side of the screw, inside the shaft comes out through the groove. Rectangular plug can be raised or lowered along the groove by rotating the screw lift fitted at the top of the drum. It supports weight of the drum and prevents it from sliding down during rotation. The level of drum can be adjusted by top screw lift.

Figure 9: Shaft of kymograph (Alwaz, 2021)

Kymograph Gears

The gears (Figure 10A and 10B) which are inside the base chassis of the kymograph are responsible for changing the speed of the shaft. During an experiment, the sooty drum rotates at a predetermined speed based on the selected gear in the kymograph.

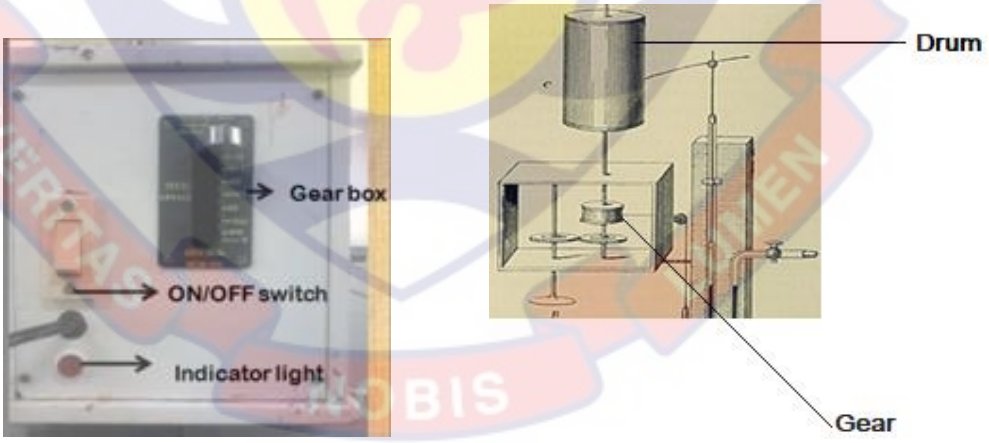

(A) (B)

Figure 10: Kymograph gear system. (A) Electrical kymograph gear box. (B) Ludwig's kymograph gear box (Alwaz, 2021)

Kymograph Lever

The gears are switched using a lever. The lever (Figure 11) has two prongs that must be brought together in order to raise or lower it and engage it in a specific speed slot. One slot with the designation (N) Neutral is where the gear detaches from the motor. Fastest: 320/640 mm per second and slowest: 0.12/0.23 mm per second.

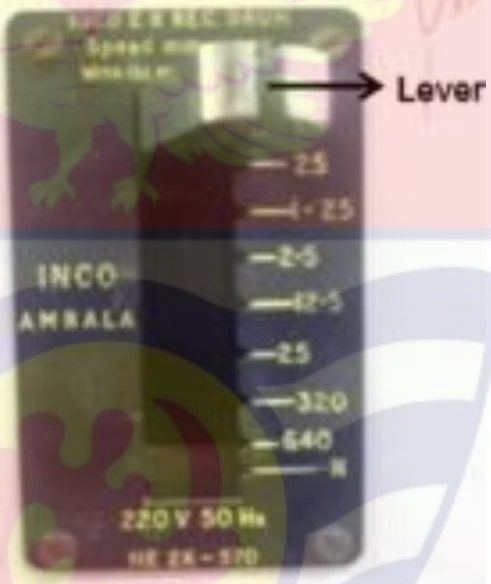

Figure 11: Kymograph gears (Alwaz, 2021)

Kymograph Clutch

A gear can be engaged or disengaged using the clutch lever (Figure 11). It is necessary to engage this clutch each time before shifting gears in order to start or stop the drum. This guards against gear damage. When the clutch lever is in the neutral (OFF) position, it is simple to rotate the cylinder by hand.

Kymograph Contact Block

At striker level, a contact block (Figure 12) is installed on the top of the kymograph body. A plastic button, two electrical terminals, and a spring contact bearing are all present.

The electrical circuit is complete when the striker presses the spring contact, bringing the two platinum points into contact with one another. When these terminals are incorporated into the main circuit, this becomes helpful. The operation of the contact block terminals is critical to the main circuit. Their purpose is to indicate the recording surface's stimulation point.

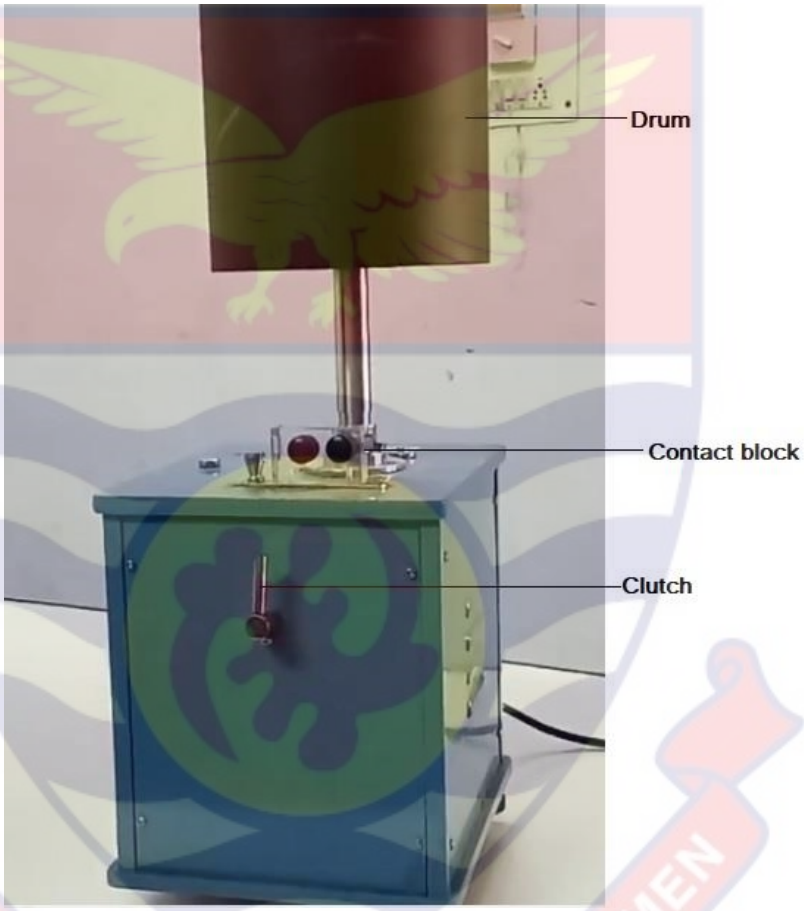

Figure 12: Electrical kymograph (www.indiamart.com, 2023)

Kymograph Contact arm/ Projecting strikers

A pair of projecting strikers (Figure 13) are fixed to the base of the vertical shaft. They can be kept closed together or drawn apart to form any desired angle between them. The striker's two arms can be pulled apart in response to two stimuli, one of which occurs when the drum rotates. The contact button will be pressed either once or twice in close association at a precise

interval of time. They are fitted firmly enough on the shaft to rotate with it and strike past the contact button (Alwaz, 2021).

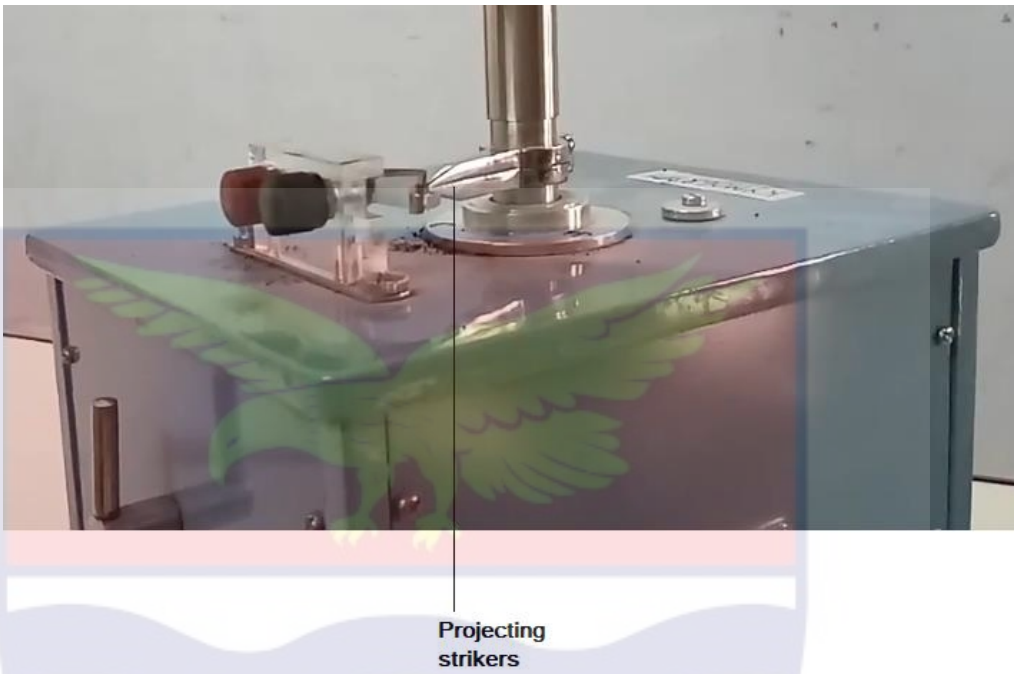

Figure 13: Kymograph projecting strikers

Kymograph Drum

The drum (Figure 12) is fixed to the kymograph's shaft. On top of the drum is a drum grip clasp that secures the drum to the axle and keeps it from sliding down the shaft. The starting drum for Sherrington is 6" x 6" (15 cm x 15 cm) and is composed of aluminum alloy.

Digital Kymograph

A digital kymograph (Figure 14) is made out of a revolving drum wrapped with kymograph paper on which a stylus glides up and down to show the effects of drugs on contractile tissues. In comparison to the former type of electrically powered pulley adjustment drum, the recording drum is a microprocessor-controlled unit (www.narayanienterprises. com, 2023).

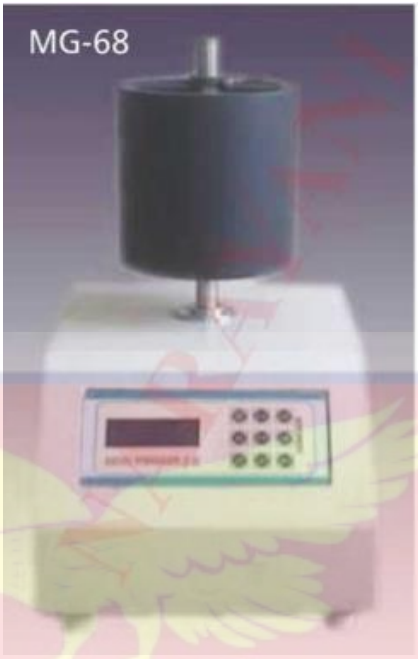

Figure 14: Digital kymograph (www.narayanienterprises.com, 2023)

Technical Features of Digital Kymograph

Most digital kymographs have the following features: Microprocessor-controlled machine with a standard 16x2 LCD display, digital speed selection, and highly accurate speeds of 0.12, 0.25, 0.75, 1.00, 1.25, 2.50 mm/sec. Other features include: digital timer and time multiplier with voice and visual alarm, Low power consumption and simple drum height adjustment. The body is sturdy and resistant to corrosion. (www.narayanienterprises.com, 2023).

The smoked-drum kymograph was superseded in most laboratories by equipment ranging from simple ink writing pens for kymograph to complicated electronic devices meant to obtain permanent recordings in physiology and pharmacology research.

A traditional simple kymograph ink writing pen device, consisting of a hollow steel pen connected to a small ink reservoir via a thin polyethylene tube, is used for kymograph recordings of heart, skeletal and smooth muscle contractions, and respiratory movements. In actual use, a number of different

problems with ink flow through the instrument can arise. Moreover, student laboratories may not always have the system. The smoked-drum kymograph is still in use today.

Mechanical Kymographs

The antique kymograph (Figure 15) is a 19th-century mechanical device that uses a floating pen attached to Poiseuille's mercury manometer. This instrument was utilized to gauge air pressure, measure tuning fork oscillations, and evaluate the performance of steam engines. A visual depiction of the movement across time that utilizes the spatial axis was presented. The instrument comprises of a paper-covered rotating cylinder that registers changes in motion or pressure by means of a swinging stylus (www.lasvegaspolygraphs.com, 2022).

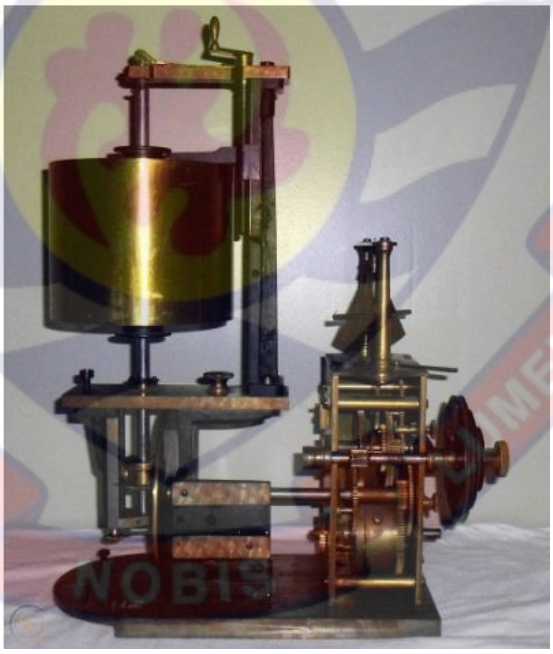

Figure 15: Mechanical kymograph (www.lasvegaspolygraphs.com, (2022)

Carl Ludwig's contribution to image registration in physiology has remained a significant landmark in the field for more than a century. He introduced a groundbreaking method of studying physical functioning and

established entire schools of physiological inquiry. The kymograph, an instrument he invented, was a crucial tool in the rapid advancement of scientific medicine during the 19th century. Its historical importance has cemented its place in medical history, and it continues to be a reference point for subsequent scientific advancements polygraphs

Conventional Mechanical Kymograph

The drive system of mechanical kymograph (Figure 16) consists of a constant speed electric motor and a precise gearbox that are housed in the base. Additionally, a sturdy plate clutch is included. The gear ratios can be engaged by sliding the lever into the surface speed-marked slot or by using a knob in separate variants. The main cylinder has a diameter of 6 inches and is made of stainless steel. It has been standardized to be universal and interchangeable with other cylinders. Double electric contact arms secure the main spindle, and a strong double contact block is put on top of the base. Sliding the lever into the 8-surface speed slot yields gear ratios of 640 mm, 320 mm, 25 mm, 12.5 mm, 2.5 mm, 1.2 mm, 0.25 mm, and 0.12 mm per sec.

Longer records can be accommodated with a long paper extension mechanism with a single set screw. Various types of mechanical kymographs have been developed over the years.

Figure 16: Mechanical kymograph (www.iqbalscientific.com, 2023)

Physiological Records Projected on a Screen

Despite being a useful instrument for physiological examinations, kymograph with paper wrapped around drum was poorly equipped to display its output to a very small number of pupils. Therefore, the goal of French veterinarian Jean Baptiste Auguste Chauveau (1827–1917), who was well-versed in the field, was to design and construct a modified Ludwig's kymograph that could project three channels onto a screen as demonstrated in front of a class to show three physiological variables during the actual experiment, or in-vivo. His favorite demonstration involved using the clever and reliable intravascular pressure sounds created by his close collaborator Etienne Jules Marey (1830–1904) to record intracavity pressures following catheterization of

the left ventricle via the carotid artery and the right atrium and ventricle via the jugular vein.

The British neurophysiologist and Nobel Prize winner Sir Charles Scott Sherrington (1857–1952) is credited with replicating the method and building a model with a similar design in a lecture hall at the University of Liverpool. (Hoff, Valentinuzzi, Geddes, and Moore, 215).

A sketch of the brilliant idea, a true bioinstrumentation advancement that seamlessly integrates into the current biomedical engineering concept, is displayed in Figure 17 of the kymograph projector. Ludwig's whirling cylinder was swapped out for a smoked horizontal slab of glass. A strong vertical light beam was created by a carbon arc lamp and a 45° mirror. This beam broke through the glass, was caught by an upper prism-lens assembly, and was then projected onto a huge white screen in front of the audience.

The second half of the nineteenth century saw a significant advancement in optics, with the addition of telescopes and microscopes to a wide range of other optical tools and discoveries, including glass prisms and light polarization. When the kymograph was fully smoked, no light could get through, but any scratches on the surface showed as white lines. The clockwise round glass action was powered by a mechanical pulley clutch mechanism and a permanent magnet DC motor. Heat and gasses were able to escape through the lamp's chimney. Four light styluses scratched the smooth surface, three of which recorded blood pressure in various cardiac chambers and one of which served as a timer. The radial movements of the styluses were guided by four pneumatic tambours.

The precise construction and operation of the equipment are not documented, however it was probably built somewhere between 1875 and 1876.

A lateral view of the machine is shown in Figure 18a, with the four tambours on the bottom and the projecting head on top. The ventilation chimney is on the right. Figure 18b illustrates a back view.

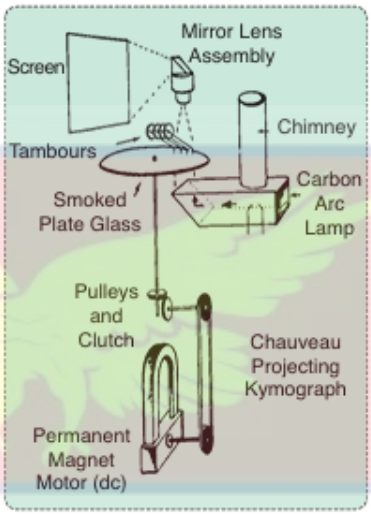

Figure 17: Chauveau's projecting kymograph scheme (Hoff *et al*., 2015)

(A) (B)

Figure 18: (A) Lateral and (B) Chauveau's projecting kymograph from the back (Hoff *et al*., 2015).

Computerized Kymograph for Muscle Contraction

Suhaeri and Vitri Tundjungsari (2014) built a computerized kymograph that uses an ultrasonic distance sensor to measure muscle contractions (Figure 19). The problems in the conventional kymograph, which includes result visualization and accuracy were improved by the researchers.

The researchers demonstrated a computerized kymograph, which uses an ultrasonic distance sensor to measure, record, and show graphical data of muscle contraction on a computer.

Hardware and software systems were built to support the computerized kymograph, and the device was tested on live frogs. The results show that the device works well, as it provides greater visualization than a normal kymograph (Figure 19 and 20).

Figure 19: Computerized kymograph system

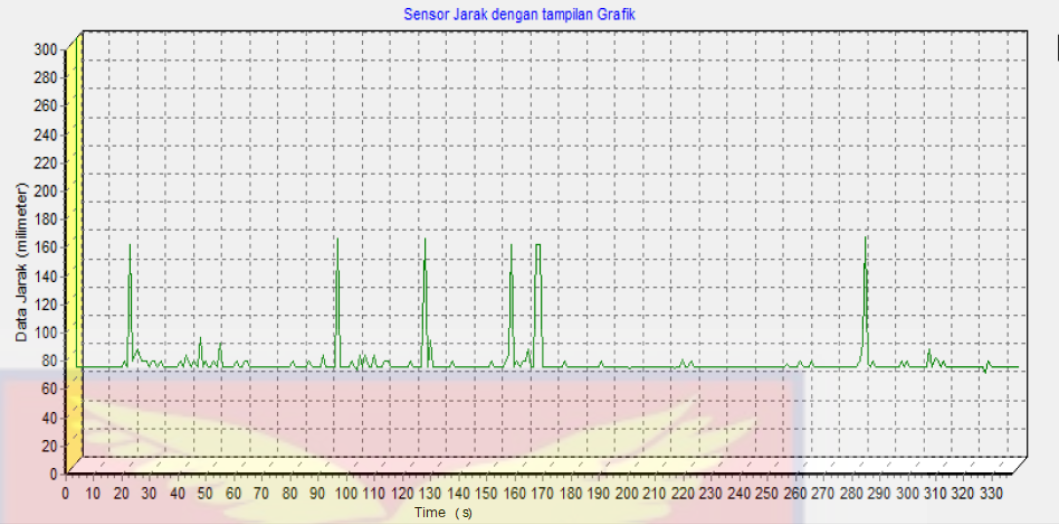

Figure 20: Computerized kymograph result

Figure 20 shows the result of Computerized Kymograph, compared with the results of conventional kymograph (Figure 21). The computerized displays time value (x axis) and distance value (y axis); whilst the conventional kymograph does not provide those value but graphics.

Figure 21: Conventional kymograph result

Several kymograph projects for motion analysis and detection have been accomplished. Spatio-temporal methods have been used in kymograph for motion analysis and detection, such as building a spatio-temporal picture representation, utilizing kymograph of video sequences (Ihor Smal, IIya Grigoriev, Anna Akhmanova, Wiro J Niessen, and Erik Meijering, 2010).

Kymographs have also been used to track picture attributes over time, such as the variable-rate particle filter's strategy for improving the accuracy of retrieved edges corresponding to the tip of microtubules from a kymograph-like image representation. Amit Mukherjee, Brian Jenkins, Cheng Fang, Richard J. Radke, Gary Banker, and Badrinath Roysam (2011) describe an automated method for profiling the velocity patterns of small organelles, Brain-derived neurotrophic factor (BDNF) granules moving along a selected section of an axon of a cultured neuron imaged using time-lapse fluorescence microscopy.

Instead of identifying granules immediately, as in normal tracking, the proposed method creates a two-dimensional spatiotemporal map (kymograph) of granule traffic along an axon segment. Smal et al. (2010) created kymographs by hand and examined granules using the Radon transform to determine particle peak velocities. Oliver Welzel, Daniel Boening, Armin Stroebel, Udo Reulbach, Jurgen Klingauf, Johannes Kornhuber, and Teja Wolfgang Groemer (2009) investigated axonal transport using kymograph column cross- and auto-correlation.

A promising tool for disease diagnostics and genomics is optical mapping using direct imaging of individual DNA molecules stretched in nanochannels with sequence-specific fluorescent tagging. Thermal mobility of the DNA during imaging is a key challenge for this technology; it blurs fluorescent patterns along the DNA, resulting in information loss.

Correcting for this effect (a process known as kymograph alignment) is a common preprocessing step in nano channel-based optical mapping workflows; a highly efficient pattern recognition algorithm has been developed

to accomplish this (Charleston Noble, Adam N. Nilsson1, Camilla Freitag, Jason P. Beech, Jonas O. Tegenfeldt, and Tobias Ambjörnsson, 2015).

Kymograph Temporal High Resolution on Neurofilament Transport Kinetics

Neurofilaments, also known as nerve cell intermediate filaments, are space-filling cytoskeletal polymers that contribute to axon cross-sectional area expansion and hence boost axonal conduction velocity (Hoffman, 1995). Neurofilaments are axonal transport payloads in addition to their structural function. They vary from membranous payloads in that they are protein polymers with a width of only 10 nm but a length of many micrometers (Brown, 2003, 2014).

In the 1970s, radioisotopic pulse-labeling studies in laboratory animals revealed axonal transport of neurofilament proteins (Hoffman and Lasek 1975; Lasek, Garner, & Brady, 1984; Brown 2016). Radiolabeled neurofilament proteins produced in neuronal cell bodies were found to travel along axons at 0.1-2mm at day 21 (Lasek, Paggi, & Katz, 1993).

More recently, fluorescent neurofilament fusion proteins have been shown to move in the form of formed neurofilament polymers in time-lapse live-cell imaging of cultured nerve cells. These motions are not only much faster than anticipated but also uncommon and bidirectional (Roy et al., 2000; Uchida and Brown, 2004;Wang and Brown, 2001; Wang, Ho, Sun, Liem, & Brown, 2000; Yan and Brown, 2005; Yan, Jensen, & Brown, 2007). The reason for the apparent discrepancy between pulse-labeling and live-imaging studies can be attributed to the sluggish average velocity of neurofilaments, which are primarily immobile (Brown, 2000).

A temporal average of rapid movements interspersed with extended pauses accounts for the slow pace of neurofilament transport over extended periods; the movement is quick for seconds but slow for hours or days (Brown, Wang, & Jung, 2005; Craciun, Brown, & Fried man, 2005; Jung and Brown 2009; Li, Jung, & Brown, 2012).

Microtubules are the tracks for neurofilament movement, and microtubule motor proteins propel the motions (Francis, Roy, Brady, & Black, 2005; Prahlad, Helfand, Langford, Vale, & Goldman, 2000; Shah, Flanagan, Janmey, & Leterrier, 2000). Although the movements are bidirectional, anterograde movements predominate. He et al., 2005; Helfand, Loomis, Yoon, & Goldman, 2003; Shah et al., 2000; Uchida, Alami, & Brown, 2009; Wagner et al., 2004) appear to drive retrograde movements, while kinesin-1 appears to promote anterograde movements.

Nevertheless, there are still a lot of unanswered questions and an uncertain connection between these motors. For instance, what controls the length and frequency of pauses, how many motors are needed to move a single neurofilament, how motors interact to control directionality and reversals in neurofilaments, and how neurofilament length is affected by the kinetics of neurofilament movement? The fact that neurofilaments are macromolecular assemblies with diffraction limits significantly lower than those of light microscopes presents a significant obstacle in addressing these problems (Uchida, Monsma, Fenn, & Brown, 2016).

Previously, Daniel, Fenn, Brown, Johnson, Peng, and Jung (2017) used relatively long exposures (1 s) and time-lapse imaging with long time intervals (4 or 5 s) to capture enough signal and optimize the length of our movies while

limiting photo bleaching. While low temporal resolution research revealed a lot about the dynamics of neurofilament transport, higher temporal resolution is required to study questions about motor interaction and regulation.

Daniel et al. (2017) overcame this by imaging neurofilament movement at video rates, taking advantage of the increased speed and sensitivity of modern Electron Multiplying Charge-Coupled Devices (EMCCD) cameras.

This enhanced frame rate allowed for kymograph analysis of neurofilament movement with a >100-fold increase in temporal resolution. To analyse this data, Daniel et al. used edge detection to characterize the filament end trajectories and a novel computational filtering approach to automatically identify runs and stops in the pixelated and noisy traces. Daniel, Fenn, Brown, Johnson, Peng, and Jung (2017) used kymograph analysis with high temporal resolution to find novel characteristics of neurofilament transport kinetics.

Negative Temperature Coefficient Thermistors

NTC is an abbreviation for Negative Temperature Coefficient, which implies that as resistance decreases, temperature also increases. Its temperature sensitivity coefficient is about five times higher than that of silicon temperature sensors as shown in Figure 22. The temperature sensivity of NTCs is also ten times higher than the resistance temperature detectors (RTDs). They usually operate within a temperature range of -50 to +150 ^{o}C. The non-linearity of NTC with resistance to temperature relationship poses a significant challenge as shown in Figure 23 when using analogue circuits to accurately measure temperature. Rapid development of digital circuits (microcontrollers) have resolved the problem with the help of equation 1-3.

Figure 22: Thermistor sensor head

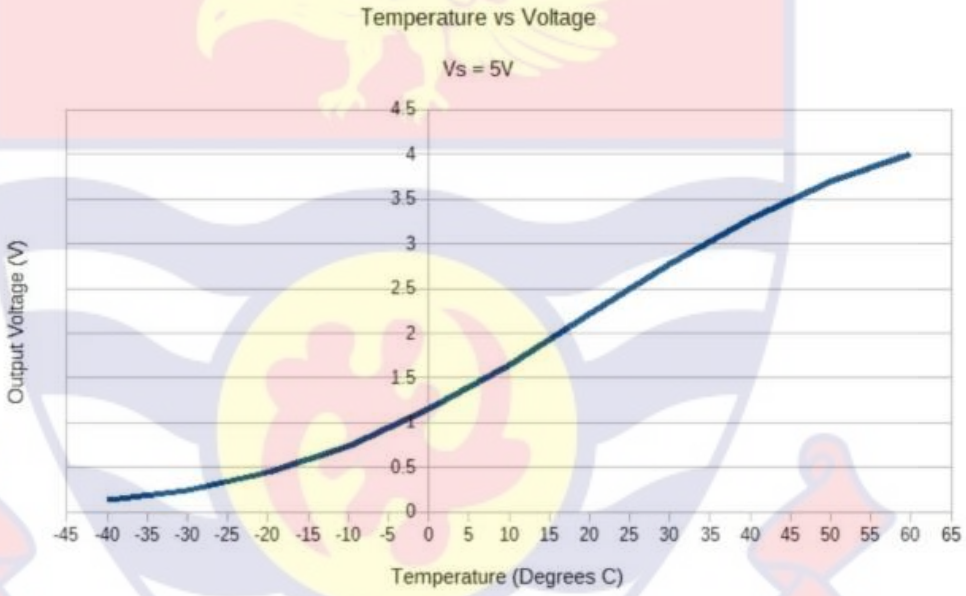

Figure 23: NTC temperature verses voltage curve (www.jameco.com, 2024).

First-Order Approximation

The first-order approximation, which is the most straightforward to apply, states that:

$$\Delta R = k\Delta T \qquad (1)$$

Where k represents the negative temperature coefficient, T represents the temperature difference, and R represents the resistance change produced by the temperature change. This first-order approximation is only valid for a narrow

temperature range and can only be used when k is practically constant throughout (eepower.com, 2023).

Beta Formula

Another equation yields acceptable results, with an accuracy of 1°C over the temperature range of 0°C to +100°C. It is determined by a single material constant that is measurable (eepower.com, 2023).

The equation is as follows:

$$R(T) = R(T_O)e^{\beta \frac{1}{T} - \frac{1}{T_O}} \quad (2)$$

Where R(T) is the resistance at temperature T in Kelvin and R(T0) is a temperature T0 reference point. The Beta formula necessitates two-point calibration and is often only accurate to 5°C across the whole usable range of the NTC thermistor.

Steinhart-Hart equation

The Steinhart-Hart formula, published in 1968, is the best known approximation to date:

$$T = \frac{1}{A+B(lnR)+C(lnR)^3} \quad (3)$$

Where:

Where A, B, and C are empirically determined coefficients, and ln R is the natural logarithm of resistance at temperature T in Kelvin. The coefficients are frequently given by thermistor vendors as part of the datasheet. The Steinhart-Hart formula is frequently accurate to 0.15°C for the temperature range of -50°C to +150°C. If greater precision is required, the temperature range must be reduced, and accuracy of better than 0.01°C over the temperature range of 0°C to +100°C is achievable (2023, eepower.com).

Choosing the Right Approximation

The method for calculating temperature from resistance data must be selected based on available processing power as well as real tolerance requirements. In certain circumstances, a first-order approximation is adequate, whereas in others, even the Steinhart-Hart equation is insufficient, and the thermistor must be calibrated point by point, necessitating a large number of measurements and the building of a lookup table (eepower.com, 2023).

Control of Muscle Tension

A muscle's force is related to its length and shortening velocity. Muscles generate the most force when they are at their resting (ideal) length and the least amount of force when they are shortened or stretched relative to their resting length, according to the force-length link. The force-velocity relationship demonstrates that the velocity and force of muscular contraction influence the power produced, with an optimum power output occurring at one-third of maximum velocity (Alwaz, 2021).

Force-Length Relationship

The overlap between sarcomere length and muscle force as governed by actin and myosin. Power (equation 1-5) is sometimes easier to explain in terms of constant force (F) acting on an object moving at constant velocity, v. If F is the force acting on the body (tissue) through displacement Δd then work done Δw will be:

$$\Delta w = F.\Delta d \tag{4}$$

The average power is given by:

$$P_{av} = \frac{\Delta w}{\Delta t} \tag{5}$$

$$P_{av} = F.\frac{\Delta d}{\Delta t} \tag{6}$$

$$\text{But } \frac{\Delta d}{\Delta t} = v_{av} = Average\ velocity \quad (7)$$

Therefore, average power:

$$P_{av} = F.v_{av} \quad (8)$$

As a result, the product of applied force and average velocity of the body yields the average power.

If the force acts at angle **θ** to the tissue, the tissue displacement then:

$$P = Fv\cos\theta \quad (9)$$

Equation (5) expresses the relationship between power, force, and velocity.

For rotational motion,

Work = torque x angular displacement

P = W/t = (Torque x angle of displacement) / time

Power, P = Torque x angular velocity.

Load Regulation

Load regulation controls how much the output voltage changes throughout a certain range of load current values, typically from no load (NL) to full load (FL). It is commonly stated as a percentage and may be calculated using the formula in equation 10:

$$\text{Load regulation} = \left(\frac{V_{NL}-V_{FL}}{V_{FL}}\right)100\% \quad (10)$$

where Voltage No Load (VNL) is the output voltage when no load is applied and Voltage Full Load (VFL) is the output voltage when full (maximum) load is applied.

Voltage divider formula.

$$V_{out} = V_{in}\frac{(Rt)}{(R+Rt)} \quad (11)$$

Where:

Rt is the resistance of the thermistor (Rt), and R denotes a 10k ohm resistor.

The speed of the kymograph can be determined by equation 12.

$$\text{Speed} = \frac{distance\ (meters)}{time\ (second)} \qquad (12)$$

Muscle Force Generation

A muscle's force is related to its length and shortening velocity. These two fundamental features limit several essential biomechanical traits, such as running speed, strength, and jumping distance (qsstudy.com, 2022).

Chapter Summary

The scholarly articles and other relevant information used in this chapter focused on generation of kymograph, computerized kymograph systems, analogue and digital kymographs, and the uses of kymograph. However, none of the information retrieved focused on the identification of novel materials to make kymograph production more cost-effective and easily accessible.

CHAPTER THREE

MATERIALS AND METHODS

Introduction

This chapter presents electronic circuit designs and simulations, assembling of components and soldering, processes for detection and measurement of electrical signals, and procedure for data acquisition. The first section covered the use of Proteus and Multisim software for circuit designs, simulations, and engineering drawings with CorelDraw.

The second part presents computer programming, using C++ in Arduino IDE environment, collections and use of suitable materials; experimental methods and procedure for construction of chassis, assembling, soldering of different components, data acquisition involving the use of test instrument (multimeter).

Design of Kymograph

The design (Figure 24) and flowchart (Figure 25) of the kymograph depict the various processes and the computer algorithm used in the design and the implementation of the digital kymograph and the organ bath. The flowchart gives a functional perspective of a system and shows the connections between its many components.

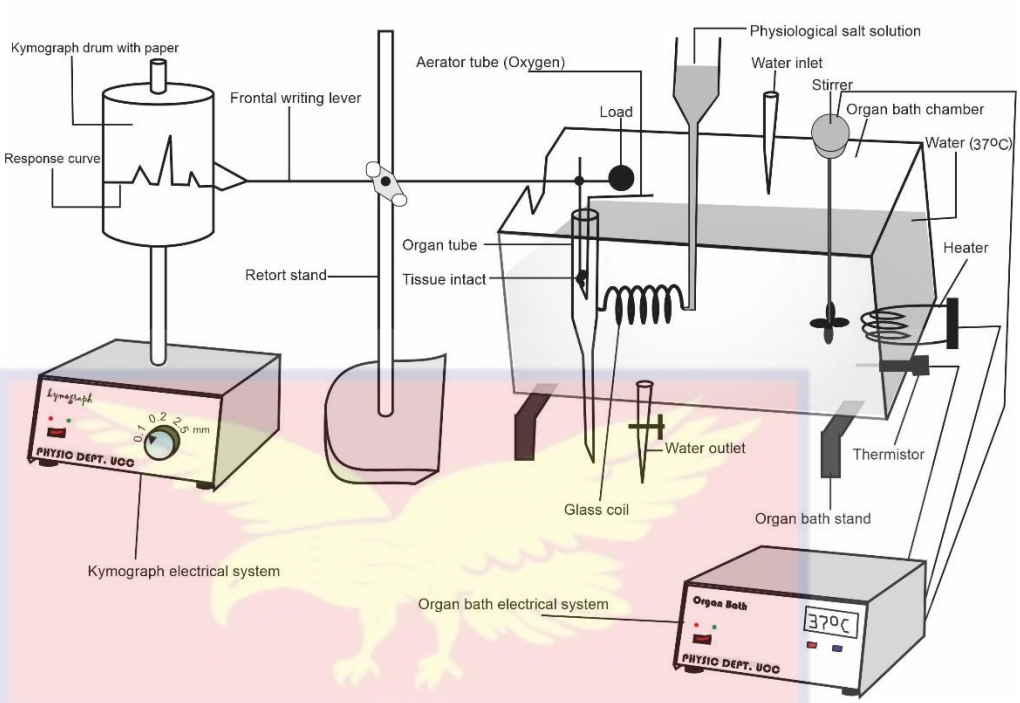

Figure 24: Schematic diagram of the kymograph and organ bath using CorelDraw 23.1.0.389 (Author's design, 2022)

Figure 25 shows the flowchart used in the construction of the digital kymograph. The flowchart was followed to design and implement the digital kymograph. The Arduino UNO R3, which is synchronized with the stepper and the stepper motor driver, was chosen as the microcontroller. The stepper motor and shaft were connected to the drum, and the link made sure the drum turned in a clockwise direction.

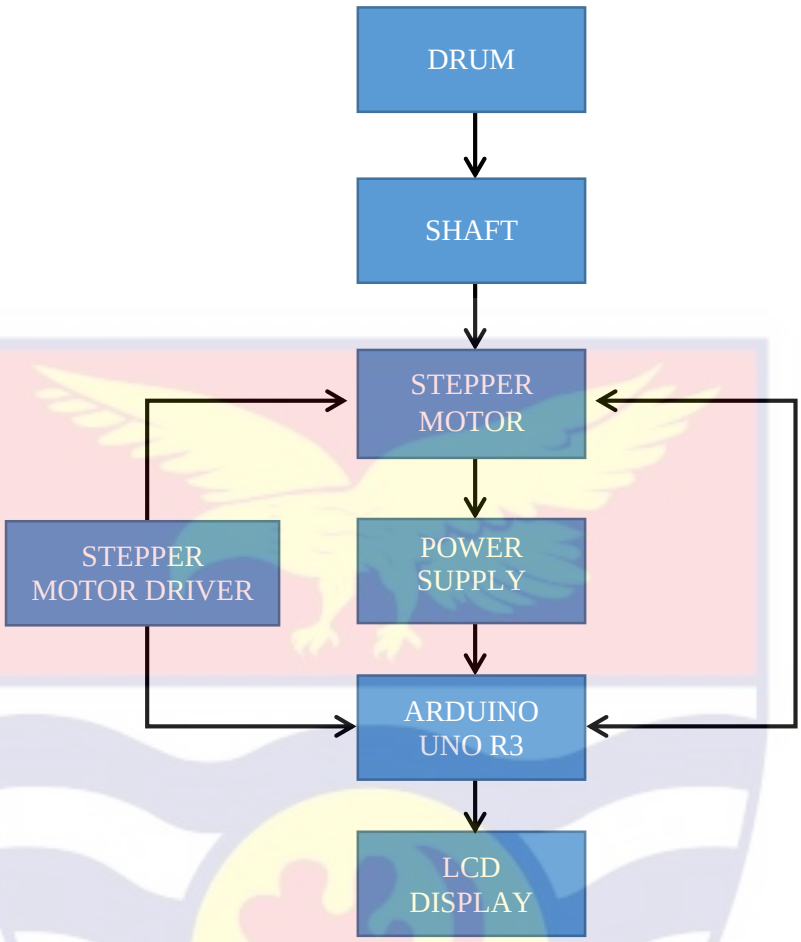

Figure 25: Kymograph flow chart diagram

The components used in the design and building of the digital kymograph are shown in Table 1.

Table 1: Kymograph components and materials

Component	Quantity
Relay 5 V	1
Arduino Uno R3	1
Arduino AT mega 2560	1
LCD (JHD162A)	1
Strip board	1
Bread board	1
Stepper motor NEMA 17	1
Stepper motor motor driver	1
Jumper wires	1
Potentiometer 10 K	2
Switches	3

Table 1: Continued	
DC adaptor	1
Galvanised steel sheet	60 cm
Aluminium bowls (unpolished)	2
Control knob	1
Carbon fibre rod	1
Rubber bushing	2
Type B USB cable	1
Stepper motor driver L298N	1
Stepper motor driver (ULN2003)	1

Arduino UNO R3

An Arduino UNO R3 (Figure 26 and Figure 27) with a small microcontroller board and a universal serial bus (USB) was plug to a computer and a number of connections were made to its sockets. Some of the connections include wires, fixed and variable resistor, LCD, relay and stepper motor driver. It was powered by 12 V. It was first programmed via the use of a computer and then disconnected to work independently to regulate the kymograph.

Arduino UNO R3 Board

Figure 26: Arduino UNO R3 development board

Arduino Uno R3 Pin Diagram

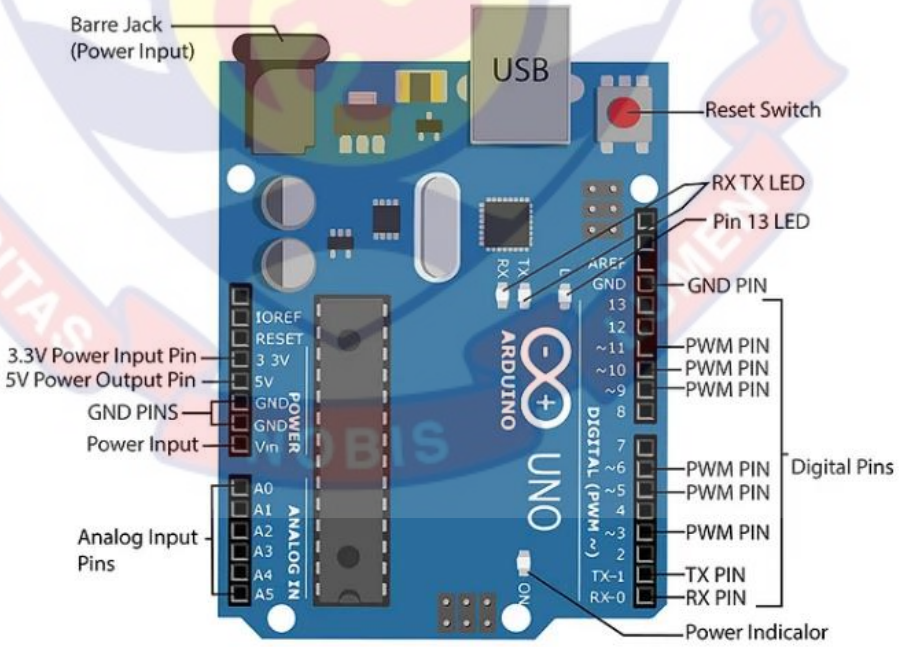

Figure 27: Arduino UNO R3 development board pin diagram

Description of Arduino UNO R3

The Arduino Uno R3 is an open source microcontroller board based on the ATmega 328 chip. This Board has 14 digital input/output pins, 6 analog input pins, Onboard 16 MHz ceramic resonator, Port for USB connection, Onboard DC power jack, An ICSP header and a microcontroller reset button. It contains everything needed to support the microcontroller. Using the board is also very easy, simply connect it to a computer with a USB cable or power it with DC adapter or battery to get started.

The Uno differs from all preceding boards in that it does not use the FTDI USB-to-serial driver chip. Instead, it features the Atmega16U2 and Atmega8U2 up to version R2) programmed as a USB-to-serial converter. While the Arduino UNO can be powered via the USB connection, its power source was connected externally in this research.

External (non-USB) power can come either from an AC-to-DC adapter (wall-wart) or battery. The adapter can be connected by plugging a 2.1mm center-positive plug into the board's power jack. Also leads from a battery can be inserted in the GND and Vin pin headers of the Power connector. The board can operate on an external supply of 6 to 20 volts. If supplied with less than 7V, however, the 5V pin may supply less than five volts and the board may be unstable. If using more than 12V, the voltage regulator may overheat and damage the board. The recommended range is 5v to 12v for Arduino Uno.

Arduino AT mega 2560 Pin out

The Arduino ATmega 2560 as shown in Figure 28 uses a processor with more input output pins. It was used in this research to develop the first prototype

of the digital kymograph and the organ bath. It has a surface mount chip that is fixed permanently to the board. Unlike Arduino Uno the microcontroller on the ATmega 2560 cannot be replaced, if the processor is accidentally damaged.

Figure 28: Arduino AT mega 2560 Pin Out

The extra connectors are arranged at the end of the board. Extra features provided by the Mega include, 54 input/output pins, 128KB of flash memory for storing sketches and it has fixed data, 8KB of RAM and 4KB of EEPROM as compared to the Uno's 32KB.

NEMA 17 Stepper Motor

NEMA 17 stepper motor (Figure 28) is a bipolar stepper motor which is 42x42x48 mm and has a step angle of 1.8 degrees **(**200 steps/revolution) with a 1.7 x 1.7 inch faceplate. It contains four wires, with a holding torque of 44 Ncm (62.3 oz.in) and a draw of 1.68A per phase. It has a recommended driving voltage of 12-24V. The NEMA 17 stepper motor can be synchronised with a motor driver and an Arduino as shown in Figure 30.

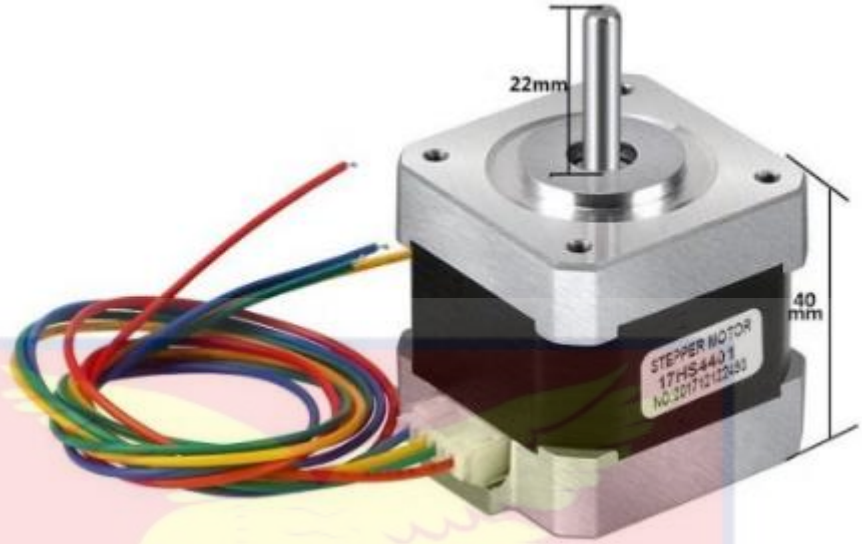

Figure 29: NEMA 17 Stepper Motor

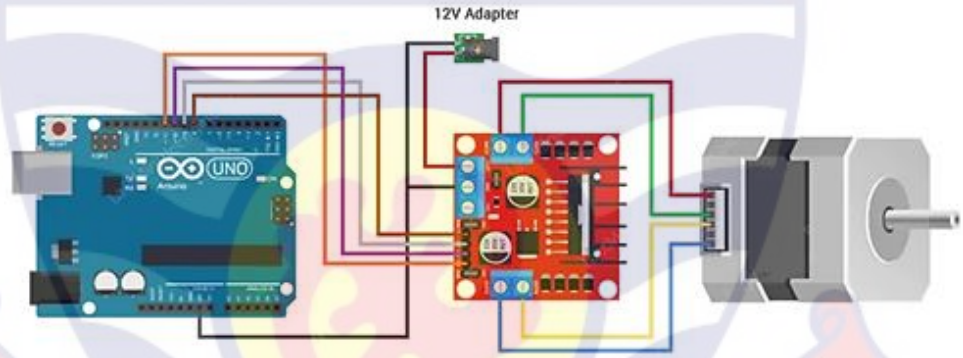

Figure 30: Wiring NEMA 17 Stepper Motor with L298N and Arduino

The Stepper Motor Driver (L298N)

The Motor Driver shown in Figure 31 and Figure 32 is an essential device that provides the required voltage and current to a stepper motor so that it gets a smooth operation. In this research, the H-Bridge motor driver (L298N) was used to smoothly regulate the speed of the kymograph. When a stepper motor driver receives a pulse input, it can convert it into an angular displacement signal. Stepper drivers cause stepper motors to rotate in a predetermined direction at a step angle. The displacement is determined by the pulse quantity provided by the controller, and the motor speed is limited to the

pulse frequency. A stepper motor plus a stepper driver make up a stepper system.

A stepper system's performance is determined by both the stepper driver and the motor. The twin H-Bridge motor driver L298N as shown in Figure 31, enables simultaneous control of two DC motors' speeds and directions. DC motors with voltages between 5 and 35V and peak currents up to 2A can be driven by this module. Single 2-phase, single 4-phase, or two DC motors can be driven using a dual-channel L298N H-bridge driver.

Inductive loads, including relays, solenoids, DC, and stepping motors, can be driven by the driver between 5 and 35 volts using typical TTL logic level inputs. Reliability is further enhanced by the use of diodes with freewheeling protection and large-capacity filter capacitors.

Figure 31: L298N Dual H Bridge PWM Stepper Motor Drive Controller Board Module

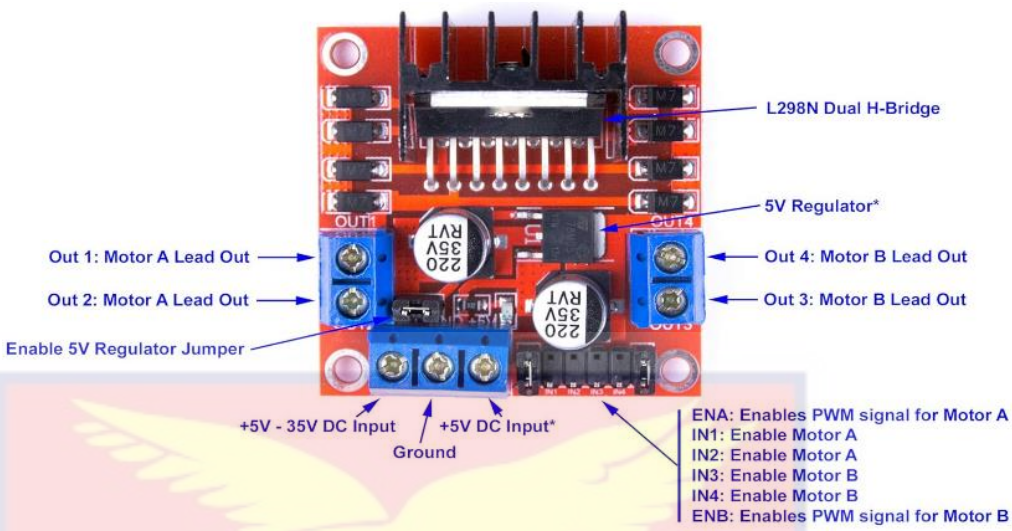

Figure 32: L298N Dual H Bridge PWM Stepper Motor Drive Controller Board Module input and output connections

16x2 Liquid Crystal Display (LCD)

The JHD162A 16×2 LCD as shown in Figure 33 is a liquid crystal display that can show 16 characters in each of its two rows, providing a total of 32 characters of information. It's commonly used to display alphanumeric information in various electronic devices. The LCD consists of 16 rows and 2 columns of 5×7 or 5×8 LCD dot matrices. LCD is available in a 16 pin package with back light ,contrast adjustment function and each dot matrix has 5×8 dot resolution. The JHD162A has two built in registers namely data register and command register. Data register is for placing the data to be displayed and the command register is to place the commands. The 16×2 LCD module has a set of commands each meant for doing a particular job with the display. In this research, it was synchronised with an Arduino to provide information on the operation of the kymograph.

LCD modules are an essential part of many embedded system designs that employ Arduino to improve the user interface of the system. All that is

needed to assemble the circuit is an Arduino board, a breadboard, jumper wires, and a 16x2 character LCD display.

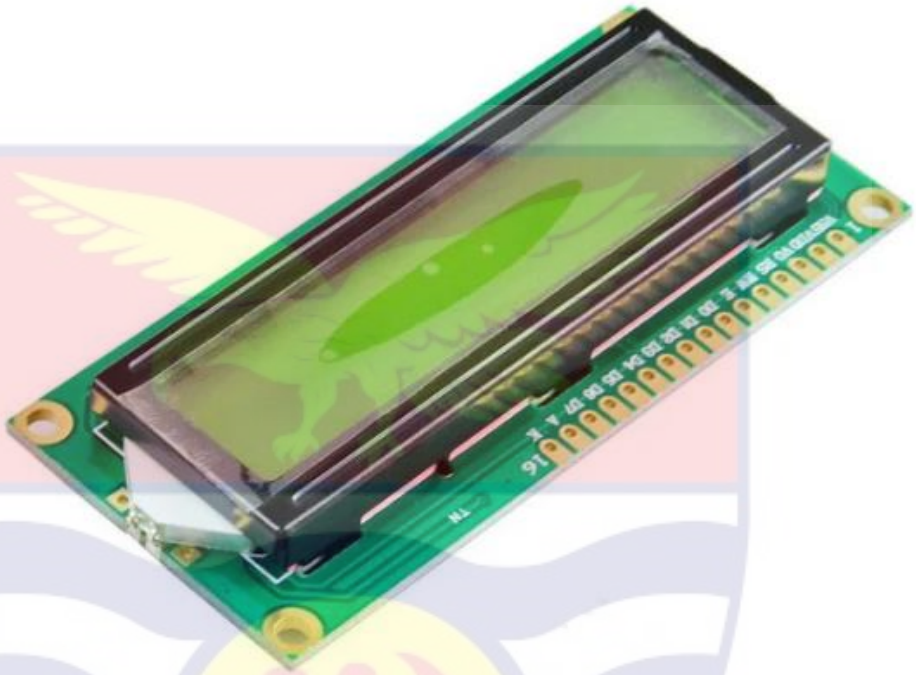

Figure 33: Interfacing 16×2 LCD display to an Arduino board

JHD162A 16×2 LCD RS (Register Select)

A 16X2 LCD has two registers (Figure 34), namely, command and data. The register select is used to switch from one register to other. RS=0 for the command register, whereas RS=1 for the data register. The command register stores the command instructions given to the LCD. A command is an instruction given to an LCD to do a predefined task such as initializing it, clearing its screen, setting the cursor position and controlling display. Processing for commands happens in the command register. The data register stores the data to be displayed on the LCD. The data is the ASCII value of the character to be displayed on the LCD. When data is sent to LCD, it goes to the data register and is processed there. When RS=1, the data register is selected. Figure 34 shows

the pin connections of JHD162A 16×2 LCD. Figure 35 also shows the LCD connections with Arduino and external components.

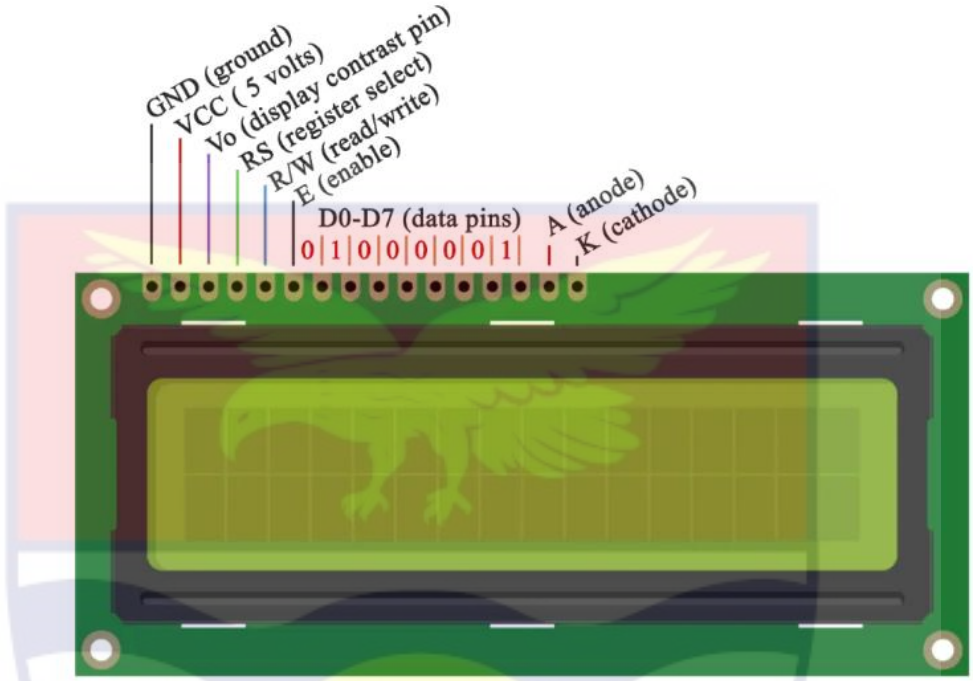

Figure 34: JHD162A 16×2 LCD pin diagram

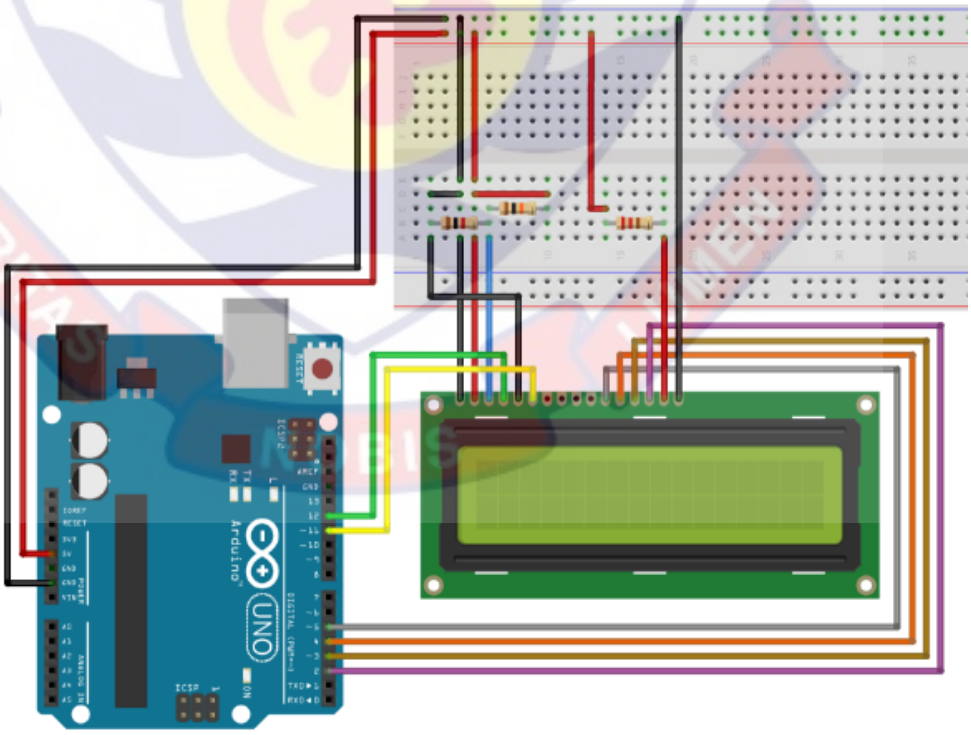

Figure *35:* JHD162A 16×2 LCD interfaced with an Arduino board

Figure 36 shows the design of the digital kymograph. Physical assembling of the components for the kymograph were implemented after the simulation. Figures 36-54 show the construction processes of the kymograph. A galvanized steel metal plate was cut into specific size and then molded into shape to form the base. Arc welding was used to piece the various parts together. This ensures a strong bond among the various parts used in the construction of the base of the kymograph.

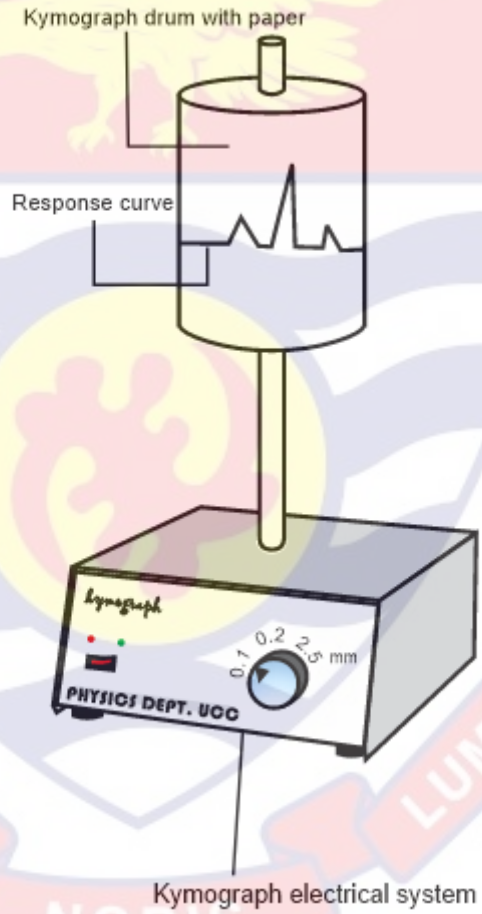

Figure 36: Kymograph electrical system and drum (Author's design, 2022)

The internal components were fixed in the base frame and the control panel and other knobs were attached to the base frame. The base is 24 cm x 21cm x 13 cm in size. The height of the shaft is 35 cm. The drum height is 14 cm and the diameter is 20.5 cm. The height of the kymograph is 40 cm. The

weight of drum is 0.56 kg. The material used for the shaft is carbon fiber (Figure 37). This is the first time a carbon fiber has been used for kymograph construction and has been proved to be very effective. Carbon fiber materials are used to build aircraft and spacecraft parts, race car bodies, golf club shafts, bicycle frames, fishing rods, vehicle springs, sailboat masts, and a variety of other components that require light weight and great strength. Due to its strength and light weight, carbon fiber can help to extend the life of a stepper motor. Carbon fiber is also extremely corrosion resistant.

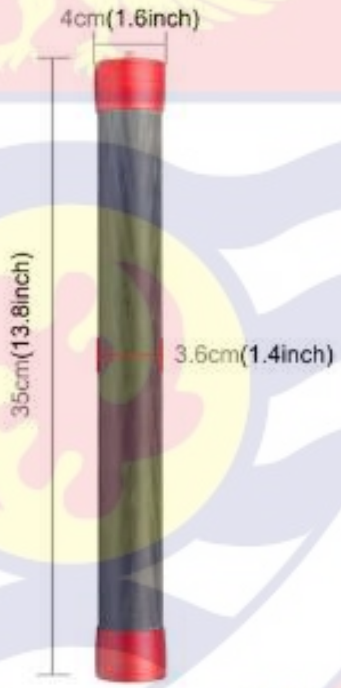

Figure 37: Carbon fiber rod for the kymograph shaft

Construction of Digital Kymograph

The base of the digital kymograph is made up of galvanised steel, which is a robust metal that is also resistant to corrosion. Highly resistant to corrosion materials were used for the construction of the kymograph. This makes it an effective instrument to be used in all research laboratories including corrosion prone areas. The base of the digital kymograph was sprayed with an oil paint as

shown in Figure 38, which protects the surface of the base of the kymograph from corrosion.

Figure 38: Sprayed kymograph base

Circuit designs and simulation for the digital kymograph were done in Proteus 8.7 SP3 Professional as shown in Figure 39 to create and verify the circuit boards; this will ensure that the circuit boards and other peripheral components are practicable.

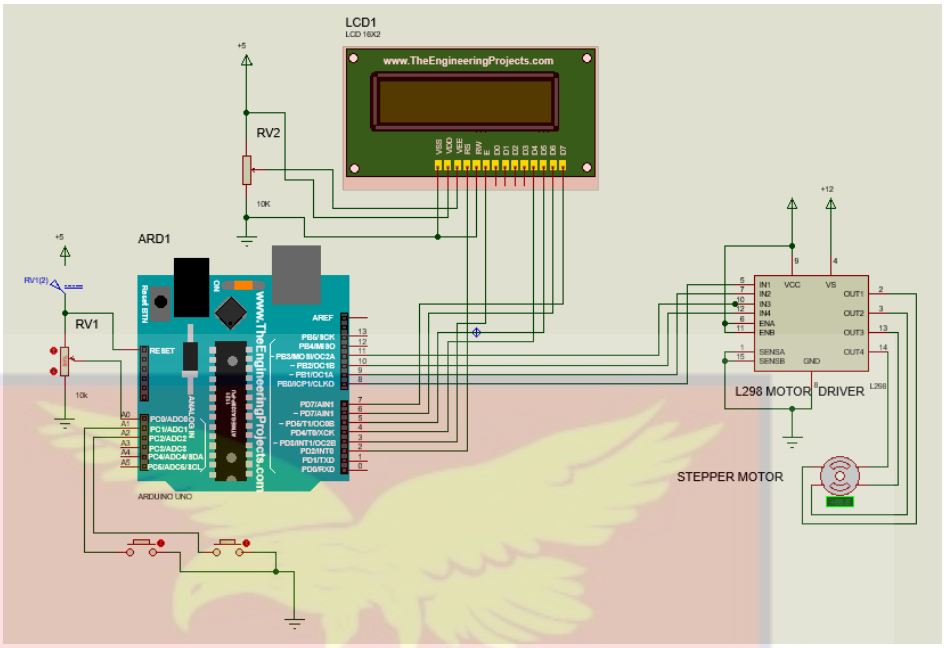

Figure 39: NEMA 17 Stepper Motor with stepper motor driver (L298N) and Arduino in Proteus 8.7 SP3 Professional

The flow chart for the programming as shown in Figure 40 was designed before the sketches (codes) were developed and uploaded onto the microcontroller (Arduino UNO R3), Figure 41.

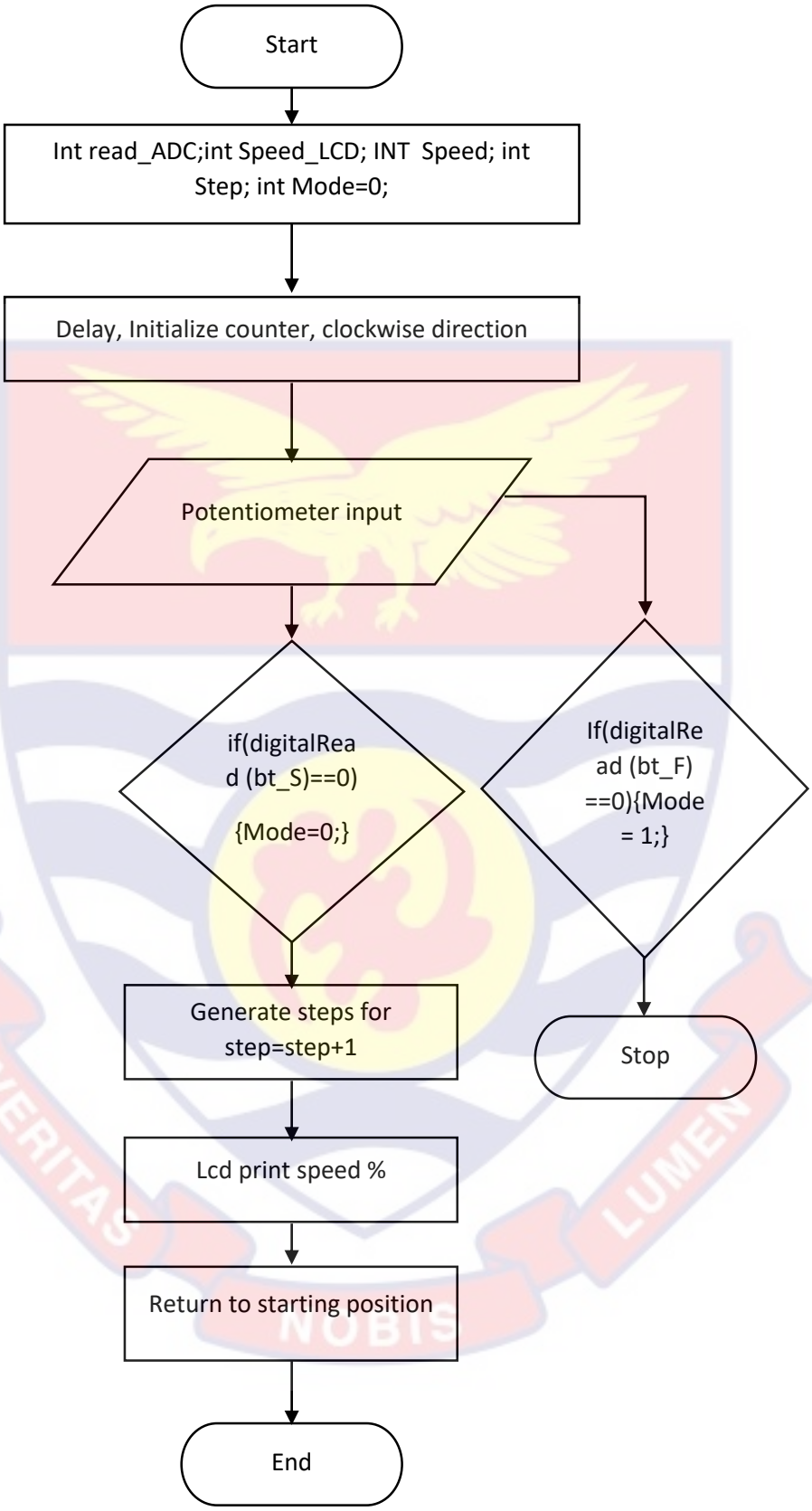

Figure 40: Programming flow chart for the development of the kymograph

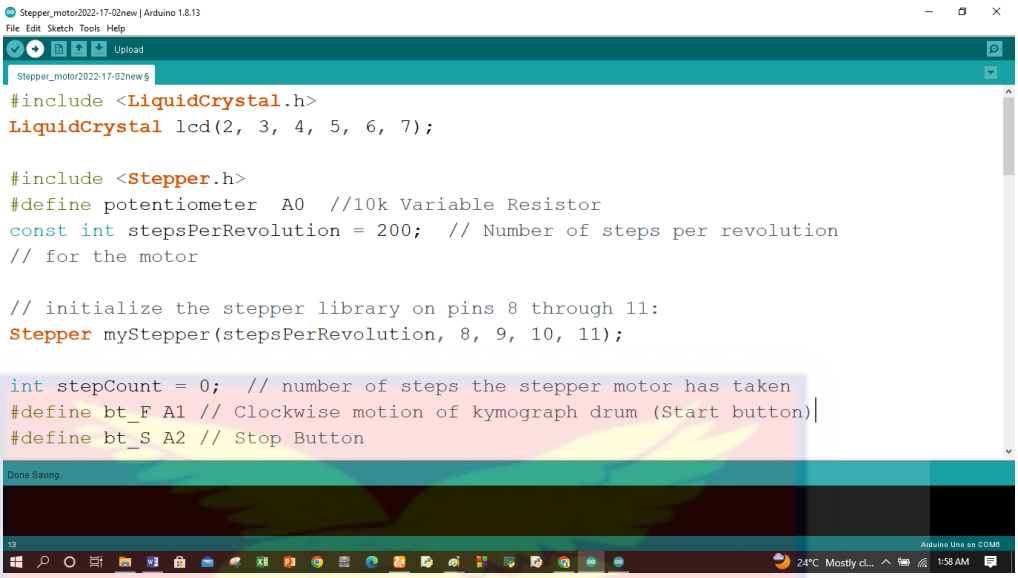

Figure 41: C++ program (sketches) in Arduino IDE 1.8.13 developed for the kymograph

Arduino codes for kymograph

The codes below were upload onto a microcontroller to regulate and direct the movement of the stepper motor and the kymograph drum. C++ was used to program the stepper motor and the driver in Arduino IDE as shown in Figure 41.

```
#include<LiquidCrystal.h>
LiquidCrystal lcd(2,3,4,5,6,7);

#include <Stepper.h>
#define potentiometer  A0  //10k Variable Resistor
const int stepsPerRevolution = 200;  // number of steps per revolution for the motor

// initialize the stepper library on pins 8 through 11:
Stepper myStepper(stepsPerRevolution, 8, 9, 10, 11);

int stepCount = 0;  // number of steps the motor has taken
#define bt_F A1 // Clockwise motion of kymograph
#define bt_S A2 // Stop Button

int read_ADC;
```

```
int Speed_LCD;
int Speed;
int Step;
int Mode=0;

void setup() {
 pinMode(potentiometer, INPUT); // declare potentiometer as input

pinMode(bt_F, INPUT_PULLUP); // declare bt_F as input
pinMode(bt_S, INPUT_PULLUP); // declare bt_S as input

lcd.begin(16,2);
lcd.setCursor(0,0);
lcd.print("DIGITAL KYMOGRAPH");
lcd.setCursor(0,1);
lcd.print("OTENG'S PROJECT");
delay(2000); // Waiting for a while
lcd.clear();
}

void loop() {

Speed_LCD = map(read_ADC, 0, 1023, 0, 100);


lcd.setCursor(0,0);
lcd.print("   Speed: ");
lcd.print(Speed_LCD);
lcd.print("%  ");

if(digitalRead (bt_F) == 0){Mode = 1;} //For Clockwise motion of kymograph
if(digitalRead (bt_S) == 0){Mode = 0;} //For Stop
```

Complete Arduino code for the programing of the digital kymograph is show at the appendix A.

Development of Kymograph Electrical System

An external power supply of 12 V was connected to the 12V NEMA 17 bipolar stepper motor. The VS connector was wired with an external 12V power supply. A 5V was supplied to the logic circuitry of the L298N, using the on-

board 5V regulator to derive 5V from the motor power supply, the 5V-EN jumper was unattached.

The enable pin A (ENA) and enable pin B (ENB) jumpers were not disabled; they were left in place to ensure that the motor was always turned on. The L298N module's input pins (IN1, IN2, IN3, and IN4) were linked to the four Arduino digital output pins (8, 9, 10, and 11). The motor's first and second phases were linked to terminal A (OUT1 and OUT2), while the third and fourth phases were attached to terminal B (OUT3 and OUT4). LCD screen was connected to the veroboard such that each pin has its own separate line on the board. A potentiometer was also connected such that the middle terminal was connected to A0 and the other two terminals were connected to ground and 5 V. Each pin has its own separate line on the Arduino board. A 5 V and ground (GND) were connected to liquid crystal display's (LCD's) A and K pins respectively to power the backlight of the LCD.

Pins D4, D5, D6, and D7 were connected to the digital output pins 4, 5, 6, and 7 of the Arduino. The LCD's pins 2 and 3 were connected to the Arduino board's pins Reset (RS) and E, respectively. Pins Write only (RW), VDD, and VEE of the LCD were connected to a potentiometer to adjust the contrast of the LCD.

Single pole single throw (SPST) push buttons were grounded and connected to A1 and A2 of the Arduino analogue inputs. A1 initiates the kymograph process, and A2 terminates it. To control the speed of the kymograph, a 10 K potentiometer was attached to Arduino pin A0. The Arduino board was connected to the PC, and the kymograph program was uploaded to it (Figure 42).

Arduino Code – Controlling NEMA 17 Stepper Motor

The Arduino Integrated Development Environment (IDE) or Arduino Software was installed onto a computer. The software was synchronized with Arduino boards to upload programs. Programs written using Arduino Software (IDE) are called sketches. These sketches are written in the text editor and are saved with the file extension onto the microcontroller on the Arduino board. A sketch (program) was uploaded to Arduino UNO R3 from the Arduino IDE to make the stepper motor spin clockwise.

Proteus design suite software was used with powerful features to rapidly design, simulate and test the kymograph and the organ bath circuit boards before the circuit boards were implemented, as shown in Figure 42.

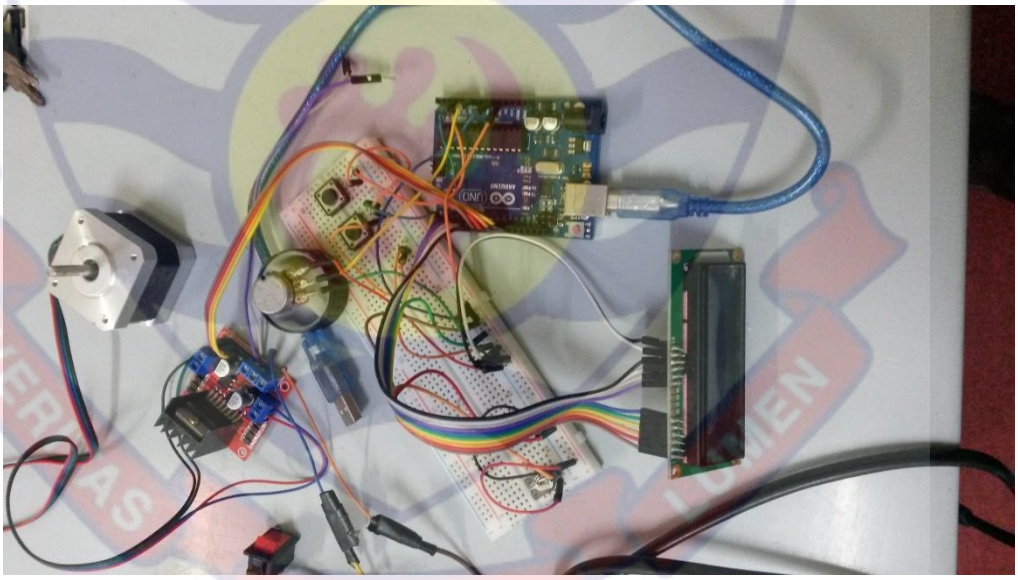

Figure 42: Complete assembly and connection of the various components of the prototype (kymograph)

Design and Simulation of Standby Mode Circuit

The standby mode circuit (Figure 43) contributes to energy conservation and device protection. Standby mode is used to conserve power on a device when it is not in use. It lets the kymograph quickly resume operation when

necessary and conserves energy while not in use. The device uses just 0.25 Watts of electricity when it is in standby mode as shown in Figure 44.

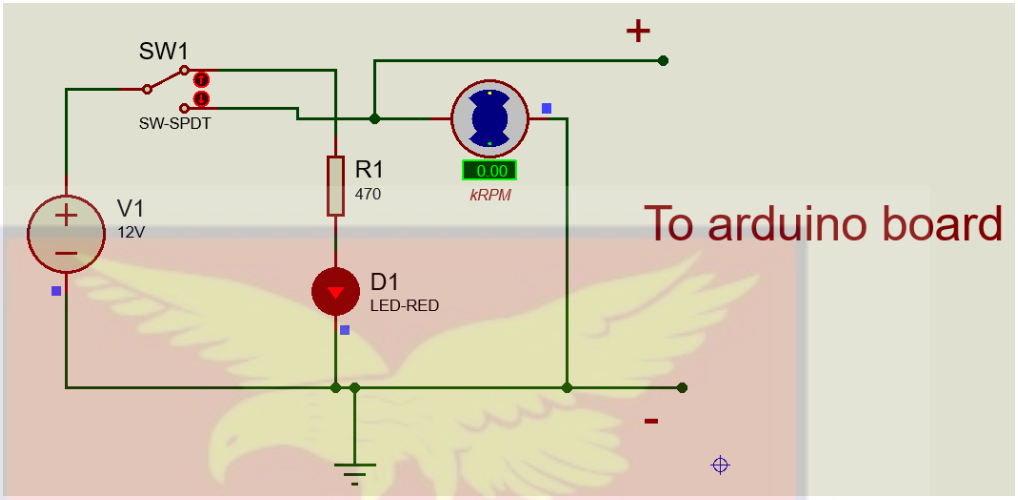

Figure 43: Standby mode circuit diagram

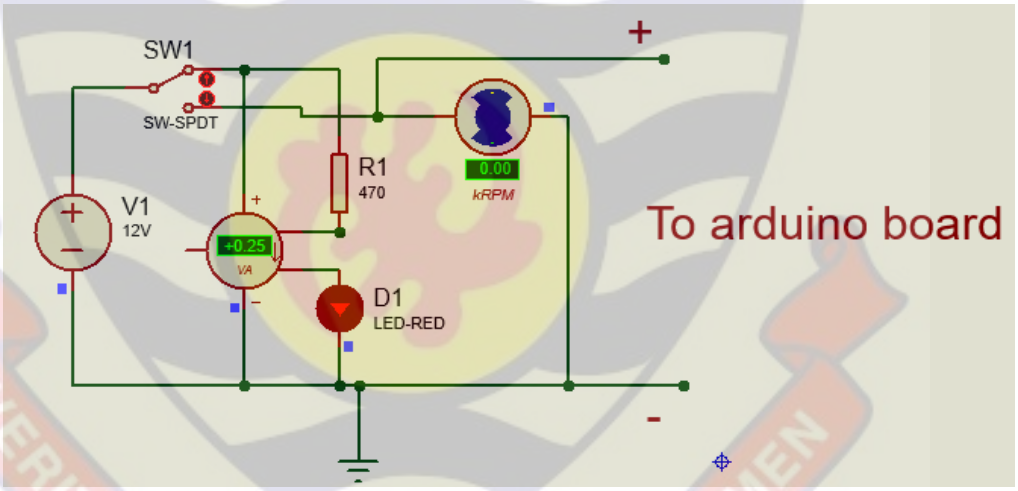

Figure 44: Standby mode circuit diagram with watt meter

Prototype Construction of Kymograph

A prototype was first designed, simulated and constructed, as shown in Figure 45 using plastic drum, Arduino UNO R3, 12 VDC power supply and stepper motor driver (ULN2003). After the prototype was successful, the final design and construction was carried out.

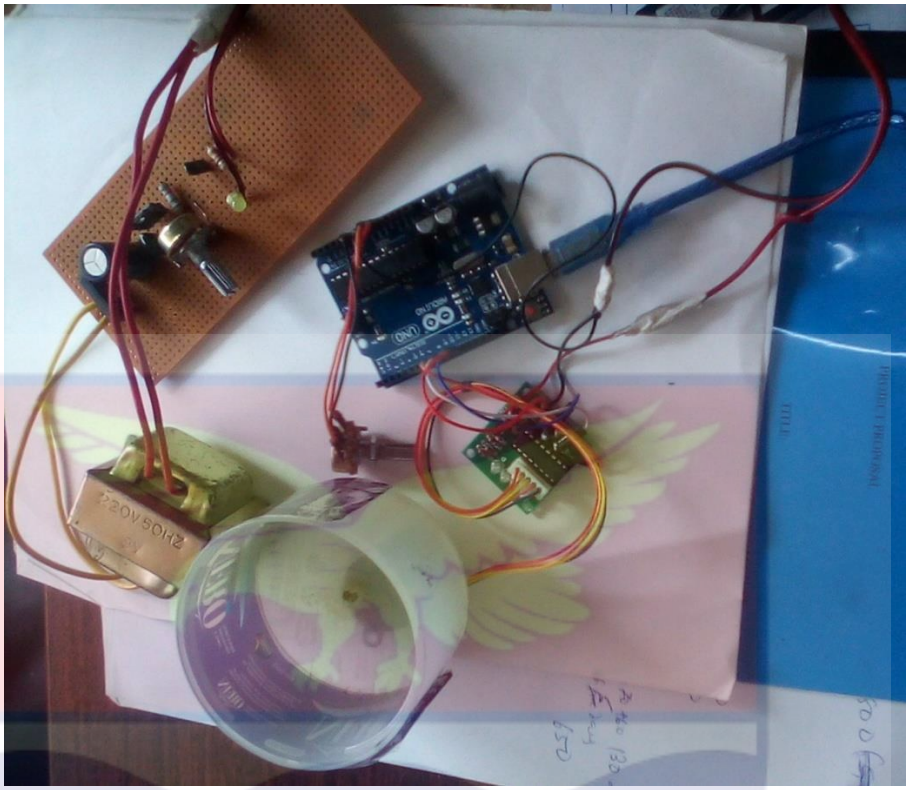

Figure 45: Prototype construction of kymograph with plastic drum, Arduino Uno R3 and 12 DC power supply

Construction of Kymograph Chassis

Anti-slip pads obtained from gas cylinder seals were used to support the base of the kymograph in order to increase safety and also prevent unwanted movement of the digital organ bath and the stepper motor as shown in Figure 46.

.

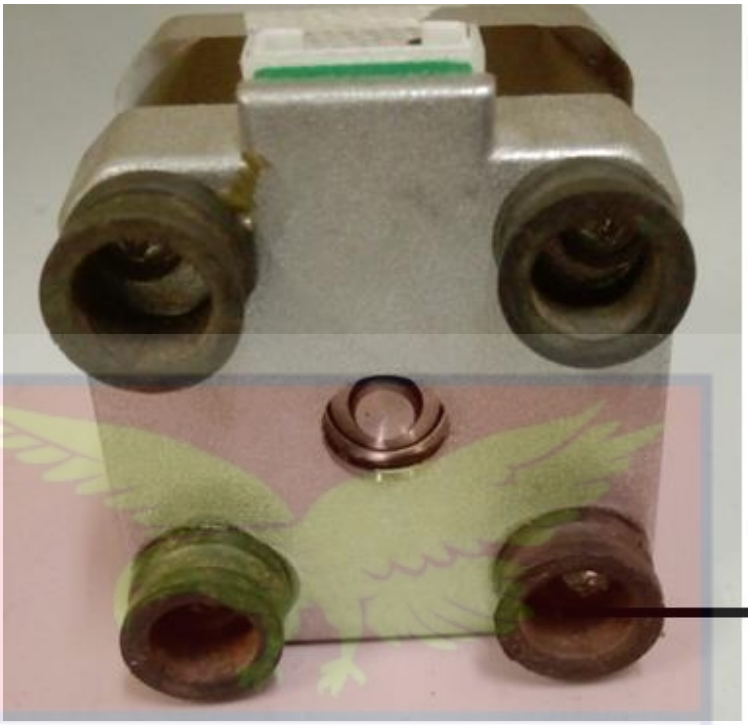

Figure 46: Anti-slip pads for prevention of the movement of the stepper motor

All electrical and electronic circuits for the kymograph were enclosed in the base of the kymograph. Figure 47 shows the electrical and electronic system base and shaft of the kymograph.

Figure 47: Kymograph electrical base system with a carbon shaft

Construction of Kymograph Drum

Two unpolished aluminum bowls as shown in Figure 48 were obtained from aluminum factory in Ghana.

Figure 48: Two aluminum bowls (unpolished), used for the drum

The two bowls were polished and interlocked to form the drum as shown in Figure 49 and 50 for the kymograph. Figure 51(A) and Figure 51(B) show the completion of the setup after the attachment of the aluminium drum.

Figure 49: Bottom view of the polished and interlocked aluminium bowls

Figure 50: Complete assembly of kymograph drum

(A) (B)

Figure 51: *(A)* Complete assembly of kymograph, front and side views. (B) Complete assembly of kymograph, front view

Calibration of Kymograph

The standard speeds of kymographs are measured in millimeters per second. The speeds of kymograph ranges from: 0.12, 0.25, 0.50, 0.75, 1.00, 1.25, 2.50, 0.300 mm/sec. The speed of the designed kymograph was determined in millimeters per second as required and it ranges between 0.25 mm/s to 3.00 mm/s. A pointer fixed to the retort stand, measurement tape and digital start/stop clock were used to determine the speed ranges of the kymograph (Figures 52). Figure 53 shows the final assembly after calibration.

Figure 52: Kymograph calibration

Figure 53: Kymograph final assembly after calibration

Kymograph Vibration Test

To ascertain the stability of the kymograph when the drum is rotating, a vibration test was conducted. A vibrometer, version 1.6.15 was used to determine a possible vibration generated by the kymograph. Modified Mercalli intensity scale of 1-2 MMI was observed which is considered as a very weak vibration. This also means the kymograph is stable. The setup for the vibration test is shown in Figure 54.

Figure 54: Vibration test setup for studying the stability of the kymograph

Power Supply Design and Construction of the organ bath

The components utilized in the building of the dc power supply are shown in Table 2.

Table 2: Electronic Components of organ bath DC power supply

Component	Values
Transformer	12 V
Diodes (1-4)	1N4007
LEDs (1 and 2)	Yellow and Red
Capacitor 1	2200 µF
Capacitor 2	0.1 µF
Capacitor 3	1 µF
Capacitor 4	470 µF
Capacitor 5	470 µF
Power regulator	LM317
Variable resistor (R3)	10 kΩ
Fixed resistor (R2)	1 kΩ
Fixed resistor (R1)	100 Ω
Fixed resistor (R4)	470 Ω

Figure 55 shows the flowchart of the power supply with regulated output which was used in the construction of the DC power supply for powering the organ bath and the kymograph. The flowchart was followed to design and implement the power supply.

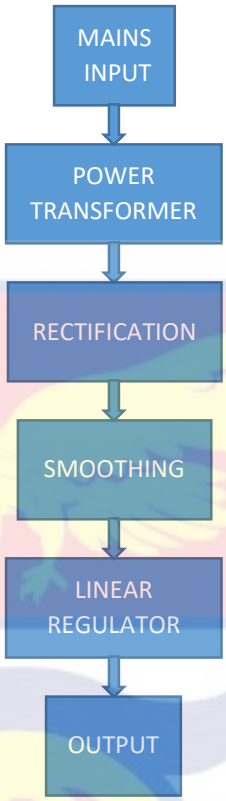

Figure 55: Flow chart for developing the power supply with regulated output for the organ bath and kymograph

Step-down Transformer

Electrical energy can be passively transferred between one or more circuits using a transformer. Any coil in the transformer experiences fluctuating current, which causes the core's magnetic flux to change. This, in turn, causes variations in the electromotive force (EMF) across any other coils wound around the same core. It is possible to transfer electrical energy between two distinct coils without there being a physical or conductive link between the two circuits. The induced voltage effect in any coil caused by a fluctuating magnetic flux surrounding the coil is described by Faraday's law of induction, which was discovered in 1831. AC voltage levels are adjusted with transformers; these transformers are referred to as step-up or step-down types, depending on

whether the voltage level is being increased or decreased. The type of transformer used in this research is a step down transformer (220 V to 12 V), Alternating Current Voltage (ACV) as shown in Figure 56.

Figure 56: 12 V Step down transformer for the development of the electrical system for the organ bath

Full-Wave Power Supply Circuit Construction

All active electronic components used in this study require a steady dc power source, which was provided by a power adaptor or a dc power supply. The power supply designed and constructed converted AC (alternating current) to dc (direct current).

All electronic circuits, including the Arduino board and air pump, are powered by the voltage supplied by a dc source. The voltage was reduced from 220 V to 12 V using a transformer. The transformer modifies alternating current voltages based on the turns ratio between the main and secondary windings.

A full-wave rectifier was developed and connected to the secondary's output voltage with 1N4007 diodes. The rectifier converts the alternating current input voltage to a pulsing direct current voltage. A 2,200 µF filtering capacitor was connected across the rectified output voltage. The filter reduces rectified voltage fluctuations and produces a generally smooth dc voltage.

The circuit included two linear power regulator components, LM317 and LM7805. For fluctuations in the input line voltage or the load, the regulators maintain a constant dc voltage. There are two output voltages on the power supply circuit: 12 V and 5 V. The 12 V was wired to the Arduino board, while the 5 V was wired to the air pump.

Figure 57 is the schematic diagram for the dc power supply. The input signal was sinusoidal and the output was linear (dc) as shown in Figure 58; the unrectified voltage from the power source was 12.2 V and the rectified voltage was 12.3 V (Figure 59). In this study, the dc power supply was used to supply adjustable dc voltage to the organ bath and the microcontroller (Arduino).

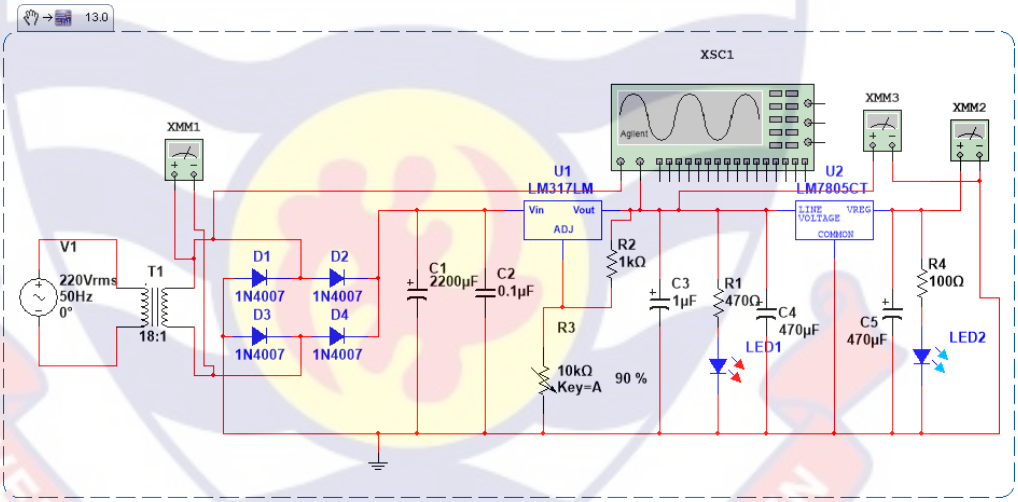

Figure 57: Schematic diagram of dc power supply using Multisim 13.0 for powering organ bath

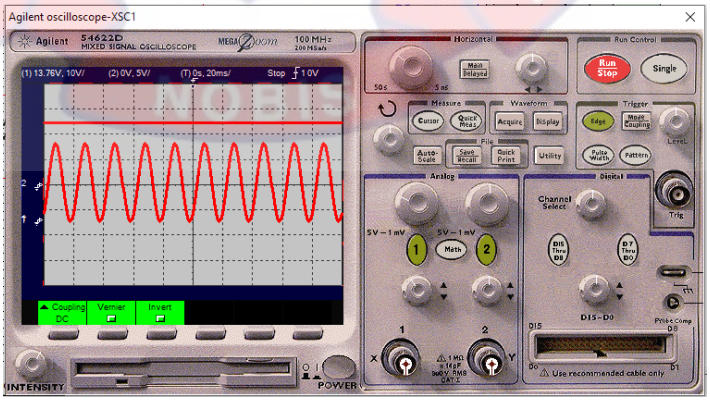

Figure 58: Simulated Cathode Ray Oscilloscope reading the input and output signals

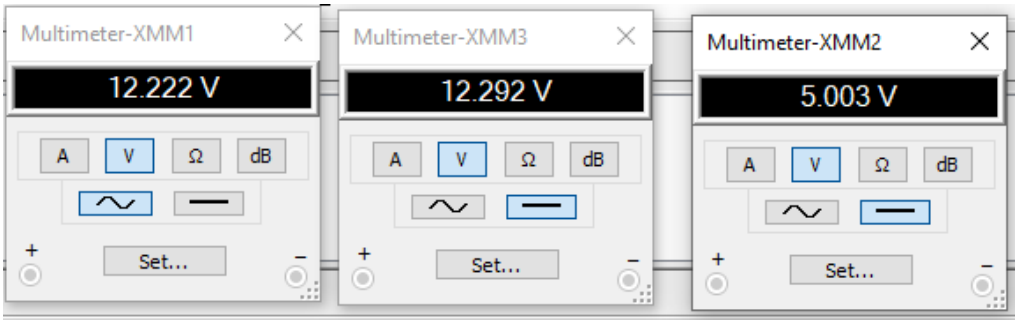

Figure 59: DC power supply schematic diagram output voltages, generated from Multisim, X-MM1 is AC input, X-MM3 is dc output after rectification from LM317 regulator, and X-MM2 is dc out rectification 5 V from LM7805 regulator.

Percent Regulation of the power supply

Without any load, the output voltage of the LM 317 power regulator was 12.3 V. The ouput load voltage from LM 317 power regulator was 12.0 V and the output voltage obtained from 7805 power regulator was 5.2 V, without load. The output voltage obtained from 7805 power regulator with load was 5 V.

The percent regulation is defined as the performance of a voltage regulator experessed as a percentage. It could be in terms of input (line) or load regulation.

The no-load output voltage of the 7805 regulator was 5.1 V, and the full-load output voltage was 5.0 V.

Therefore load regulation is:

Load = 2%

The no-load output voltage of the LM 317 regulator was 12.3 V, and the full load output voltage was 12.0 V.

Therefore load regulation of LM 317= 2.5%

A good power transformer should exhibit a regulation percentage of less than 3% (www.allaboutcircuits.com, 2023). The load regulation obtained in this study was less than 3%, which indicates the efficiency of the power regulator

and the transformer used in the construction of the dc power supply as shown in Figure 60.

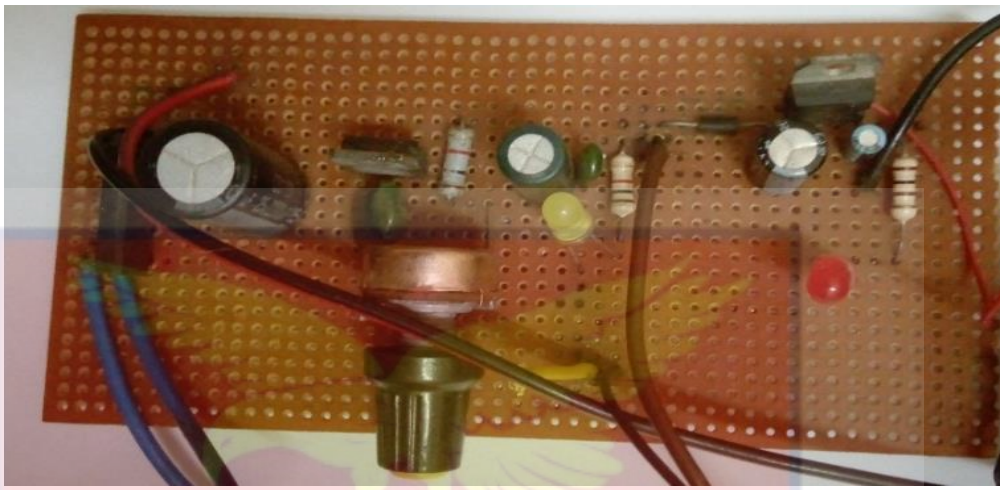

Figure 60: Power supply circuit board containing assembled components

Organ Bath Design and Construction

The components utilized in the design and construction of the organ bath are shown in Table 3.

Table 3: Organ bath components and materials

Component	Quantity
Relay 5 V	1
Arduino Uno R3	1
Arduino AT mega 2560	1
LCD	1
Strip board	1
Bread board	1
Thermistor (NTC), 10K	1
Transistor BC 547	1
Resistor 10 K fixed	3
Variable resistor 10 K	2
Diode 1N4007	1
Heating element	1
Air pump	1
DC motor	1
DC adaptor	2
Materials	
Perspex glass	
Angle iron metal (2 cm x 2 cm)	

Construction of Organ Bath Circuit and Chassis

The electronic and the electrical systems of the organ bath were tested on a breadboard before permanent fixing of the components were done on a veroboard.

Organ Bath Electrical and Electronic System

A potentiometer was connected such that the middle terminal was connected to A0 and the other two terminals were connected to ground and 5 V of Arduino UNO board. Each pin has its own separate line on the Arduino board. A 5 V and GND were connected to LCD's A and K pins respectively to power the backlight of the LCD.

Pins D4, D5, D6, and D7 were connected to the Arduino digital output pins 4, 5, 6, and 7, respectively. Pins 2 and 3 of the LCD were connected to the Arduino board's pins RS and E, respectively. To modify the contrast of the LCD, pins RW, VDD, and VEE of the LCD were connected to a potentiometer.

The Arduino board was connected to the PC, and the program for the organ bath was installed onto it. Pin 13 of the Arduino board was connected to one lead of a 10 k resistor, and the other lead of the resistor was connected to the base of a transistor (BC 547). The transistor's collector was connected to one of the terminal coils of the 5 V relay (Figure 54). A DC heating element was synchronized with the normally open pin of a 5 V relay and a DC adapter.

The organ bath chamber measures 35cm in length, 26 cm in breadth, and 19cm in height. The base frame supported the Perspex container and other devices in it.

A prototype as shown in Figure 61 and Figure 62 was first designed and constructed using plastic container, Arduino board, soldering iron

(heating element), 5 V DC fan, a thermistor and breadboard. After the successful completion of the prototype, the final design and construction was carried out. A 5 V relay was connected to turn on or off the heating element when the output pin of the Arduino is high or low to ensure optimum temperature of 37^{o}C.

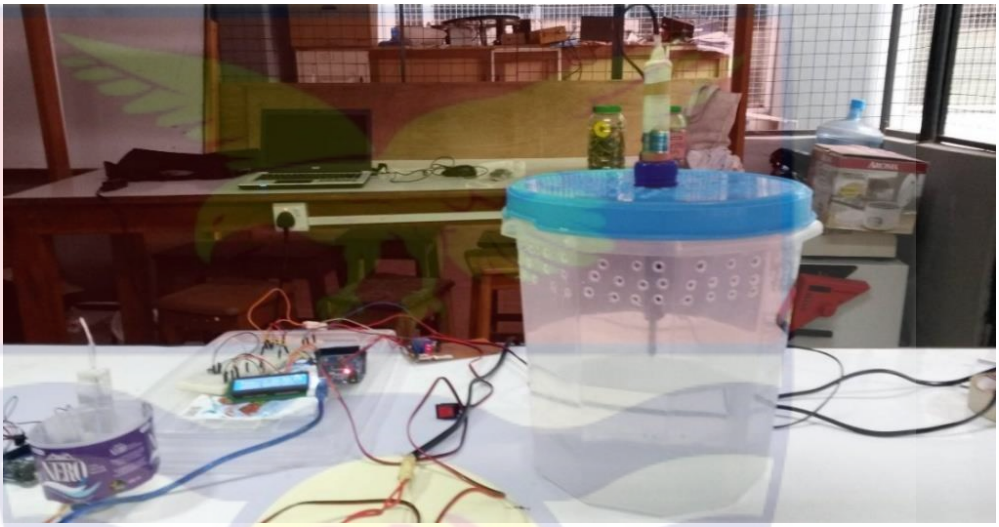

Figure 61: Prototype construction of kymograph and organ bath using plastic container

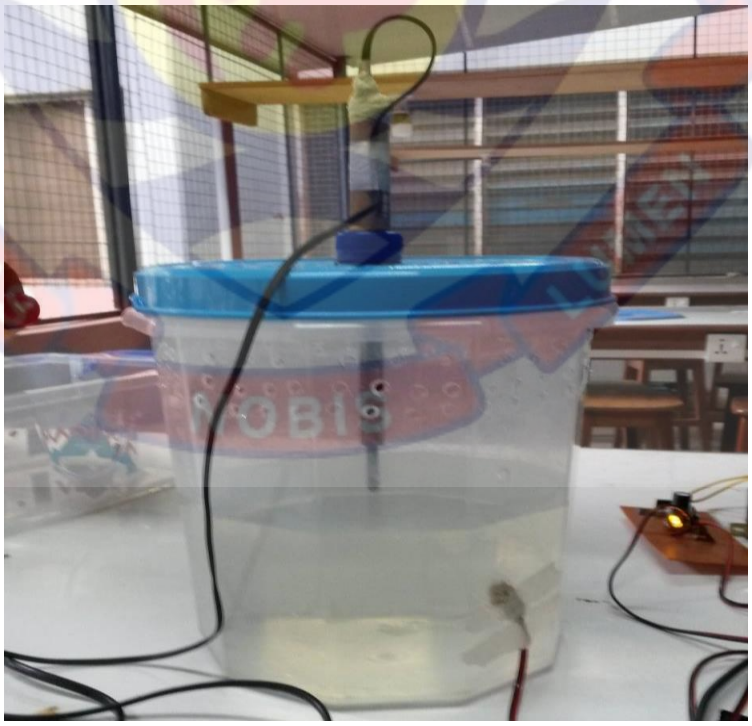

Figure 62: Prototype construction of organ bath with plastic container

Five volts (5 V) Relay Module

A relay is an electromagnetic switch that is used to turn on and off relatively large currents as shown in Figure 63 and Figure 64. The 5 V relay module utilized in the final work is a Single Pole Double Throw (SPDT) Relay, with five terminals as shown below:

Figure 63: 5 V relay module used for switching on and off the heating element

This project's relay is a 5V operating voltage relay that allows 7A/250VAC electricity to pass through. To configure the relay, a basic driver circuit consisting of a transistor, diode, and resistor was employed. A transistor was used to amplify the current so that the full current (from the DC source (5 V battery)) could flow through the coil and fully energy it. A diode was utilized to avoid reverse current. Figure 64 (A) shows relay pin connections and Figure 64 (B) show Terminal coils of the relay used in this research.

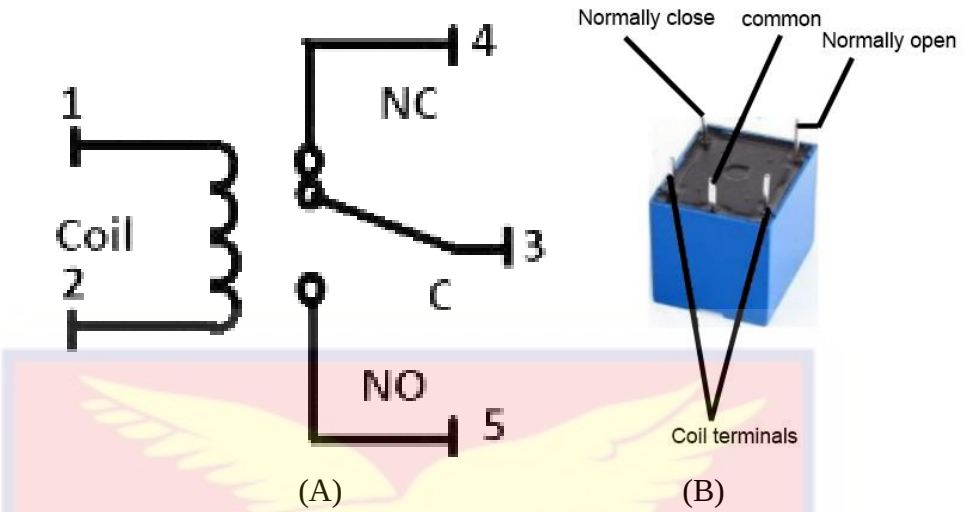

Figure 64: (A) Relay pin connections. (B) Terminal coils

Arduino Codes and the Programming of the Organ Circuit

Figure 65 shows the circuit diagram used for the development of the organ bath in Proteus 8.7 SP3 Professional. Simulation was also done in Proteus to ensure that all synchronised components can be implemented.

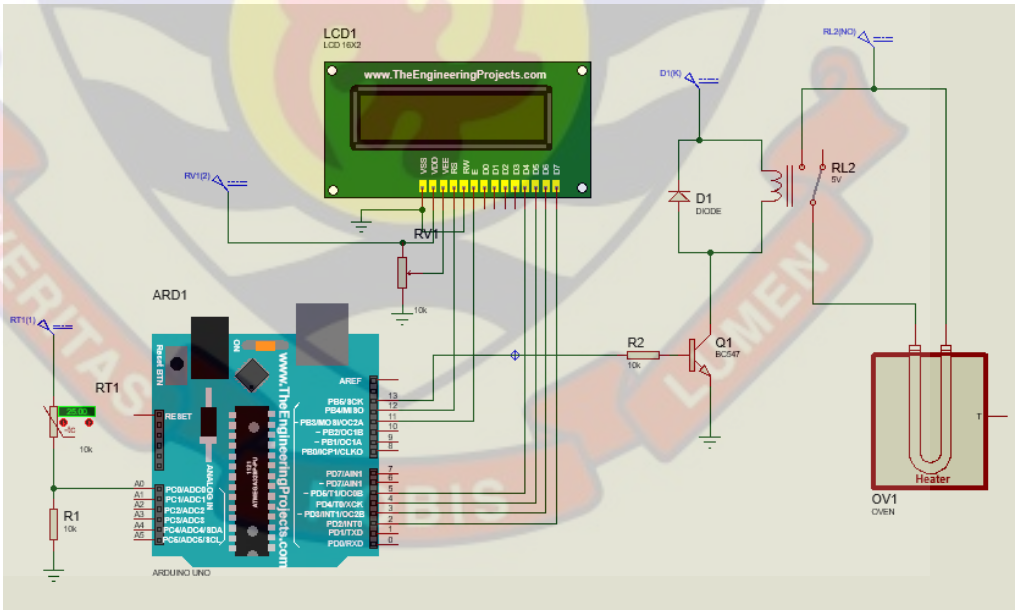

Figure 65: Organ bath simulated circuit diagram from Proteus 8.7 SP3 Professional

Figure 68 shows the flowchart used in the designing and the programming of the organ bath. The image shown in Figure 68, Figure 69 and Figure 70 show

the various components and the microcontroller used during the test period of the organ bath.

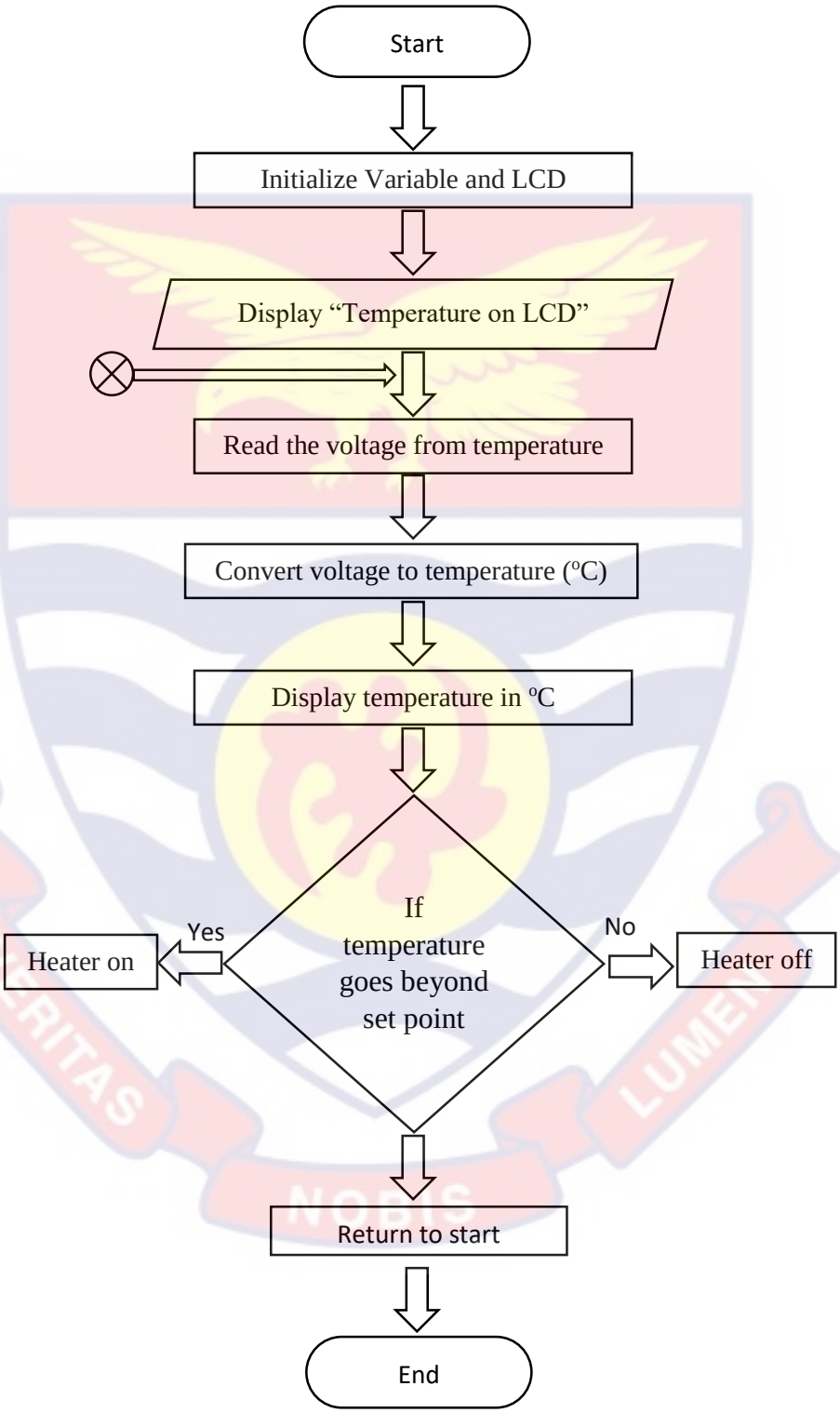

Figure 66: Programming flow chart for the development of the organ bath

Figure 67 and Figure 68 show the assembled components (electronic system) and the power supply circuit of the organ bath. Figure 69 shows the housing for the organ bath power supply circuit board.

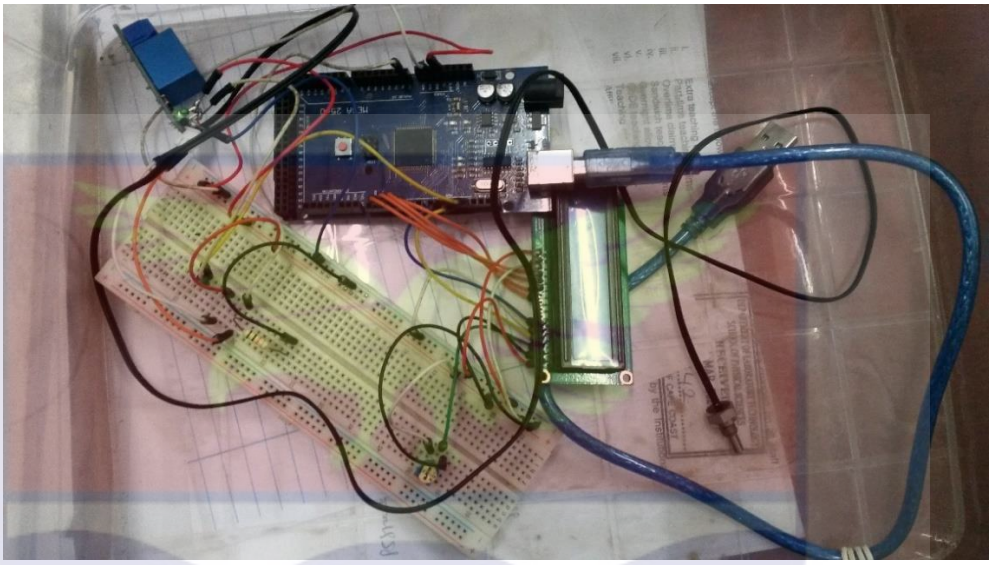

Figure 67: Organ bath electronic system with bread board, RTD, 5 V relay and Arduino ATmega 2560

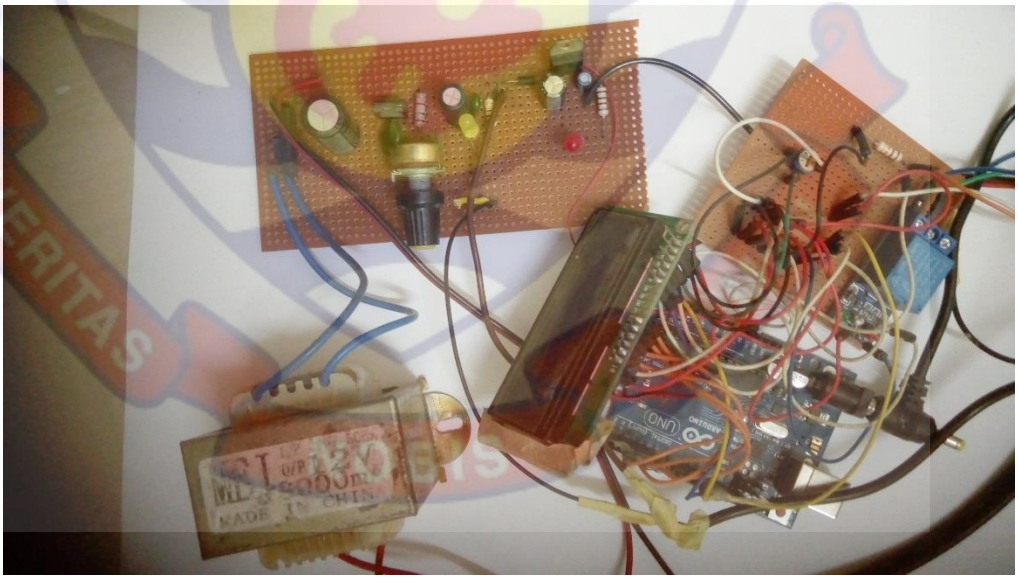

Figure 68: Assembled components and power supply circuit of organ bath

Figure 69: Housing for organ bath power supply circuit board

The complete frame work of the stand is shown in Figure 70. Figure 71 shows the complete frame work of the organ bath Perspex container (chamber).

Figure 70: Complete framework of the stand for the development of the organ bath

Figure 71: Complete frame work of the organ bath Perspex container

The complete setup of the organ bath is shown in Figure 72. It include aerator, heating element and the stirrer.

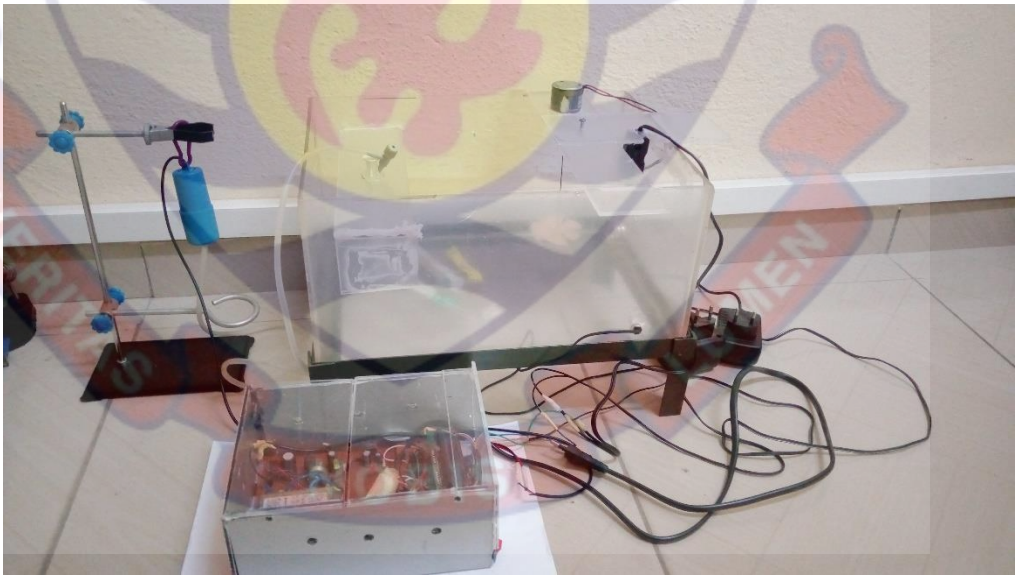

Figure 72: Complete setup of the organ bath chamber and electrical system

Organ Bath Arduino Codes or Sketches

The codes below were upload onto a microcontroller for the regulation of the organ bath temperature. C++ was used to program the organ bath in Arduino IDE as shown in Figure 73.

```
//Benjamin Oteng
//Department of Physics
//University of Cape Coast
//Cape Coast

//Digital Temperature Regualator for Organ Bath

#include <LiquidCrystal.h>

int ThermistorPin = 0;
int Vo;
float R1 = 10000;
float logR2, R2, T;
float c1 = 1.009249522e-03, c2 = 2.378405444e-04, c3 = 2.019202697e-07;
int RELAY = 13;

LiquidCrystal lcd(12, 11, 5, 4, 3, 2);

void setup() {
  pinMode(RELAY, OUTPUT);
Serial.begin(9600);
// set up the LCD's number of columns and rows:
  lcd.begin(16, 2);
  // Print a message to the LCD.
  lcd.print("OTENG B. PROJECT");
  lcd.setCursor(0,1); //Move coursor to second Line and display temperature
regulator
  lcd.print("Temp. Regulator");
  delay(4000);
}

void loop() {

  Vo = analogRead(ThermistorPin);
  R2 = R1 * (1023.0 / (float)Vo - 1.0);
  logR2 = log(R2);
```

```
T = (1.0 / (c1 + c2*logR2 + c3*logR2*logR2*logR2));
T = T - 273.15;
//T = (T * 9.0)/ 5.0 + 32.0;

lcd.print("Temp. = ");
lcd.print(T);
lcd.print(" C");

lcd.setCursor(0,1);
lcd.print("ORGAN BATH-UCC");
delay(1000);
lcd.clear();
```

Complete Arduino code for the programing of the digital organ bath is show at the appendix B.

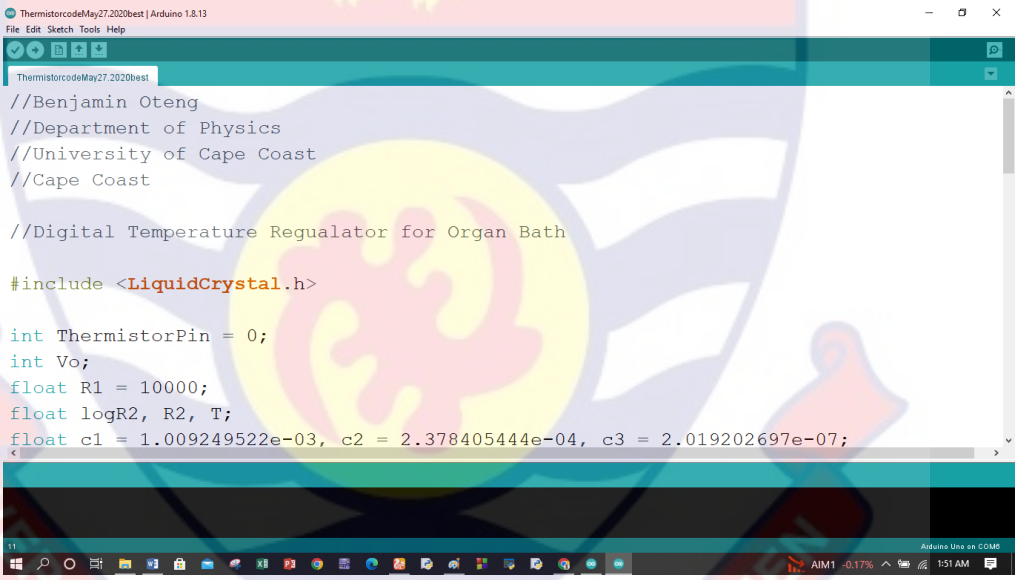

Figure 73: C++ program (sketches) in Arduino IDE 1.8.13 developed for the organ bath

The Organ Bath Temperature based System is made up of several components, including an Arduino board, an LCD display, a relay, and a thermistor. The relay and thermistor are the main components of the system. If the temperature rises above 37.1^{o}C, the relay will turn off at a preset value from the program, and if the temperature falls below (36.9^{o}C), the relay will turn on, keeping the temperature of the organ bath at around 37^{o}C.

The programmed Arduino board handles the entire triggering and temperature setting operation. It also displays information about the temperature change in every half second on the organ bath status on the LCD panel based on the program installed on the microcontroller. Figure 74 shows voltage divider circuit integrated in the thermistor design and construction.

Thermistor Temperature Calculation:

Voltage divider circuit:

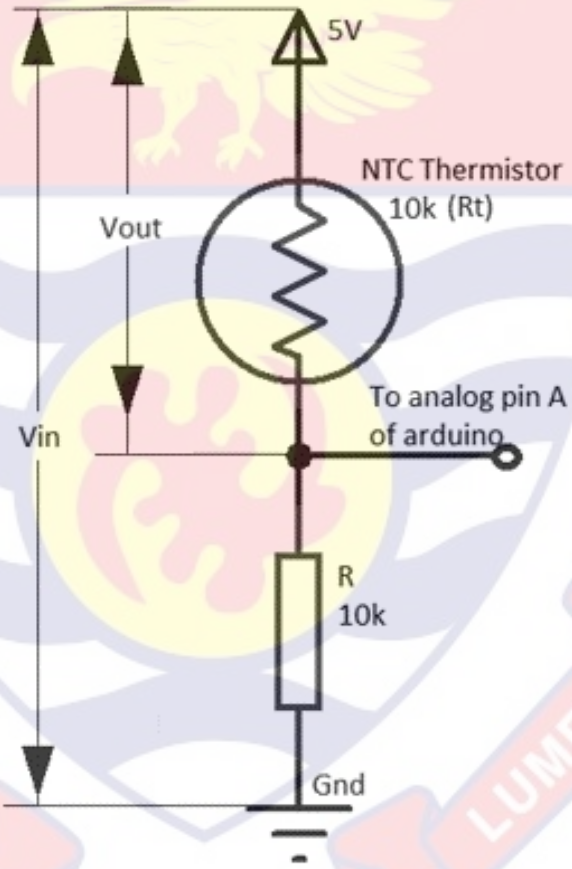

Figure 74: Thermistor voltage divider circuit

A voltage divider circuit was integrated to generate a passive linear circuit which produces an output voltage (Vout) that is a fraction of its input voltage (Vin). The output voltage of the voltage divider was synchronised with the Arduino UNO R3 to regulate the temperature of the organ bath.

This equation (equation 11) is used to calculate thermistor resistance based on the measured output voltage Vo. Which is the voltage, Vout value from the ADC value at Arduino pin A0, as illustrated in the Arduino Code in Appendix B.

Calculation of Temperature From the Thermistor Resistance

The thermistor resistance can be computed mathematically by using the Stein-Hart equation (equation 3).

The constant values for the thermistor used in the study are: $A=1.009249522x10^{-3}$, $B=2.378405444x10^{-4}$, $C=2.019202697x10^{-7}$. These constant values were taken from the thermistor's datasheet; an additional way is to utilize three resistance measurements at different temperatures, and then the Constants values are entered into the Thermistor calculator online to get the constants.

To compute the temperature, three different temperatures of the thermistor are carried out. The temperatures evenly spaced and at least 10 degrees apart. After obtaining the value of Rt from equation 10, the data are entered into the Stein-hart equation to obtain the temperature in Kelvin. A little change in the output voltage causes the temperature to vary.

Chapter Summary

The developed Arduino based kymograph and organ bath are highly corrosion resistance. Proteus 8.7 SP3 Professional and NI Multisim 13.0 were used in the design and simulation of all the circuit diagrams. The microcontrollers in this research were programmed using C++. The kymograph is made up of an aluminum drum, a carbon fiber shaft, and a galvanized steel base. The galvanised based was pieced using arc welding. The organ bath

chamber was built by using Perspex glass. The Perspex glass was also pieced using epoxy and super glue.

The instrument has two standby modes, a circuit and coded program. This study improves on the previous style of electrically operated pulley adjustment drum.

Lack of molds, specifically designed machines and tools for creating faster components (parts) of the kymograph served as a constraint in the prototype construction.

CHAPTER FOUR

RESULTS AND DISCUSSION

Introduction

The development of the digital kymograph and the organ bath in this research will help researchers and students have easy access to sustainable and affordable kymograph for extended study in physiology. The results and discussion on the digital kymograph design and implementation are presented in this chapter. C++ language was used to program the microcontroller. Two separate microcontrollers were used for the kymograph and the organ bath. Multisim 13.0 and Proteus 8.7 Professional were used for the circuit design and simulations.

The information provided is divided into four parts. The first part reports on information and analysis on the digital kymograph, the second part presents the power supply constructed for the generation of power to the organ bath in this research, the third part reports on the parameters obtained from the digital organ bath and the forth part discusses the findings from the construction of the digital kymograph.

The Digital Kymograph

The base of the kymograph is 24 cm x 21cm x13 cm in size, this size was chosen for portability. The height of the shaft is 35cm. The drum height is 14 cm, the diameter is 20.5 cm and the weight is 0.56 kg. The height of the kymograph is 40 cm. The following speeds were determined: 0.25 mm/s, 0.50 mm/s, 0.75 mm/s, 1.00 mm/s, 1.25 mm/s, 2.50 mm/s, and 3.00 mm/s. The material used for the shaft is carbon fiber, it is the first time a carbon fiber

material has been introduced in the construction of kymograph and it proved to be effective.

Figure 76 shows the result of the implemented prototyped digital kymograph, experimented with muscle contraction and relaxation. The results show that the prototype digital kymograph with organ bath provide better display than the conventional kymograph. The speeds obtain from the research conforms with standard speeds of digital kymograph.

The prototype digital kymograph also provides more accurate result because it reduces friction force and complicated gear system which are common problems with conventional kymograph, which employ smoke-drum (Suhaeri *et al.*, 2014). A standard graph paper can be attached to the drum of the prototype digital kymograph (Figure 75) directly to display the result of the muscle contraction, this leads to more accurate result than the smoke-drum. This will also lead to a better result interpretation.

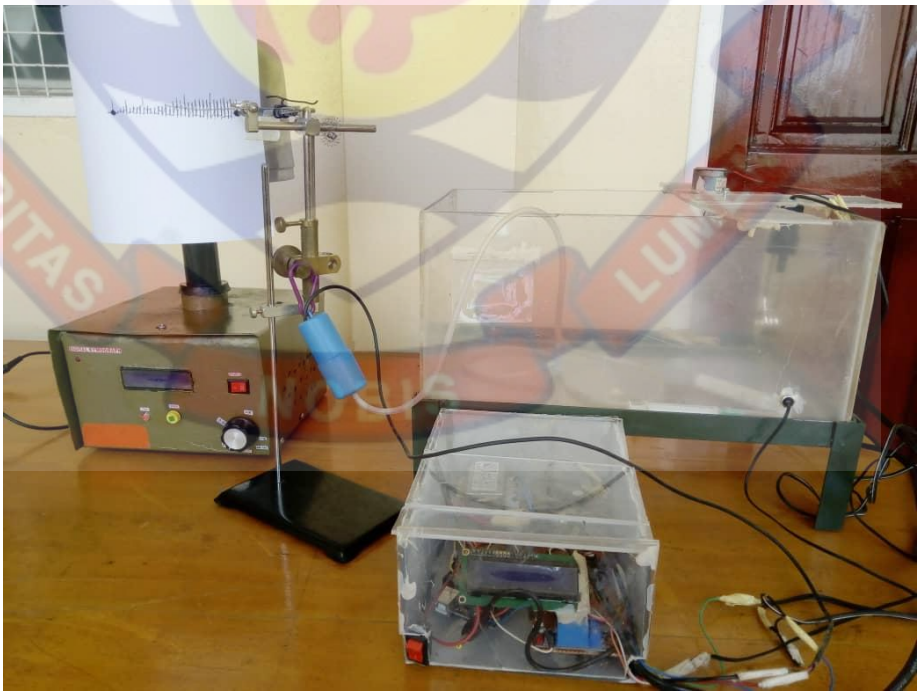

Figure 75: Complete setup of the interfaced digital kymograph and organ bath (Author's construction)

Figure 76: Kymograph response on muscle contraction

Carbon fiber is highly corrosion resistant and chemically stable. The utilization of carbon fiber (Figure 37) can increase the lifespan of the stepper motor since it is strong and lightweight and has a little impact on the weight of the stepper motor's stator and rotor. Curing epoxy is added to carbon fiber during manufacturing. Although the curing epoxy can react to sunlight and other elements, the carbon fiber itself is made from a chemically stable material and is corrosion-resistant making it a perfect choice for applications in harsh environments, there is no known corrosion index found in previous work (kymograph) done.

Galvanise steel was also used to construct the base, which is also a strong metal and highly resistant to corrosion. The research used highly resistant to corrosion materials in the construction of the kymograph. This makes it an effective instrument to be used in the coastal areas as well. The zinc coating of hot-dipped galvanized steel will last in the harshest soil is between 35-50 years and in less corrosive soil, 75 years or more (bucket-outlet, 2024).

The drum is made of aluminum, which is also resistant to corrosion. Two unpolished aluminum bowls were acquired from a factory. They were polished and then interlocked to form the drum of the kymograph. In rural area's atmosphere, the corrosion rate averages 0.03 µm/year (0.001 mils/year). In

industrial locations, the corrosion rates average 0.8–0.28 µm/year (0.03–0.11 mils/year) (Zaki, 2006).

Arduino code

Complete Arduino code for the programing of the digital kymograph is show at the appendix A.

Digital kymograph key features:

i. Microprocessor controlled unit
ii. 16x2 LCD Display
iii. 0.25, 0.50, 0.75, 1.00, 1.25, 2.50, 3.00 mm/sec accurate speeds
iv. Standby mode, stop and start buttons
v. Very low power consumption (24 W)
vi. Easy detachable drum
vii. Sturdy, extremely corrosion resistant body

Table 4: Kymograph system specifications

Parameter	Value
Speeds	7
Drum Dimensions	Height: 14 cm Diameter 20.5 cm
Height of Shaft	35.5 cm
Height of Kymograph	40 cm
Power Requirements	220/230 V AC 50 Hz DC 12 V, 2 A

Circuit Design and Simulation

Proteus 8.7 SP3 Professional was used in the design and the simulation of the circuit diagram and accessories for both the digital kymograph (Figure

39) and the organ bath (Figure 65). Multisim 13.0 was used in the design and the simulation of the power supply circuit as shown in Figure 57.

Assembled Components and Accessories of Kymograph

All the electrical systems and chassis were put together to form the complete digital kymograph as shown in Figure 52. Anti-slip pads obtained from gas cylinder seals were used to support the base of the kymograph.

Calibration of Kymograph

The speed of the kymograph was determined in millimeters per second as required. A pointer fixed on retort stand, counter and measurement tape were used to determine the speed ranges of the kymograph (Figure 52). Determination of the speeds were based on equation 12. Highly accurate speeds obtained are as follows: 0.25, 0.50, 0.75, 1.00, 1.25, 2.50 and 3.00 mm/sec, which is consistent with existing speed values for commercial kymograph (newmeditech.com, 2011).

Kymograph Vibration

To ascertain the stability of the kymograph when the drum is rotating, a vibration test was conducted. A Vibrometer software (smart tools) version 1.6.15 was employed to determine the vibration. As the drum rotated at various speeds, the vibrations at various speeds were determined as well as shown in Figure 77.

According to the study, the system experienced a slight vibration for 120 seconds while maintaining a consistent angular movement between 0.25 and 0.75 mm. The process of rotation is quite steady between 0.25 mm/s and 3.00 mm/s.

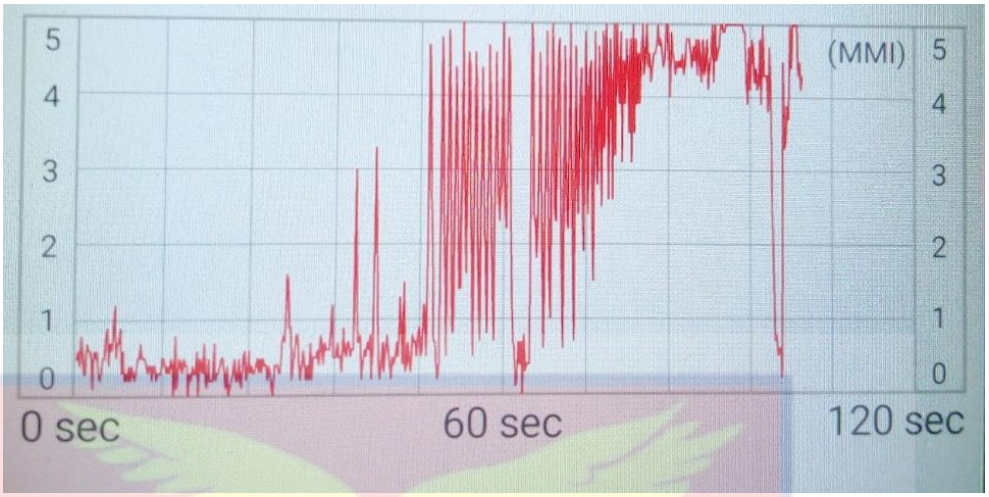

Figure 77: Kymograph vibration test response

Organ Bath Construction

Figure 59 is the schematic diagram for the DC power supply. The input signal from the mains supply (AC) was sinusoidal and the output was regulated. The unrectified voltage from the power source was 12.2 V and the rectified voltage was 12.3 V and 5.0 V). In this research, the DC power supply (Figure 69), was used to supply 12.3 V to the organ bath and 5 V to the microcontroller (Arduino).

The load regulation (LM7805) was 2% and LM317 regulator 2.5% the percentages obtained are less than 3% which indicates the efficiency of the power regulators and the transformer employed in the construction of the power system. This also relates to similar study by allaboutciruits, 2023. In that study, a load regulation of less than 3% is regarded as efficient power system. Complete Arduino code for the programing of the digital organ bath is show at the appendix B. The chassis stand was constructed using iron of 37 cm x 28 cm x 10 cm size as shown in Figure 70. Perspex glass was used to develop the chamber for the organ bath (Figure 71). The size of the Perspex glass is 36 cm x 26 cm x 18.5 cm.

Chapter Summary

Figure 75 depict the interfaced digital kymograph and organ bath. The resulting kymograph and organ bath can be used to analyze tissues in vivo and in vitro. Other researchers and producers have conducted similar studies using various materials such as steel, brass, iron, and wood (www.indiamart.com, 2023). This research introduces new materials, aluminium and carbon fiber. The speeds of kymograph ranges from: 0.12, 0.25, 0.50, 0.75, 1.00, 1.25, 2.50, 0.300 mm/sec. The speed of the designed kymograph was determined in millimeters per second as required (newmeditech.com, 2011) and it ranges between 0.25 mm/s and 3.00 mm/s. The organ bath constructed regulate the temperature at 37^{o}C. A muscle contraction was used to evaluate the hardware and software systems that were created to support the kymograph. For use in teaching and research by scholars and students, the kymograph with organ bath is being developed to enhance academic study.

CHAPTER FIVE

SUMMARY, CONCLUSIONS AND RECOMMENDATIONS

Overview

The purpose of this research is to design and build a low-cost, corrosion-resistant Arduino based kymograph for measuring the level and time of a variety of physiological parameters for use in teaching and research, particularly in developing laboratories.

Many basic pieces of equipment used in research and academic institutions can be swiftly and inexpensively constructed to suit the purpose of the more complicated and costly imported ones. Instead of a foreign-made kymograph, a locally-made digital kymograph with a spinning upright cylinder (drum) that can display continuous recording on a paper surface wrapped around it has been created and manufactured. The apparatus produced can be used to study physiological investigations such as muscle movement, nerve circulation, and respiration. Physics and other engineering disciplines can use the equipment to study waveforms and vibrations.

Summary

Proteus 8.7SP3 Professional and NI Multisim 13.0 were used for the schematic diagram and simulation of the hardware and software systems. The device has a 12.0 V input voltage and a current of 2.0 A. It includes a 12-volt cooling fan, a stepper motor and driver, an Arduino UNO R3 board, a standby mode circuit, a display unit, stop and start buttons, and a speed regulator (0.25,0.50,0.75,1.00,1.25,2.50, 3.00 mm/sec). Carbon fiber is used for the shaft, aluminum for the drum, and galvanised steel for the main chassis. The organ

bath runs at 37 degrees Celsius and is composed of Perspex glass and a microcontroller.

Conclusions

The prototype digital kymograph demonstrates better result by providing muscle contraction value. It is also easier to use than the conventional kymograph. Recently, the instrument had being used to study physiological parameter (hand muscle contraction), at the University of Cape Coast. The experiment in the laboratory shows that students can interpret better using the instrument than the conventional one. The digital kymograph prototype exhibits superior performance by furnishing the value of muscle contraction. In addition, it is simpler to operate than a traditional kymograph. At the University of Cape Coast, the device has recently been utilized to investigate a physiological parameter (hand muscle contraction). The lab experiment demonstrates that students can interpret results more accurately with our technology than with the conventional one.

However, the system did exhibit a little tremor for 120 seconds during the vibration test, all the while maintaining a steady angular movement between 0.25 and 0.75 mm. From 0.25 mm/s to 3.00 mm/s, the rotational process is quite stable, as Figure 77 illustrates.

In this study an Arduino based digital kymograph has been developed interfacing an organ bath for physiological tissue analysis. The extremely corrosion resistant body and well-made apparatus is a novel edifice based on a developed C++ program. The device has been integrated with a standby mode circuit. This prevents the operation of the equipment when there is power interruption. Unlike conventional kymographs, the newly constructed device

which is cost-effective and efficient has a fiber rod as the shaft which is light in weight, strong and corrosion resistant, thus prolonging the life span of the stepper motor since the shaft doesn't exert a lot of pressure. The calculated efficiency of the power load regulation was not above the stipulated 3% threshold. The speed ranges obtained are also within the standard ranges for digital kymograph. In this case, the study is novel and adds knowledge to academia and research.

Recommendations

For further research the following recommendations are made;

1. The use of carbon fiber for the shaft is recommendable, and hence further research could be done to employ it for the development of the drum. This may make the kymograph light weight and robust.
2. In order to collect data remotely, improve understanding and visualization, future research could include sophisticated algorithms, distant precision sensors and wireless transmission signals. This will provide reliable data to researchers for better interpretation and informed decision-making in real-time monitoring, which will have a substantial impact on medical research as well as the pharmaceutical industry.

REFERENCES

Allaboutcircuits (2023, July 27). Voltage regulation. Retrieved https://www.allaboutcircuits.com/textbook/alternating-current/chpt-9/voltage-regulation/.

Alistair, M. K. (2016). “Do Not Kill Guinea Pig before Setting up Apparatus”: The Kymograph's Lost Educational Context. Retrieved from https://philarchive.org/rec/KWADNK.

Alper, J. D., Tovar, M., & Howard, J. (2013). Displacement-weighted velocity analysis of gliding assays reveals that Chlamydomonas axonemal dynein preferentially moves conspecific microtubules. *Biophysical Journal*, 104, 1989–1998.

Alwaz, N. (2021, August 20). Study of Kymograph. Retrieved from https://www.youtube.com/watch?v=x24TXiQYNfY.

Britanica (2020). Invention by Ludwig. Retrieved from https://www.britannica.com/biography/Carl-F-W-Ludwig#ref32614

Brown, A. (2000). Slow axonal transport: Stop and go traffic in the axon. *Nature Reviews Molecular Cell Biology*, 1, 153–156.

Brown, A. (2003). Axonal transport of membranous and nonmembranous cargoes: A unified perspective. *Journal of Cell Biology*, 160, 817–821.

Brown, A. (2014). Slow axonal transport. In M. Caplan (Ed.), *Reference Module in Biomedical Sciences. Elsevier*.

Brown, A. (2016). Axonal transport. In D. W. Pfaff & N. D. Volkow (Eds.), Neuroscience in the 21st Century: From Basic to Clinical (pp. 333–379). New York: Springer Publishing.

Brown, A., Wang, L., & Jung, P. (2005). Stochastic simulation of neurofilament transport in axons: The "stop-and-go" hypothesis. *Molecular Biology of the Cell*, 16, 4243–4255.

Bucket-outlet (2024, June 16). Does galvanized steel rust. Retrieved from https://www.bucket-outlet.com/Does-Galvanized-Steel-Rust.htm.

Burton, P. R., & Wentz, M. A. (1992). Neurofilaments are prominent in bullfrog olfactory axons but are rarely seen in those of the tiger salamander, Ambystoma tigrinum. *Journal of Comparative Neurology*, 317, 396–406.

Chaphalkar, A. R., Jain, K., Gangan, M. S., & Athale, C. A. (2016). Automated multi-peak tracking kymography (AMTraK): A tool to quantify sub-cellular dynamics with sub-pixel accuracy. PloS One, 11, e0167620.

Colakoglu, G., & Brown, A. (2009). Intermediate filaments exchange subunits along their length and elongate by end-to-end annealing. *Journal of Cell Biology*, 185, 769–777.

Craciun, G., Brown, A., & Friedman, A. (2005). A dynamical system model of neurofilament transport in axons. *Journal of Theoretical Biology*, 237, 316–322.

Daniel, F., Brown, A., Johnson, C. A., Peng, J., & Jung, P. (2017, January 6). Kymograph analysis with high temporal resolution reveals new features of neurofilament transport kinetics. *Willy K. S,* Retrieved from https://neurofilament.osu.edu/wp-content/uploads/2018/11/Fenn_ Johnson_2018.pdf.

dbpedia.org (2021, November 11). Kymograph. Retrieved from https://dbpedia.org/page/ Kymograph.

Deriche, R. (1987). Using Canny's criteria to derive a recursively implemented optimal edge detector. *International Journal of Computer Vision*, 1, 167–187.

Efimov, A., Schiefermeier, N., Grigoriev, I., Ohi, R., Brown, M. C., Turner, C. E., & Kaverina, I. (2008). Paxillin-dependent stimulation of microtubule catastrophes at focal adhesion sites. *Journal of Cell Science*, 121, 196–204.

Francis, F., Roy, S., Brady, S. T., & Black, M. M. (2005). Transport of neurofilaments in growing axons requires microtubules but not actin filaments. *Journal of Neuroscience Research*, 79, 442–450.

Gouveia, S. M., & Akhmanova, A. (2010). Cell and molecular biology of microtubule plus end tracking proteins: End binding proteins and their partners. *International Review of Cell and Molecular Biology*, 285, 1–74.

He, Y., Francis, F., Myers, K. A., Yu, W., Black, M. M., & Baas, P. W. (2005). Role of cytoplasmic dynein in the axonal transport of microtubules and neurofilaments. *Journal of Cell Biology*, 168, 697–703.

Helfand, B. T., Loomis, P., Yoon, M., & Goldman, R. D. (2003). Rapid transport of neural intermediate filament protein. *Journal of Cell Science*, 116, 2345–2359.

Hoffman, P. N. (1995, March 4). The synthesis, axonal transport, and phosphoryla- tion of neurofilaments determine axonal caliber in myelinated nerve fibers. *Sage Journals*, 1(2). Retrieved from https://journals.sagepub.com/doi/abs/10.1177/107385849500100204.

Hoffman, P. N, & Lasek, R. J. (1975, December 6). The slow component of axonal transport. Identification of major structural polypeptides of the axon and their generality among mammalian neurons. *National Library of Medicine,* 351-66. Retrieved from https://pubmed.ncbi.nlm.nih. gov/49355/.

Hoff, Valentinuzzi, Geddes & Moore (2015, April 10). Physiological records projected on a screen. Retrieved from https:// ieeexplore.ieee.org/stamp/stamp. jsp?arnumber=7156279.

iqbalscientific (2022, June 13). Mechanical kymograph. Retrieved https://www.iqbalscientific.com/shop/kymograph-3/

Jameco (2024, June 2). Thermistors/Temperature Measurement with NTC Thermistors. Retrieved from https://www.jameco.com/Jameco/ workshop/TechTip/temperature-measurement-ntc-thermistors.html

Jung, P. & Brown, A. (2009). Modeling the slowing of neurofilament transport along the mouse sciatic nerve. *Physical Biology*, 6, 046002.

Kaech, S. & Banker, G. (2006). Culturing hippocampal neurons. *Nature Protocol*, 1, 2406–2415.

Lasek, R.J., Paggi, P., & Katz, M. J. (1993). The maximum rate of neurofilament transport in axons: a view of molecular transport mechanisms continuously engaged. *ScienceDirect*,616 (2), 58-64.

Lasek, R. J., Garner, J. A., & Brady, S. T. (1984). Axonal transport of the cytoplasmic matrix. *Journal of Cell Biology*, 99, 212s–21s.

Lattal, K.A. (2004). Steps and pips in the history of the cumulative recorder. *Journal of the Experimental Analysis of Behavior*, 82, 329–355.

Lindsley, O. R. (2010). Skinner on measurement. Kansas City, KS: Behavior Research Company.

Ludington, W. B., & Marshall, W. F. (2009). Automated analysis of intracellular motion using kymographs in 1, 2, and 3 dimensions, Vol. 7184.

Li, Y., Brown, A., Jung, P. (2014). Deciphering the axonal transport kinetics of neurofilaments using the fluorescence photoactivation pulse-escape method. *Physical Biology*, 11, 026001.

Li, Y., Jung, P., & Brown, A. (2012). Axonal transport of neurofilaments: a single population of intermittently moving polymers. *Journal of Neuroscience*, 32, 746–758.

Matus, M. (2011). Temperature Measurement in Dimensional Metrology – Why the Steinhart–Hart Equation works so well. Wabern, Switzerland.

Monsma, P. C., Li, Y., Fenn, J. D., Jung, P., & Brown, A. (2014). Local regulation of neurofilament transport by myelinating cells. *Journal of Neuroscience*, 34, 2979–2988.

Morris, E. K., & Smith, N. G. (2004). On the origin and preservation of cumulative record in its struggle for life as a favored term. *Journal of the Experimental Analysis of Behavior*, 82, 357–373.

Mukherjee, A., Jenkins B., Fang C., Radke R. J., Banker G., Roysam B. (2011, September 8). Automated kymograph analysis for profiling axonal transport of secretory granules. *ScienceDirect*, 15 (3), 354-367. Retrieved from https://www.sciencedirect.com/science/article/abs/pii/S1361841510001350.

Mukhopadhyay, R., Kumar, S., & Hoh, J. H. (2004). Molecular mechanisms for organizing the neuronal cytoskeleton. *Bioessays*, 26, 1017–1025.

Newmeditech (2011, March 3). Kymograph. Retrieved http://newmeditech.com/secure /wp-content/uploads/2011/09/Kymograph.pdf.

Welzel, O., Boening, D., Stroebel, A., Reulbach, U., Klingauf, J., Kornhuber J., & Groemer, T. (2009). Determination of axonal transport velocities via image cross-and autocorrelation, *European Biophysics Journal* no. 38, pp. 883–889.

Prahlad, V., Helfand, B. T., Langford, G. M., Vale, R. D., & Goldman, R. D. (2000). Fast transport of neurofilament protein along microtubules in squid axoplasm. *Journal of Cell Science*, 113, 3939–3946.

Reis, G. F., Yang, G., Szpankowski, L., Weaver, C., Shah, S. B., Robinson,J. T.,... Goldstein, L. S. (2012). Molecular motor function in axonal transport in vivo probed by genetic and computational analysis in Drosophila. *Molecular Biology of the Cell*, 23, 1700–1714.

Roy, S., Coffee, P., Smith, G., Liem, R. K. H., Brady, S. T., & Black, M. M. (2000). Neurofilaments are transported rapidly but intermittently in axons: Implications for slow axonal transport. *Journal of Neuroscience*, 20, 6849–6861.

Schindelin, J., Arganda-Carreras, I., Frise, E., Kaynig, V., Longair, M., Pietzsch, T.,... Schmid, B. (2012). Fiji: An open-source platform for biological-image analysis. *Nature Methods*, 9, 676–682.

Schneider, C. A., Rasband, W. S., & Eliceiri, K. W. (2012). NIH Image to ImageJ: 25 years of image analysis. *Nature Methods*, 9, 671–675.

Seitz, A., & Surrey, T. (2006). Processive movement of single kinesins on crowded microtubules visualized using quantum dots. *EMBO Journal*, 25, 267–77.

Semanticscholar (2024, March 2). Physiology of the Muscular System 397 Bone Tendon Fascia Muscle Epimysium Perimysium Endomysium Fascicle Muscle fiber. Retrieved from https://www.semanticscholar.org/paper/ Chapte-r-11-Physiology-of-the-Muscular-System-397-%28/b2dc6 1049eece8ad89fe9ba894fb601a58c885a1/figure/8

Shah, J. V., Flanagan, L. A., Janmey, P. A., & Leterrier, J.-F. (2000). Bidirectional translocation of neurofilaments along microtubules mediated in part by dynein/dynactin. *Molecular Biology of the Cell*, 11, 3495–3508.

Sil (2022, October 7). Physiological instruments. *Cambridge Scientific Instrument Company Ltd*. https://www.sil.si.edu/DigitalCollections/trade-literature/scientific-instruments/pdf/sil14-51682.pdf.

Soppina, V., Rai, A. K., Ramaiya, A. J., Barak, P., & Mallik, R. (2009). Tug-of-war between dissimilar teams of microtubule motors regulates transport and fission of endosomes. Proceedings of the National Academy of Science of the United States of America, 106, 19381–19386.

Stepanova, T., Slemmer, J., Hoogenraad, C. C., Lansbergen, G., Dortland, B. D., Zeeuw, C. I.,... Galjart, N. (2003). Visualization of microtubule growth in cultured neurons via the use of EB3-GFP (end-binding protein 3-green fluorescent protein). *Journal of Neuroscience*, 23, 2655–2664.

Suhaeri, & Tundjungsari, V. (2014). Computerized Kymograph for Muscle Contraction Measurement Using Ultrasonic Distance Sensor. *International Journal of Advanced Computer Science and Applications*, Vol (5).

Smal, I., Grigoriev, I., Akhmanova, A., Niessen, W., & Meijering, E. (2010). Microtubule dynamics analysis using kymographs and variable-rate particle filters, Image Processing. *IEEE*, pp. 1861–1876.

Taylor, N. J., Wang, L., & Brown, A. (2012). Neurofilaments are flexible polymers that often fold and unfold but they move in a fully extended configuration. Cytoskeleton (Hoboken), 69, 535–544.

Trivedi, N., Jung, P., & Brown, A. (2007). Neurofilaments switch between distinct mobile and stationary states during their transport along axons. Journal of Neuroscience, 27, 507–516.

Uchida, A., Alami, N. H., & Brown, A. (2009). Tight functional coupling of kinesin-1A and dynein motors in the bidirectional transport of neurofilaments. *Molecular Biology of the Cell*, 20, 4997–5006.

Uchida, A., & Brown, A. (2004). Arrival, reversal and departure of neurofilaments at the tips of growing axons. *Molecular Biology of the Cell*, 15, 4215–4225.

Uchida, A., Colakoglu, G., Wang, L., Monsma, P. C., & Brown, A. (2013). Severing and end-to-end annealing of neurofilaments in neurons. *Proceedings of the National Academy of Science of the United States of America*, 110, E2696–E705.

Uchida, A., Monsma, P. C., Fenn, J. D., & Brown, A. (2016). Live-cell imaging of neurofilament transport in cultured neurons. *Methods in Cell Biology*, 131, 21–90.

Utsic (2023). Horizontal Kymograph. Retrieved https://utsic.utoronto.ca /wpm_instrument/horizontal-kymograph-2/.

Valentinuzzi, M. E. Beneke, K. & González, G. E. (2012). "Ludwig: The bioengineer," *IEEE* Pulse, vol. 3, no. 4, pp. 68–78.

Virtual laboratory (2022). Experimental set up: Machine-driven kymograph. Retrieved https://vlp.mpiwg-berlin.mpg.de/animations/ kymograph.html.

Wellcomeimages.org (2024). Carl F. W. Ludwig's kymograph. Retrieved from https://wellcomecollection.org/works/kvz5um7n.

Wagner, O. I., Ascano, J., Tokito, M., Leterrier, J. F., Janmey, P. A., & Holzbaur, E. L. (2004). The interaction of neurofilaments with the microtubule motor cytoplasmic dynein. *Molecular Biology of the Cell*, 15, 5092–5100.

Wang, L., & Brown, A. (2001). Rapid intermittent movement of axonal neurofilaments observed by fluorescence photobleaching. Molecular *Biology of the Cell*, 12, 3257–3267.

Wang, L., & Brown, A. (2010). A hereditary spastic paraplegia mutation in kinesin-1A/KIF5A disrupts neurofilament transport. *Molecular Neurodegeneration*, 5, 52.

Wang, L., Ho, C.-L., Sun, D., Liem, R. K. H., & Brown, A. (2000). Rapid movement of axonal neurofilaments interrupted by prolonged pauses. *Nature Cell Biology*, 2, 137–141.

Yan, Y., & Brown, A. (2005). Neurofilament polymer transport in axons. *Journal of Neuroscience*, 25, 7014–7021.

Yan, Y., Jensen, K., & Brown, A. (2007). The polypeptide composition of moving and stationary neurofilaments in cultured sympathetic neurons. *Cell Motility & Cytoskeleton*, 64, 299–309.

Yau, K. W., Schatzle, P., Tortosa, E., Pages, S., Holtmaat, A., Kapitein, L. C., & Hoogenraad, C. C. (2016). Dendrites in vitro and in vivo contain microtubules of opposite polarity and axon formation correlates with uniform plus-end-out microtubule orientation. *Journal of Neuroscience*, 36, 1071–1085.

Zaki, A. (2006, January 11). Principles of Corrosion Engineering and Corrosion Control. *ScienceDirect*. Retrieved from https:// www.sciencedirect.com /topics/ engineering/ aluminum-corrosion.

Zhang, K., Osakada, Y., Xie, W., & Cui, B. (2011). Automated image analysis for tracking cargo transport in axons. *Microscopy Research & Techniques*, 74, 605–613.

APPENDICES

KYMOGRAPH PROGRAM, ORGAN BATH PROGRAM AND L298N MOTOR DRIVER MODULE

APPENDIX A

KYMOGRAPH PROGRAM

```
#include<LiquidCrystal.h>
LiquidCrystal lcd(2,3,4,5,6,7);

#include <Stepper.h>
#define potentiometer  A0  //10k Variable Resistor
const int stepsPerRevolution = 200;  // number of steps per revolution for your motor

// initialize the stepper library on pins 8 through 11:
Stepper myStepper(stepsPerRevolution, 8, 9, 10, 11);

int stepCount = 0;  // number of steps the motor has taken
#define bt_F A1 // Clockwise motion of kymograph
#define bt_S A2 // Stop Button

int read_ADC;
int Speed_LCD;
int Speed;
int Step;
int Mode=0;

void setup() {
 pinMode(potentiometer, INPUT); // declare potentiometer as input

pinMode(bt_F, INPUT_PULLUP); // declare bt_F as input
pinMode(bt_S, INPUT_PULLUP); // declare bt_S as input

lcd.begin(16,2);
lcd.setCursor(0,0);
lcd.print("DIGITAL KYMOGRAPH");
lcd.setCursor(0,1);
lcd.print("OTENG'S PROJECT");
delay(2000); // Waiting for a while
lcd.clear();
}

void loop() {
```

```
Speed_LCD = map(read_ADC, 0, 1023, 0, 100);


lcd.setCursor(0,0);
lcd.print("   Speed: ");
lcd.print(Speed_LCD);
lcd.print("%  ");

if(digitalRead (bt_F) == 0){Mode = 1;} //For Clockwise motion of kymograph
if(digitalRead (bt_S) == 0){Mode = 0;} //For Stop

lcd.setCursor(0,1);

if(Mode==0){ lcd.print("      Stop      ");}
if(Mode==1){ lcd.print("Drum in motion");}
// read the sensor value:
 int sensorReading = analogRead(A0);
 // map it to a range from 0 to 100:
 int motorSpeed = map(sensorReading, 0, 1023, 0, 100);
 // set the motor speed:
 if (motorSpeed > 0) {
   myStepper.setSpeed(motorSpeed);
   // step 1/100 of a revolution:
   myStepper.step(stepsPerRevolution / 100);
 }
}
```

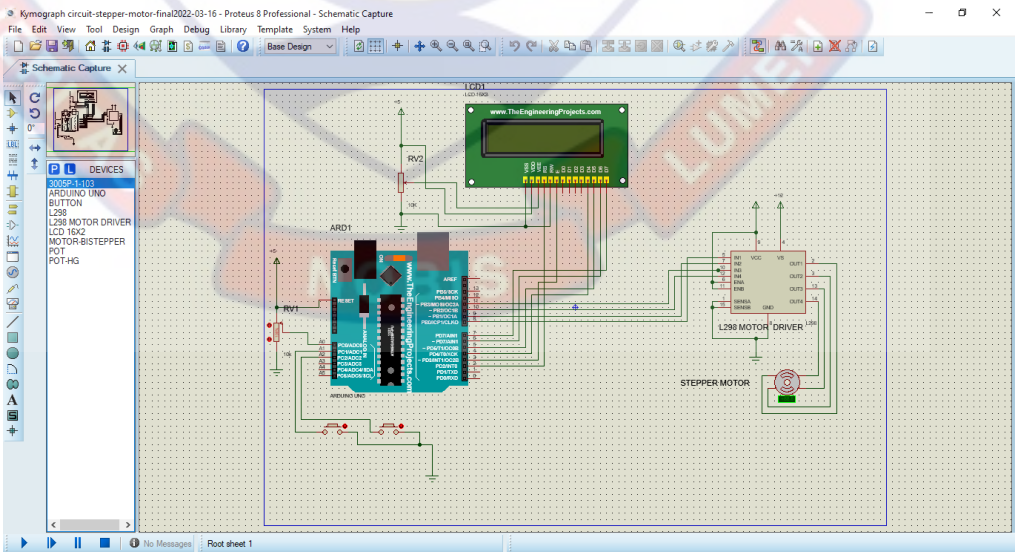

Figure 78: Kymograph simulated circuit diagram with NEMA 17 stepper motor with L298N and Arduino in Proteus 8.7 SP3 Professional IDE

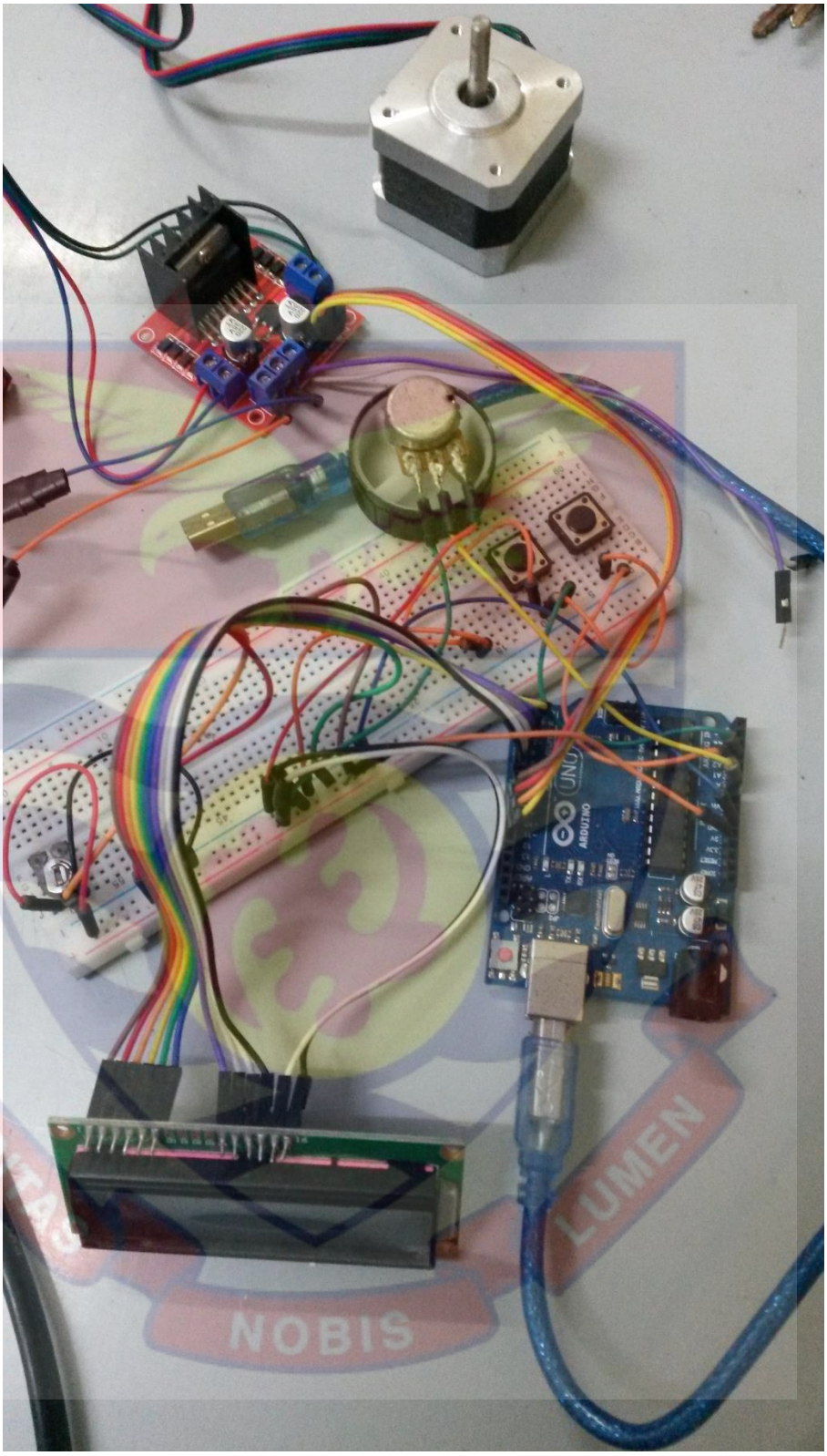

Figure 79: Implemented kymograph simulated circuit using Arduino UNO R3, LCD, Stepper motor and driver, and digital switches on breadboard.

APPENDIX B

ORGAN BATH PROGRAM

```
//Benjamin Oteng
//Department of Physics
//University of Cape Coast
//Cape Coast

//Digital Temperature Regualator for Organ Bath

#include <LiquidCrystal.h>

int ThermistorPin = 0;
int Vo;
float R1 = 10000;
float logR2, R2, T;
float c1 = 1.009249522e-03, c2 = 2.378405444e-04, c3 = 2.019202697e-07;
int RELAY = 13;

LiquidCrystal lcd(12, 11, 5, 4, 3, 2);

void setup() {
  pinMode(RELAY, OUTPUT);
Serial.begin(9600);
// set up the LCD's number of columns and rows:
  lcd.begin(16, 2);
  // Print a message to the LCD.
  lcd.print("OTENG B. PROJECT");
  lcd.setCursor(0,1); //Move coursor to second Line and display temperature
regulator
  lcd.print("Temp. Regulator");
  delay(4000);
}

void loop() {

  Vo = analogRead(ThermistorPin);
  R2 = R1 * (1023.0 / (float)Vo - 1.0);
  logR2 = log(R2);
  T = (1.0 / (c1 + c2*logR2 + c3*logR2*logR2*logR2));
  T = T - 273.15;
  //T = (T * 9.0)/ 5.0 + 32.0;
```

```
 lcd.print("Temp. = ");
 lcd.print(T);
 lcd.print(" C");

 lcd.setCursor(0,1);
 lcd.print("ORGAN BATH-UCC");
 delay(1000);
 lcd.clear();

   {
    if(T>=37.1)//if temperature above 37.1 degrees
    {
    digitalWrite(RELAY,LOW);// Turn off heater
        }
    else
    {
if(T<=36.9)//if temperature is under 36.9 degrees
    digitalWrite(RELAY,HIGH);// Turn on  heater

   }

   }
}
```

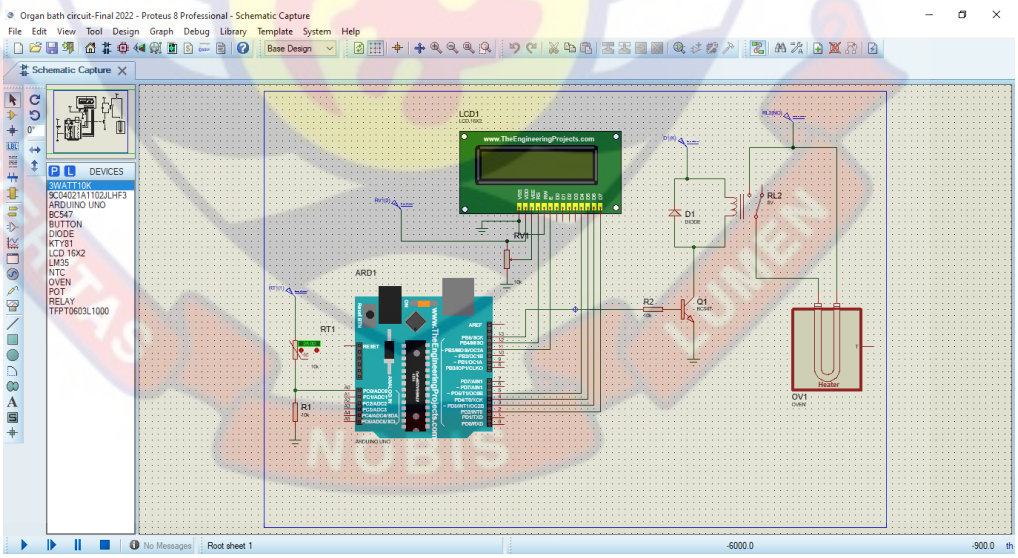

Figure 80: Organ bath simulated circuit diagram in Proteus 8.7 SP3 professional IDE

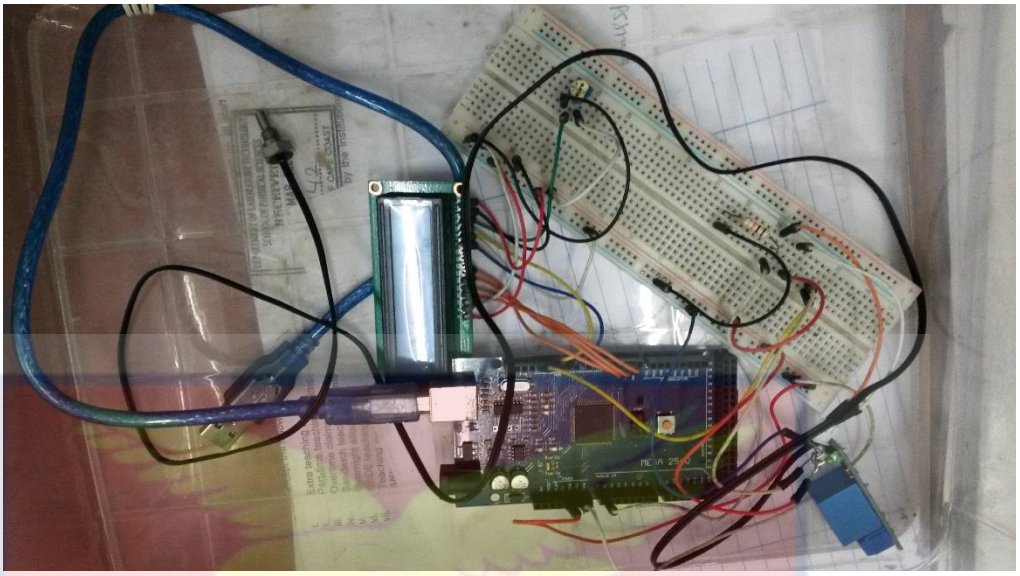

Figure 81: Implemented organ bath simulated circuit using Arduino ATmega 256, relay, thermistor, LCD and breadboard.

APPENDIX C

DC POWER SUPPLY DESIGN

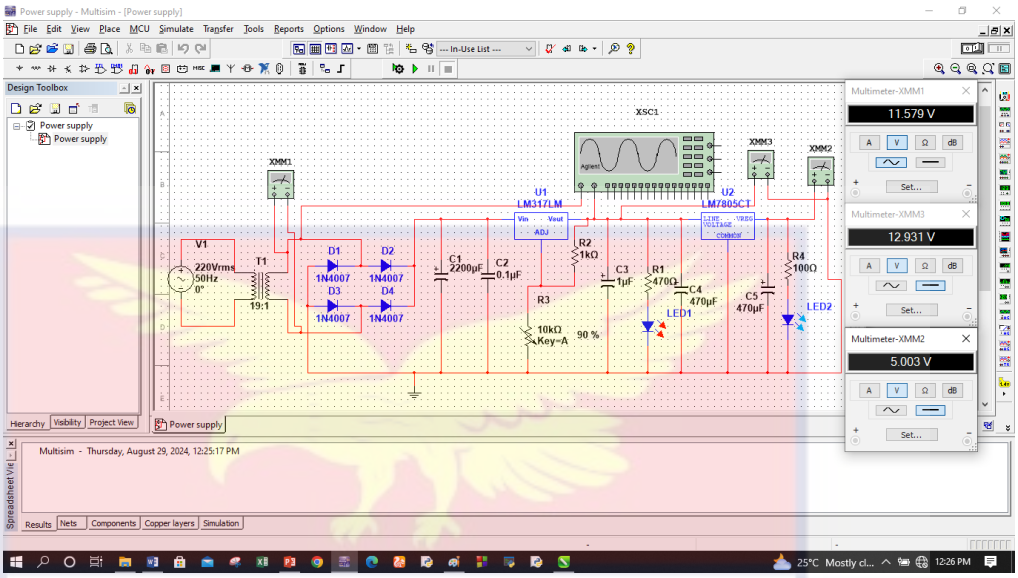

Figure 82: Organ bath DC power supply design using Multisim 13.0

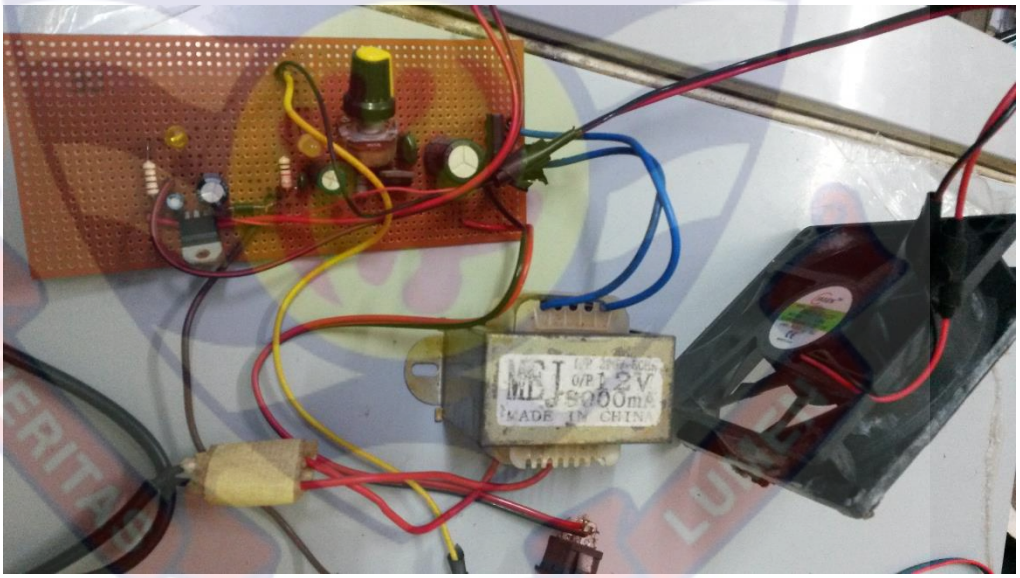

Figure 83: Implemented DC power supply circuit

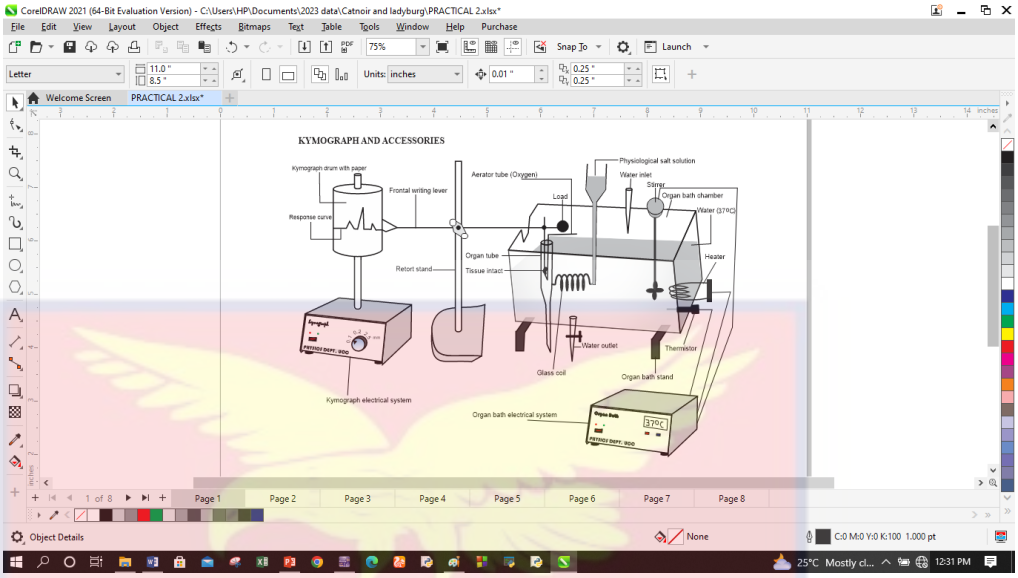

Figure 84: Schematic diagram of the kymograph and organ bath using CorelDraw 2021

Figure 85: Implemented kymograph and organ bath

Figure 86: Top view of kymograph base

Figure 87: Bottom view of kymograph base

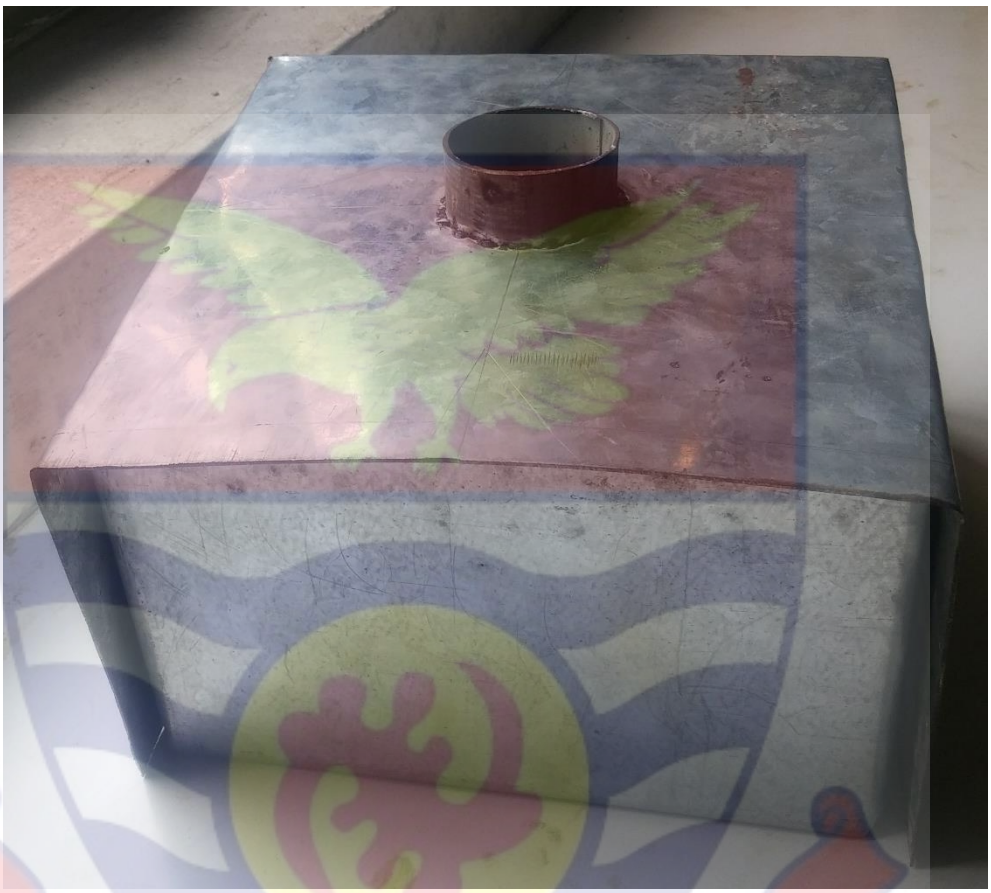

Figure 88: Enclosed kymograph electrical and electronics housing

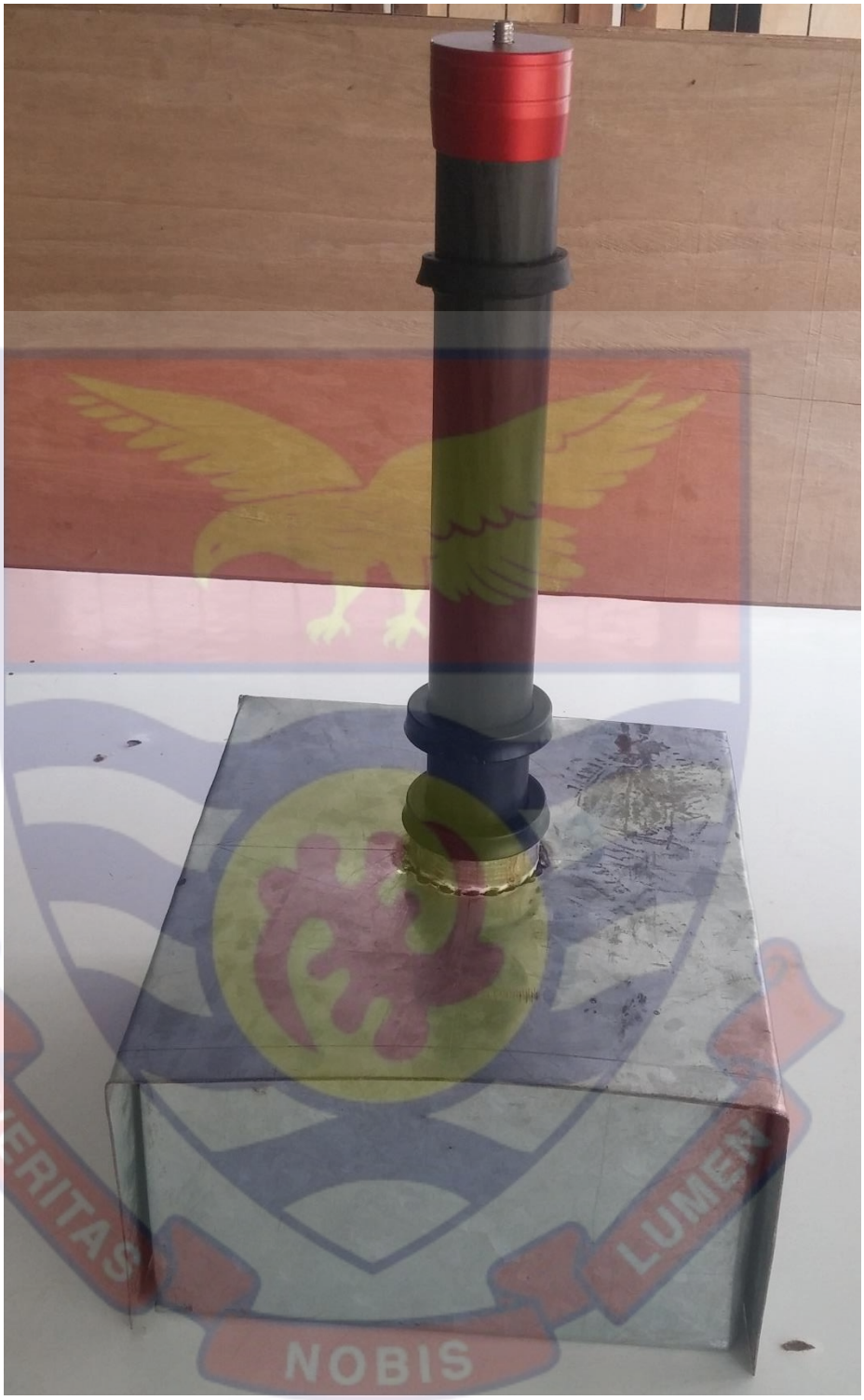

Figure 89: Kymograph base with carbon fiber shaft

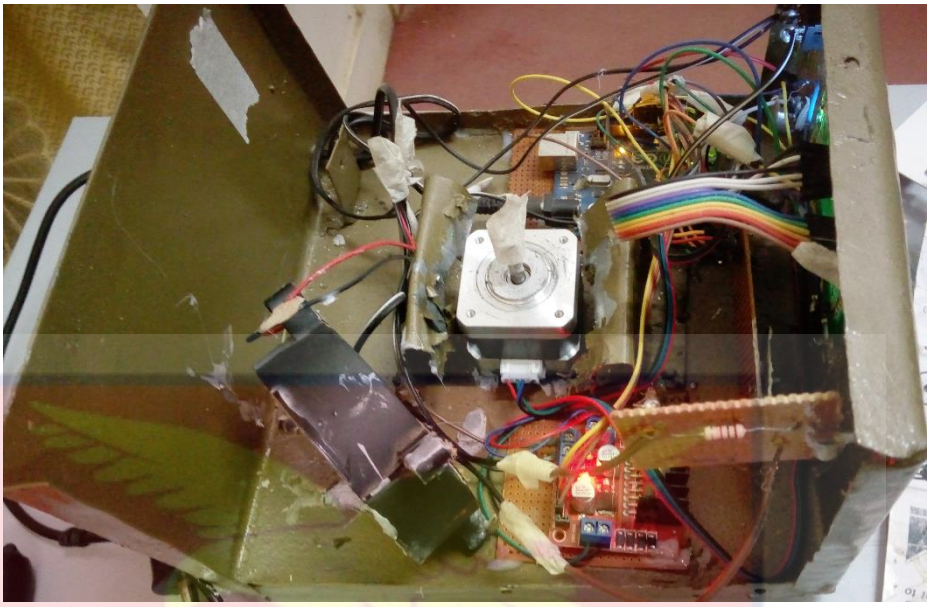

Figure 90: Kymograph electrical system

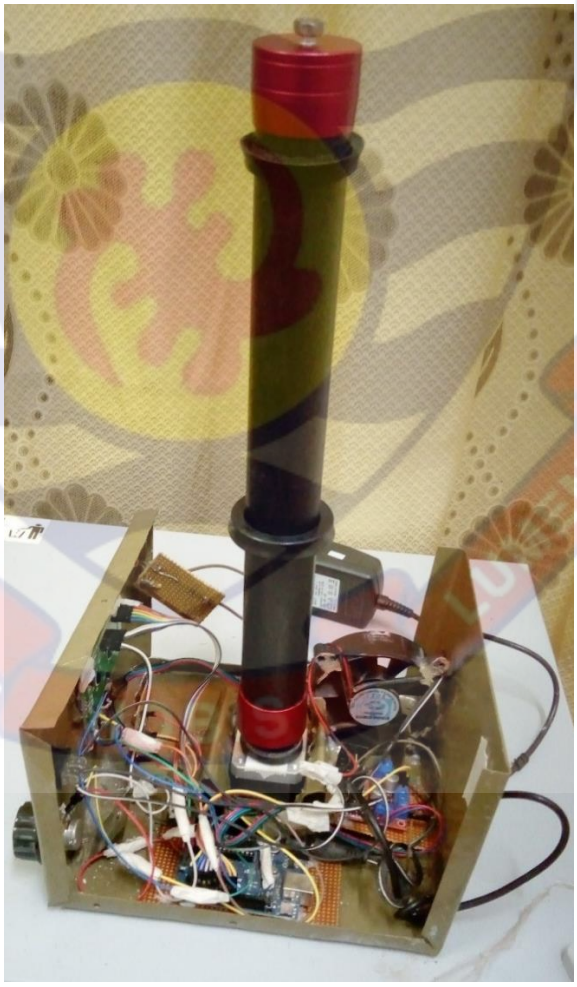

Figure 91: Kymograph base with electronic and electrical wiring

Figure 92: Two unpolished bowl used for kymograph drum

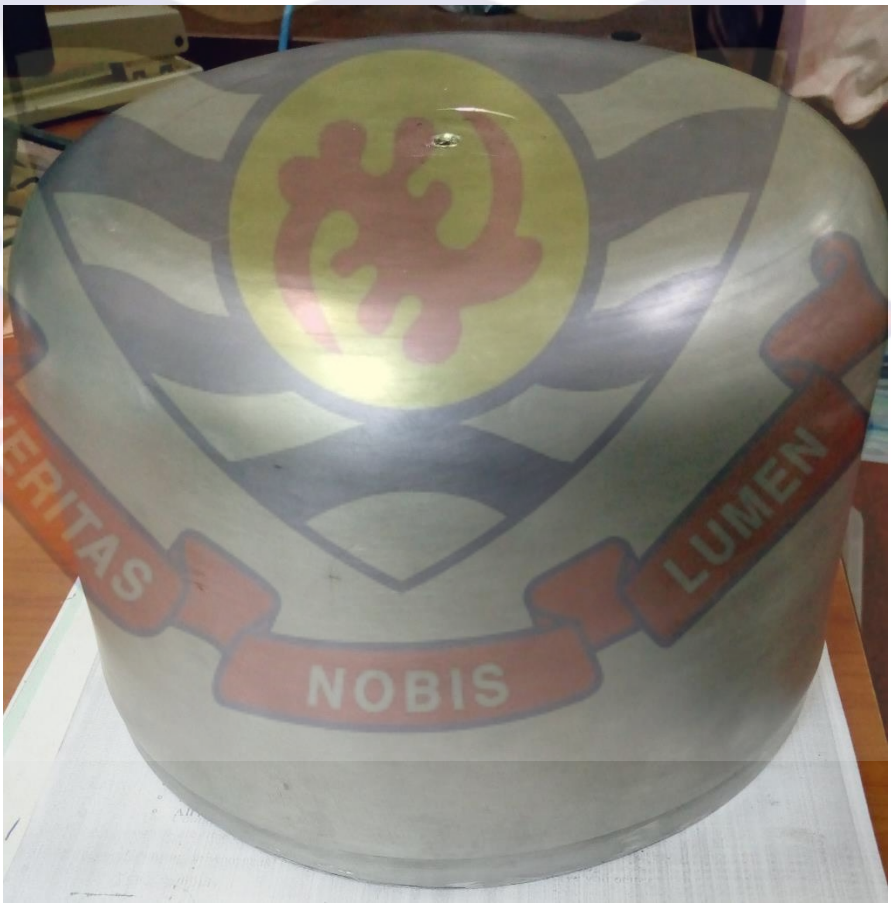

Figure 93: Kymograph aluminium drum

Figure 94: Kymograph electrical system with carbon fiber shaft

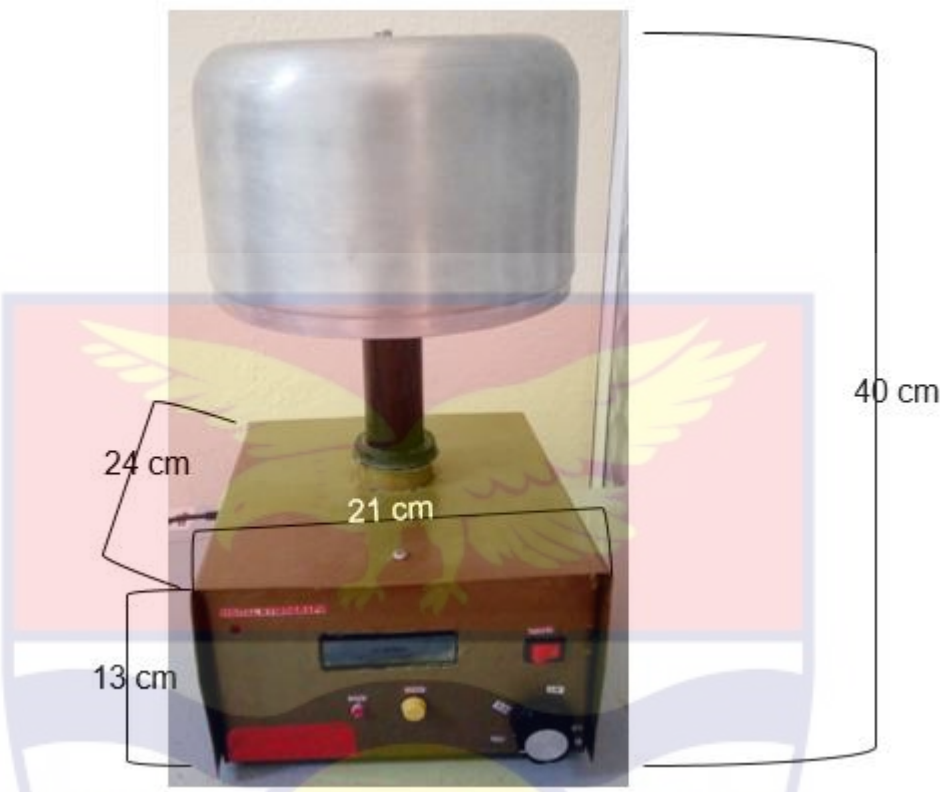

Figure 95: Front view of the calibrated kymograph

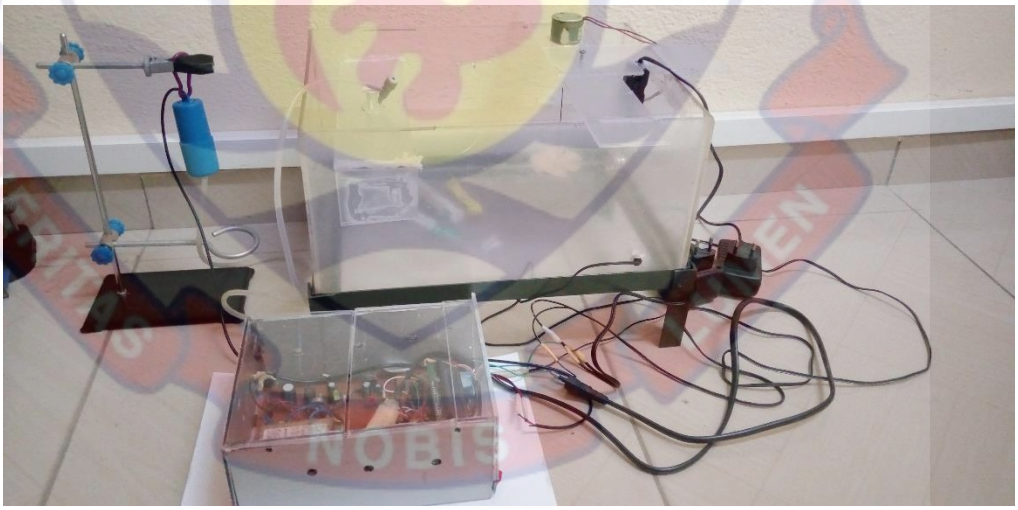

Figure 96: Organ bath setup after construction

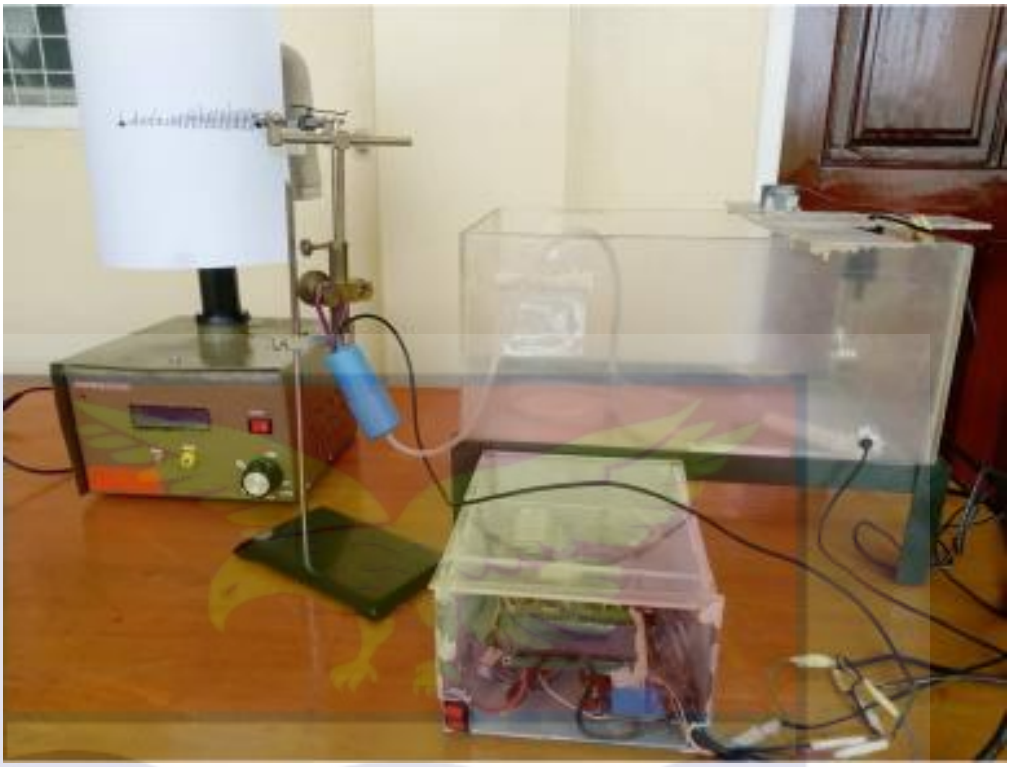

Figure 97: Implemented interfaced kymograph and organ bath

APPENDIX D

L298N MOTOR DRIVER MODULE

Table 5: L298N Module Pinout Configuration

Pin Name	Description
IN1 & IN2	Motor A input pins. Used to control the spinning direction of Motor A
IN3 & IN4	Motor B input pins. Used to control the spinning direction of Motor B
ENA	Enables PWM signal for Motor A
ENB	Enables PWM signal for Motor B
OUT1 & OUT2	Output pins of Motor A
OUT3 & OUT4	Output pins of Motor B
12V	12V input from DC power Source
5V	Supplies power for the switching logic circuitry inside L298N IC
GND	Ground pin

Features and Specifications of Driver Model: L298N 2A

- Driver Chip: Double H Bridge L298N
- Motor Supply Voltage (Maximum): 46V
- Motor Supply Current (Maximum): 2A
- Logic Voltage: 5V
- Driver Voltage: 5-35V
- Driver Current:2A
- Logical Current:0-36mA
- Maximum Power (W): 25W
- Current Sense for each motor
- Heatsink for better performance
- Power-On LED indicator